PRODUCTION AND PROPERTIES OF GLASS BONDED APATITE-WOLLASTONITE BIOCERAMICS

ÇEKDAR VAKIFAHMETOĞLU

JANUARY 2005

PRODUCTION AND PROPERTIES OF GLASS BONDED APATITE-WOLLASTONITE BIOCERAMICS

A THESIS SUBMITTED TO
THE GRADUATE SCHOOL OF NATURAL AND APPLIED SCIENCES
OF
MIDDLE EAST TECHNICAL UNIVERSITY

BY

ÇEKDAR VAKIFAHMETOĞLU

IN PARTIAL FULFILLMENT OF THE REQUIREMENTS
FOR
THE DEGREE OF MASTER OF SCIENCE
IN
METALLURGICAL AND MATERIALS ENGINEERING

JANUARY 2005

Approval of the Graduate School of Natural and Applied Science

Prof. Dr. Canan Özgen
Director

I certify that this thesis satisfies all the requirements as a thesis for the degree of Master of Science.

Prof. Dr. Tayfur Öztürk
Head of Department

This is to certify that we have read this thesis and that in our opinion it is fully adequate, in scope and quality, as a thesis for the degree of Master of Science.

Prof. Dr. Muharrem Timuçin
Supervisor

Examining Committee Members

Prof. Dr. Abdullah Öztürk	(METU, METE)	
Prof. Dr. Muharrem Timuçin	(METU, METE)	
Prof. Dr. Rıza Gürbüz	(METU, METE)	
Prof. Dr. Sezer Aygün	(METU, CHEM)	
Prof. Dr. Feza Korkusuz	(METU, PES)	

I hereby declare that all information in this document has been obtained and presented in accordance with academic rules and ethical conduct. I also declare that, as required by these rules and conduct, I have fully cited and referenced all material and results that are not original to this work.

Name, Surname: Çekdar Vakıfahmetoğlu

Signature :

ABSTRACT

PRODUCTION AND PROPERTIES OF GLASS BONDED APATITE-WOLLASTONITE BIOCERAMICS

Vakıfahmetoğlu, Çekdar
MSc., Department of Metallurgical and Materials Engineering
Supervisor: Prof. Dr. Muharrem TİMUÇİN

January 2005, 132 pages

Apatite containing bioceramic materials are considered to be potentially useful for replacement or repair of natural bone. In the present study, the aim was to produce a new composite bioceramic containing crystalline apatite and wollastonite phases with a bimodal grain size distribution. The manufacturing scheme was based on the liquid phase sintering process in which the compacts pressed from powders of apatite (HAP or Si-HAP) and pseudowollastonite was sintered in the presence of a liquid phase. Three distinct fluxing agents, magnesium flux (MCAS), sodium feldspar and sodium frit (NCAS), were prepared to act as additives for generating the liquid phase during sintering. Among those, the use of sodium frit resulted in the expected bimodal microstructural assembly.

During the sintering studies, it was discovered that the apatite component of the ceramic was prone to compositional modifications by reaction with the liquid phase. This interaction resulted in a formation of

siliconized HAP which crystallized in the form of rod-like grains. Meanwhile wollastonite grains tended to exhibit faceted equiaxed morphology and bonded to rod-like apatite grains with the help of a glassy phase.

The results showed significant enhancement in the mechanical properties of apatite-wollastonite composites compared to phase pure hydroxyapatite. For example, the sample with 47.5 wt% Si-HAP_2 + 47.5 wt% W + 5 wt% $NCAS_{frit}$ had the highest value of flexural strength, 83.6 MPa, which was almost twice that of hydroxyapatite, 46.3 MPa. The results for other properties such as compressive strength, hardness and fracture toughness also demonstrated the benefit of apatite-wollastonite composite approach.

Keywords: Reactive liquid phase sintering, calcium hydroxyapatite, wollastonite, silicone substituted hydroxyapatite, mechanical properties.

.

ÖZ

CAM BAĞLI APATİT-VOLASTONİT BİYOSERMİKLERİNİN ÜRETİMİ VE ÖZELLİKLERİ

Vakıfahmetoğlu, Çekdar
Yüksek Lisans, Metalurji ve Malzeme Bölümü
Tez Yöneticisi: Prof. Dr. Muharrem TİMUÇİN

Ocak 2005, 132 sayfa

Apatit içeren biyoseramik malzemeler kemik onarım ve replasmanında kullanılma açısından yüksek potansiyele sahiptirler. Bu çalışmada; apatit ve volastonit kristal fazlarını içeren iki-elemanlı yeni bir kompozit biyoseramik malzeme üretimi amaçlanmıştır. Hazırlanan apatit (HAP veya Si-HAP) ve volastonit toz karışımı yüksek sıcaklıkta oluşan sıvı faz yardımı ile sinterlenmiştir. Üç farklı katkı maddesi, sırasıyla; magnezyum akı (MCAS), sodyum feldspar ve sodyum akı (NCAS), sinterleme sırasında sıvı faz oluşturması için kullanılmıştır. Bu katkı maddeleri arasından sodyum akının (NCAS) kullanımı istenilen iki-elemanlı mikroyapıya ulaşılmasını sağlamıştır.

Çalışmalar sırasında, karışımın apatit bileşeninin sıvı faz etkileşimlerine dayalı kompozisyon değişimlerine açık olduğu tespit edilmiştir. Bu etkileşim sonucunda oluşan silikonlanmış hidroksiapatit fazı çubuksu yapılara dönüşerek kristalize olmuştur. Bu arada volastonit taneleri

yuvarlak yapılara bürünmüş ve çubuksu apatit tanelerine sıvı fazdan katılaşan cam fazı sayesinde yapışmıştır.

Mekanik test sonuçları, üretilen apaitit-volastonit kompozit biyoseramiklerinin dayançlarının saf hidroksiapatite göre daha yüksek seviyede olduğunu göstermiştir. Örneğin; 47.5 wt% Si-HAP_2 + 47.5 wt% W + 5 wt% $NCAS_{frit}$ kompozit seramiği 83.6 MPa ile en yüksek eğme dayancını göstermiştir. Bu dayanç saf hikroksiapatit seramiğinin eğme dayancının neredeyse iki katına eşittir (46.3 MPa). Basma gerilimi, sertlik ve kırılma dayancı gibi diğer mekanik özelliklerin yüksekliği de üretilen bu kompozit seramiklerinin avantajları arasında sayılabilir.

Anahtar Kelimeler: Reaktif sıvı faz sinterlemesi, kalsiyum hidroksiapatit, volastonit, silikonlanmış hidroksiapatit, mekanik özellikler.

To my

grandfather and grandmother;

Ali & Beser Duman

ACKNOWLEDGEMENTS

The author wishes to express his deepest gratitude to his supervisor Prof. Dr. Muharrem Timuçin for his guidance, advice, criticism, encouragements, patience and insight throughout the research.

The author expresses sincere appreciation to Dr. Nurşen Koç for her guidance and insight throughout the thesis.

The author also want to express sincere thanks to Cengiz Tan for taking SEM micrographs and EDS analyses and Nevzat Akgün for assisting in mechanical tests.

Thanks are to all of my instructors & friends at the Institute of Applied Mathematics, METU, especially Prof. Dr. Aydın Aytuna, Assoc. Prof. Dr. Tanıl Ergenç, Nejla Erdoğdu, and Oktay Sürücü for creating a warm and reliable working place.

A very special thanks to my mother Esma Duman and my aunt Nurcan Taş for their moral support, encouragement and unselfish love throughout my life.

Finally, the warmest thanks goes to Sinem Yardımcı for her efforts in preparing all the drawings in this thesis and for sharing and dreaming with me.

TABLE OF CONTENTS

CHAPTER

LIST OF TABLES

TABLE

LIST OF FIGURES

FIGURES

CHAPTER I

INTRODUCTION

Ceramics were started to be used in clinical applications at the beginning of the 19th century. However, the results were not successful enough until biocompatible materials emerged in the 20th century. During the last forty years a big revolution has occurred in the use of ceramics to improve the quality of human life. This revolution was due to the development of specially designed and fabricated ceramics, called *Bioceramics,* for the repair and reconstruction of diseased, damaged or worn out parts of the body [1].

Bioceramics have gained increased popularity due to their chemical and structural properties, such as strength and ability to withstand high temperatures as well as, high wear resistance and durability. These aspects have rendered bioceramics indispensable in a wide range of biomedical applications including repairing of iliac crest, reconstruction of maxillofacial defects, spinal surgery, replacement for the ossicles in the middle ear, etc [1].

Depending on many factors all materials elicit a response from host tissue after implantation. Response occurs at the implant-tissue site and it can be divided basically into four types [1]. Toxic response is the first one. It is critical that any implant material avoid a toxic response that kills cells in the surrounding tissues or releases chemicals that can migrate within tissue fluids and cause systemic damage to the patient [2]. It is worth to say that non-toxic behavior of bioceramics makes them very attractive for biomedical applications.

Second type of response is a formation of a non-adherent fibrous capsule which is formed when implant is a biologically nearly inert material such as alumina and zirconia. This is the protection mechanism of living organism and within time complete encapsulation of an implant is observed [1].

The third type, b*ioactive response,* is seen when tissue forms an interfacial bond with the implant. Bioactive ceramics, glasses and glass-ceramics such as *Bioglass®, sintered Calcium Hydroxyapatite and Apatite-Wollastonite Glass-Ceramics* elicit this kind of response and tissue ingrowth becomes possible if these materials are in porous form. This type of bonding is also observed in natural tissues while repairing [1].

The last type of response is the dissolution of implant. Biodegradable ceramics are this kind of resorbable materials. They degrade gradually by replacing natural tissue with time. The critical point of dissolution reaction is the degradation products. They must be non-toxic and they should be removed easily from cells without causing any damage to living organism.

Calcium Hydroxyapatite [HAP: $Ca_{10}(PO_4)_6(OH)_2$] seems to be the most appropriate ceramic material for an implant as artificial bones or teeth due to excellent biocompatibility and bioactivity [3]. Natural bone consists from a complex network of collagen and hydroxyapatite while synthetic HAP is merely a fine–grained polycrystalline ceramic. This structural difference makes synthetic HAP as a low strength material which has limited its use to only low-load bearing conditions. Several approaches are currently being developed to overcome this drawback. These include HAP coated metal implants [4], combining the bioactivity of HAP and the toughness and strength of the metal, glass sintered HAP ceramics [5] in which newly formed phases increase the strength of HAP, and HAP containing composites [3].

On the other hand, Bioglass®, Ceravital and Apatite-Wollastonite (A-W) glass-ceramics have been known as highly bioactive Ca-Si based bioceramics [1]. Among all of these materials, *A-W Glass-Ceramic* which contains crystalline apatite and wollastonite phases in a $MgO–CaO–SiO_2$ glass matrix has been regarded as the most promising biomaterial for heavy load bearing applications. The wollastonite phase ($CaSiO_3$) in the A-W glass-ceramic consisted of a silica chain structure which reinforced the apatite crystals, like the collagen fiber network reinforcing the biological apatite phase in natural bone. Due to this structural formation, A-W glass ceramics possessed greater strength than any other bioactive ceramics and even exceeded that of the human cortical bone [6].

A-W glass-ceramics were first prepared by controlled surface crystallization (heat treatment) of glass which was produced by conventional melt-quenching method in the pseudoternary system of CaO-SiO_2-P_2O_5-MgO-CaF in 1982. Since then, these glass ceramics have been produced in various sizes and forms like block, granular, dense and porous by sintering their powders according to the production principle set forth by Kokubo et al [6].

Although A-W glass-ceramics have many desirable mechanical properties and high bioactivity, they are prone to low facture toughness and exhibit high stiffness as compared to natural bone [7]. Since mechanical properties of the ceramics such as strength and fracture toughness as well as elastic modulus are strongly dependent on the microstructure, the formation of the resulting microstructures which are dictated by the densification mechanism, i.e. sintering, are very important.

The aim of the present thesis study was focused on to produce a high strength, highly bioactive ceramic composed of crystalline apatite and wollastonite phases bonded together with the help of a glassy phase. The ceramic was manufactured through the liquid phase sintering process in which

the glassy phase occupied considerably lesser volume as compared to A-W glass ceramics.

During the course of the present study, it was discovered that the apatite component of the ceramic was prone to compositional modifications by reaction with the liquid phase. This interaction resulted in the exchange of some of the phosphorus in the HAP structure with silicon in the liquid phase so that a so-called siliconized HAP became the apatite phase in the ceramic. The introduction of silicon into HAP was found to be accompanied with a change in the grain morphology as well. The siliconized HAP which crystallized in the form of rod-like grains could be effective in enhancing the mechanical properties of the ceramic. The changes in mechanical properties of the apatite-wollastonite composite ceramics due to this morphological variation have been the subject of investigation in this study.

CHAPTER II

PREVIOUS WORK

2.1. BIOCERAMICS

The class of ceramics used for repair and reconstruction of diseased and damaged parts of musculoskeletal system is termed as bioceramics. Bioceramics are produced in a variety of forms and phases. They serve many different functions in repair of the body including treatment of tumors, replacing parts of the cardiovascular system, especially heart valves [1]. Some of the forms, phases and functions of bioceramics are summarized in **Table 2.1**.

Table 2.1 Form, phase and function of bioceramics [1].

Form	Phase	Function
Powder	Polycrystalline Glass	Space-filling, therapeutic treatment, regeneration of tissues
Coating	Polycrystalline Glass Glass-Ceramic	Tissue bonding, thromboresistance, corrosion protection
Bulk	Single Crystal Polycrystalline Glass Glass-Ceramic Composite (Multi-Phase)	Replacement and augmentation of tissue, replace functioning parts

In most of the biomedical applications bioceramics may be used in the form of bulk materials of a specific shape, called *implants, prostheses, or prosthetic devices* [1]. Bioceramics are also used to fill space while the natural repair processes restore function. In other situations the ceramic is used as a coating on a substrate, or as a second phase in a composite, combining the characteristics of both into a new material with enhanced mechanical and biochemical properties. These properties of bioceramics are dependent on starting materials and thermal processing steps used in production [1]. Some examples of clinically used bioceramics and their production methods are given in **Table 2.2**.

Table 2.2 Examples of some bioceramics and their processing methods [1].

Type of Ceramic / Glass	Commercial Product
Glass	45S5 Bioglass®
Cast or rapidly solidified polycrystalline ceramic	HAP coating
Polycrystalline glass-ceramic	Ceravital®
Liquid-phase sintered (vitrified) ceramic	Glass- HAP
Solid-state sintered ceramic	Alumina, Zirconia
Hot pressed ceramic or glass-ceramic	A/W glass-ceramic
Sol-gel glass or ceramic	52S bioactive gel-glass
Multi-phase composite	PE-HAP

Bioceramics can be classified into three main categories relying on their interactions with living tissue [1]: First one is high strength "*Bioinert Ceramics*" [alumina (Al_2O_3), zirconia (ZrO_2) and carbon (C)]. The second one is "*Bioresorbable Ceramics",* these actively participate in the metabolic processes of an organism with the predictable results [Tricalcium phosphate (TCP), some bioglasses]. The last one, "*Bioactive ceramics*" which form

direct chemical bonds with bone or even with soft tissue of a living organism [Sintered hydroxyapatite, bioactive glasses (Bioglass®), glass-ceramics (A/W glass-ceramic) or composites (polyethylene-hydroxyapatite)].

2.1.1. Bioinert Ceramics

Alumina, zirconia, carbon and some refractory oxide ceramics are the inert bioceramics. Among these, high density α-alumina; (purity ≥ 99.5%) is the most widely used one in surgical operations due to combination of excellent corrosion resistance, good biocompatibility, low friction, high wear resistance, and high strength [8].

Alumina has been used in orthopedic surgery for more than 20 years as the articulating surface in total hip prostheses because of its exceptionally low coefficient of friction and minimal wear rates [9]. Other clinical applications of alumina include knee prostheses, bone screws, alveolar ridge (jaw bone), maxillofacial reconstructions, ossicular (middle ear) bone substitutes, kerato-prostheses (corneal replacements), and post-type dental implants. The superb tribological properties (friction and wear) of alumina occur only when the grains are very small < 4 micrometer (micron, μm) and have a very narrow size distribution. These conditions lead to very low surface roughness values (R_a = 0.02 μm). If large grains are present, they can pull out and lead to very rapid wear because of local dry friction and abrasion caused by the alumina grains in the joint-bearing surfaces [10].

Kanematsu et al. [11] studied the cytotoxicity of single crystal alumina ceramics in cell line culture. Cell cultures displayed the same colony formation and survival rates meaning that alumina has no cytotoxicity and if implanted in bone marrow it would not be toxic to circumferential tissue. Also there is no radiation concern when using the alumina ceramics.

Although alumina bioceramics have outstanding biocompatibility and wear resistance, they exhibit moderate flexural strength and toughness [1]. This limits the usage of them when the implant size increased. On the other hand, bioinert zirconia ceramics have higher flexural strength, fracture toughness and lower modulus of elasticity than alumina ceramics. This higher mechanical reliability of zirconia ceramics are the result of transformation toughening mechanism operating in their microstructure [1, 10].

Partially Stabilized Zirconia (PSZ) is the most common type of zirconia ceramics. PSZ ceramics are biocompatible and they have very high fracture toughness and bending strength [10]. The cytotoxicity of polycrystalline zirconia was speculated in cell line culture. The study revealed its noncytotoxicity but radioelement tests showed that very small traces of radiation is found even in fully refined ceramics [11].

Alumina and zirconia ceramics are both exceptionally biocompatible due to their chemical stability in the physiological environment [10]. However, the question of the long-term effects of alpha radiation from zirconia ceramics must be answered. In general, the phenomena of slow crack growth, static and cyclic fracture, stress corrosion, deterioration of toughness with time and sensitivity to tensile stresses are all serious concerns for both ceramics in high load bearing applications. Both alumina and zirconia ceramics undergo slight reduction in fracture strength with time in the physiological environment [1]. As a result of these disadvantages, these ceramics should be restricted to designs only for compressive loading or limited tensile loading conditions.

2.1.2. Bioresorbable Ceramics

Bioresorbable refers to a material which starts to dissolve (resorbed) and slowly replaced (healing-repairing) by advancing tissue (such as bone)

after contacting (placement) with the living organism [12]. Natural tissues can repair themselves and are gradually replaced throughout life by a continual turnover of cell populations. Thus, resorbable biomaterials are based on the same principles of repairing. Matching resorption rates to the repair rates of body tissues, which themselves vary enormously, depending upon type of tissue, age and health, and maintenance of strength and stability of the interface during the degradation are very important parameters to design these ceramics [12].

All resorbable materials do biologically degrade to varying degrees. Some resorbable materials dissolve very rapidly and some too slowly. Since large quantities of material can be replaced, it is essential that a resorbable biomaterial contain only metabolically acceptable substances with an optimum degree of degradation [13]. Otherwise, chronic inflammation and pain occur. This criterion imposes considerable limitations on the compositional design of resorbable biomaterials.

Calcium phosphate ceramics, calcium oxide, calcium carbonate and gypsum [$CaSO_4.2(H_2O)$, Hydrated Calcium Sulfate] are common bioresorbable materials that have been used during the last three decades. Tricalcium phosphate, [TCP: $Ca_3(PO_4)_2$], and calcium hydroxyapatite, [HAP: $Ca_{10}(PO_4)_6(OH)_2$] which is the main inorganic component of natural bone are the most widely used calcium phosphate ceramics for bone and tooth replacement because of their excellent biocompatibility [13]. HAP has low biodegradation which hinders bone ingrowth and results in chemical bonding only at the interface between bone and HAP implant. Compared with HAP, TCP ceramics are considered as resorbable bioceramics. TCP has three polymorphs: β-TCP is stable below 1180°C, α-TCP between 1180°C and 1400°C, and α'-TCP above 1470°C. Among these allotropic forms, β-TCP is

preferred as a bioceramic on account of its chemical stability, mechanical strength and resorption rate [14].

It is necessary to control the microstructure and phase constitution of a resorbable calcium phosphate ceramic to produce a given rate of resorption in the body [15]. For TCP and HAP degradation rate differentiates in the following order: α-TCP >> β-TCP >> HAP. The rate of degradation depends on many factors like surface area (powders > porous solid > dense solid), crystallinity and grain size [1]. Many studies have indicated that the dissolution of HAP in the human body after implantation is too low to achieve the optimal results. On the other hand, the dissolution rate of β-TCP ceramics is too fast for bone bonding. In order to obtain an optimum resorbability of the material, studies have focused on the Biphasic Calcium Phosphate, (BCP), ceramics composed of HAP and TCP. Several results suggest that the resorbability of BCP ceramics is largely determined by the HAP/TCP ratio [13, 16].

Porosity and grain size are two important factors which govern the mechanical properties of polycrystalline ceramics. Since, sintering directly effects these parameters it becomes very important process in production. Ryu et al. [14] investigated the sintering properties of β-TCP ceramics by addition of calcium pyrophosphate and claimed about effective sintering. Raynaud et al. [17] also investigated the probability of increasing mechanical strength of BCP ceramics by hot pressing and showed that the method increased the strength by inhibiting the grain growth. In order to improve the mechanical strength, ongoing studies are focused mainly on enhanced sinterability of these bioceramics.

Besides mechanical requirements, as a bone substitute, bioceramics should have the proper pore size, morphology, and interconnectivity for bone ingrowth and attachment to the body tissue. Porous calcium phosphate

ceramics can be produced by several techniques such as the polymeric sponge technique, foaming processes and techniques using organic additives [16, 18, 19]. The main morphological requisites for allowing bone ingrowth are the existence of open and interconnected pores, with pore diameters larger than 100μm for proper vascularisation [1, 18]. The interconnectivity of the pores can be achieved by adding pore formers. However, there is a compromise between interconnectivity and mechanical strength of bioceramics [3, 20-22]. Therefore, in today's knowledge porous or particulate, among resorbable calcium phosphate bioceramics, TCP is a successful material for resorbable, hard tissue replacements only when low mechanical strength is permissible, such as in some repairs of the jaw or head [1, 15-17].

A new approach for the of use resorbable ceramics in high load bearing applications was developed by De Aza et al [23]. They have produced a new ceramic constituting at least two phases, one bioactive and the other resorbable. Wollastonite – TCP binary system where wollastonite is the bioactive component [24] and TCP is the resorbable component [13, 15, 16], was selected for this aim. Homogenous microstructure was obtained at the eutectic point which corresponds to 60 weight percent (wt%) wollastonite and 40 wt% TCP. The ceramics produced with this composition showed good bioactive and bioresorbable responses in vitro [23]. Later on, Seo et al. [25] have produced $CaO\text{-}SiO_2\text{-}B_2O_3$ bioresorbable glass-ceramics and claimed about high biocompatibility and fast dissolution rate.

Bioresorbable composites have gained more interest in recent years. Composites produced were the combinations of natural or synthetic polymers such as polylactide or polyglycolide with bioresorbable/bioactive phases, such as HAP, TCP or bioglasses [26]. The reason for adding bioresobable/bioactive phases to polymers forming composite scaffolds is threefold [26]: (i) to enhance bioactivity, (ii) to provide adequate control of the scaffold degradation rate, and (iii) to enhance the mechanical properties and structural

integrity of scaffolds. Results on this review claimed that these composites are good candidates only for soft-tissue engineering scaffolds.

2.1.3 Bioactive Ceramics

The term “bioactive” relates to the ability of synthetic material to form a chemical bond with bone or with soft tissue [27]. Bioactive ceramics are unique synthetic materials, which induce in vivo bio-mineralization of bone-like apatite on their surfaces to integrate with living tissue. In the early 1970’s Hench [1] found that some glasses in the Na_2O-CaO-SiO_2-P_2O_5 system showed bone bonding ability, i.e. bioactivity. Since then, various kinds of bioactive ceramics (sintered HAP), glasses (Bioglass®) and glass-ceramics (A-W Glass-ceramics) with different characteristics have been developed.

2.1.3.1 Hydroxyapatite Based Bioactive Ceramics

Hydroxyapatite, HAP, $Ca_{10}(PO_4)_6(OH)_2$, has been successfully applied in medicine for several years due to its excellent biocompatibility and bioactivity [4, 12]. Unfortunately, there is a limit in usage of HAP bioceramics due to their low mechanical reliability in living organism. Additionally, when the amount of porosity increased (for tissue ingrowth), mechanical properties decrease dramatically. The affects of porosity on the fracture toughness and the compressive strength of HAP ceramics are shown in **Figure 2.1.a** and **Figure 2.1.b**, respectively.

The most suitable materials for biomedical applications are those combining high porosity and high mechanical strength without decreasing bioactivity. Therefore, in order to improve the mechanical properties of HAP ceramics for particular applications or implant configurations, numerous techniques have been investigated.

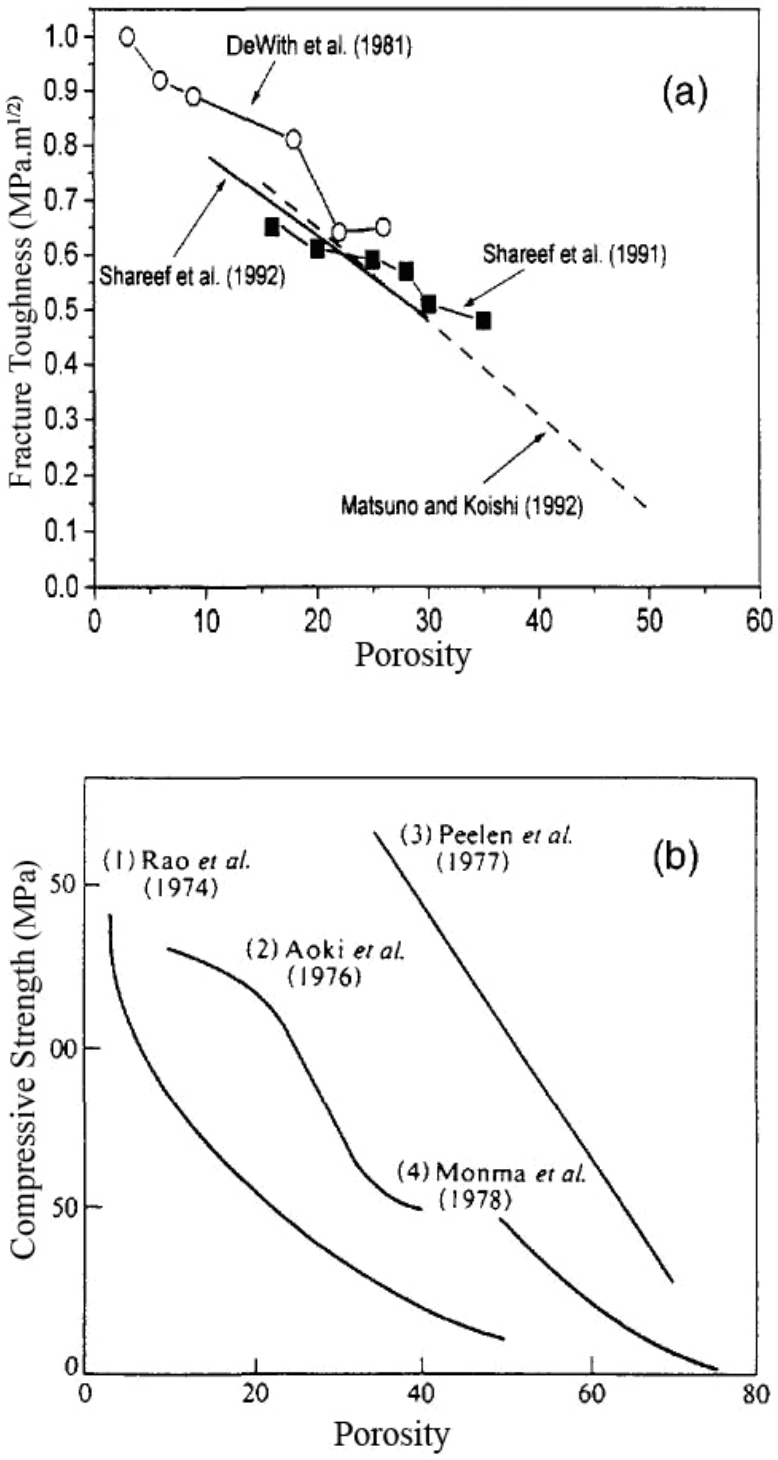

Figure 2.1 Variation in fracture toughness (a) and compressive strength (b) as a function of porosity in HAP ceramics (a [3], b [29]).

Reinforcements including particles, platelets, whiskers, long fibers, dispersoids, and nano-particles have been used in HAP ceramics to make HAP containing composite materials [3]. These composites generally have higher strength and toughness than pure HAP ceramics. DeWith and Corbijn [28] have found that the highest value in fracture toughness (K_{1C}) and flexural strength (σ_b) was achieved by HAP containing 20 to 30 volume percent, vol%, Fe-Cr long metal alloy fibers. Typical values for this composite material were K_{1C} = 6.0 MPa.$m^{1/2}$ and σ_b = 175 MPa.

Although, improved fracture toughness and mechanical strength of the HAP ceramics can be attained by ceramic/metal composite approach, the introduction of foreign materials into the HAP matrix may lead to a decrease in bioactivity and may promote decomposition of HAP into undesired phases like TCP in physiological environments [3, 5, 28]. The presence of TCP in HAP ceramic increases its biodegradability and slow crack growth susceptibility [3, 28, 30]. Moreover, the densification of the ceramic composite is decreased due to the formation of a new phase, i.e. TCP, and evaporation of water resulting from the decomposition process itself. As a consequence, mechanical strength decreases [3].

Another undesired effect associated with metal reinforcements is an increase in elastic modulus of the material. In this case the mismatch of elastic modulus between implant and tissue increases, therefore more load is carried by the implant and strength of the healed tissue becomes low [3]. In general, metal reinforcement agents enhance the mechanical strength of HAP ceramics but problems associated with high modulus, corrosion, wear, and undesired tissue reactions are still regarded as obstacles in biomedical applications.

As an implant material, ceramics have some advantageous properties like corrosion, wear resistance and higher biocompatibility when compared

with metals. Therefore some high strength ceramic materials, such as zirconia, alumina, and silicon carbide, SiC, have been used as reinforcements in HAP ceramics to produce high strength ceramic/ceramic composites [34]. Among all ceramic reinforced HAP composites, the highest mechanical strength value was obtained from HAP with partially stabilized zirconia [1]. Unfortunately, the degradation of zirconia in wet environments (like in vivo) was observed by transformation of the tetragonal zirconia to the monoclinic phase on the surface. This degradation consequently decreased the strength of the implant [35].

Alumina particles, SiC nanoparticles or platelets, and cubic zirconia reinforcement agents in HAP had better in vivo stability but their mechanical properties and biocompatibility results have still not been satisfactory [3, 31-33]. The processing route of these HAP composites aroused another problem. The sinterability of these composites by pressureless sintering was very low, therefore more expensive processes like hot pressing (HP) and/or hot isostatic pressing (HIP) were applied to overcome this problem [33]

As mentioned earlier, various kinds of fibrous materials or whiskers made of SiC, silicon nitride, Si_3N_4, carbon, alumina, zirconia and metal fibers have been applied in HAP ceramics [3, 28, 32, 34, 35]. Unfortunately, most of the metal and bioinert ceramic reinforcements decreased the biocompatibility and bioactivity of HAP ceramics. Consequently, to improve the mechanical strength of HAP ceramics without decreasing bioactivity, applications involving HAP whiskers and/or fiber have recently received much attention. Whisker-like or needle-like crystals of HAP have recently been synthesized, mainly by the hydrothermal method and precipitation routes [35-43]. However, the whiskers synthesized by these methods suffer from nonstoichiometry and low thermal stability, i.e., they partially decompose into α and β-TCP phase when the sintering temperature is increased [36, 38, 41].

Suchanek et al. [40] have reported that for HAP composite reinforced with hydrothermally synthesized HAP whiskers (30 vol% whiskers), the whiskers disappear within the HAP matrixes at sintering temperatures ≥1000°C and turn themselves into large, equiaxed grains. Taş et al. [36] studied the molten salt synthesis of HAP whiskers with various fluxes and claimed effective whisker formation. Whiskers synthesized by this method retained their initial shapes up to 1300 °C. However, trace amount of decomposition was observed. Although investigations on HAP whiskers covered a wide range of synthesis conditions, very little information on thermal and mechanical stability in biological environments were reported.

Increasing interest has been directed on sintering HAP ceramics with glass additions in recent years. There are two main motivations for sintering HAP with a glassy phase. The first one is to enhance the densification and therefore the mechanical strength by acting as a sintering aid, and the second one is to enhance bioactivity through combination of two bioactive phases [5, 44, 45]. Two main glass types were investigated as potential sintering aids for HAP ceramics [46]. The first one, calcium phosphate glasses which ensured that the ceramics produced contained merely calcium phosphate phase. Consequently, the product was probably to be bioactive. The second type of glass was based on calcium silicate system such as highly bioactive Bioglass®.

In addition to apatitic phase, inorganic part of the natural bone contains β-TCP and several ions like Na^+, Mg^{2+}, K^+ and F^-. Therefore in general, sintering of HAP ceramics by introduction of glasses within the P_2O_5-CaO-Na_2O, P_2O_5-CaO-MgO, P_2O_5-CaO-CaF_2, P_2O_5-CaO-MgO-CaF_2 and SiO_2-CaO–Na_2O systems possesses enormous potential as biomaterials, so that the ceramic obtained may have a composition similar to that of the inorganic constituent of the mineral part of bone [47]. Sintering with low glass additions promotes densification through liquid-phase sintering, resulting in

ceramic materials with enhanced mechanical properties. For example, small additions of phosphate glasses significantly enhanced the flexural strength, and fracture toughness of HAP ceramics [5, 44, 45].

Santos et al. [47] investigated the production route of HAP ceramics by addition of phosphate and bioactive silicate based glasses thought liquid phase sintering. They found that the fracture toughness of the final ceramic was enhanced due to enhanced densification and smaller grain size. Decomposition of HAP into TCP was observed, and this was taken as a cause of the enhancement of fracture toughness.

Knowles and Bonfield [44] added a series of $CaO\text{-}P_2O_5$ and $Na_2O\text{-}P_2O_5$ glasses into HAP and found similarly that, addition of glasses generally enhanced the decomposition process of HAP into α- and β-TCP phases at high temperatures. Incorporation of small amounts of $CaO\text{-}P_2O_5$ glass was found to increase bending strength of the HAP ceramics. Whereas, addition of similar amounts of $Na_2O\text{-}CaO\text{-}P_2O_5$ type glasses, decreased the bending strength of the HAP significantly [44]. Salih et al. [48] studied the in vitro behavior of HAP ceramics sintered with P_2O_5–CaO–Na_2O glass addition. They observed that calcium phosphate glass-reinforced HAP ceramics exhibited greater biological activity than pure HAP ceramics. Likewise, Santos et al. [47] studied the biological responses of calcium silicate glass reinforced HAP ceramics and found that the time required for the formation of apatite layer for these ceramics was shorter than for sintered pure HAP ceramics, indicating higher bioactivity.

In general, the presence of a glassy phase either $CaO\text{-}P_2O_5$ or $CaO\text{-}SiO_2$ in all liquid phase sintered HAP ceramics led to a faster response in bone healing; as well as reinforcing the HAP ceramic by incorporating a liquid phase at the grain boundary. But when only mechanical properties are considered HAP ceramics reinforced with calcium silicate glasses were

weaker than those containing equivalent amounts of calcium phosphate glasses [46]. Moreover in all phosphate or silicate additions, decomposition of HAP into TCP was observed. This can be regarded as an advantage or disadvantage depending on the application.

Recently, Georgiou et al. [49] studied the sintering of HAP ceramics by hot pressing. They used calcium phosphate glass as an additive and found that hot pressing accelerated the sintering process, which allowed the glass-reinforced HAP ceramic to reach densification at lower temperatures and reduced the porosity further relative to that seen in liquid phase sintered materials. Although densification was enhanced, decomposition of HAP into TCP was again observed as in pressureless sintered HAP ceramics.

Mechanical and biological properties of glass-reinforced HAP ceramics depend strongly on factors such as grain size, glass composition, level of glass addition, porosity, amounts and morphologies of formed phases [44-49]. But, in general, addition of either calcium phosphate or calcium silicate based glasses increased the bioactivity of HAP ceramics and enhanced the mechanical strength. For example; hot pressing of HAP ceramic at 1100°C with the addition of 15 wt% $CaO\text{-}P_2O_5$ glass resulted in a bending strength of 91.75 MPa [49]. Further, pressureless sintering of HAP ceramic with the addition of 25 wt% $CaO\text{-}P_2O_5$ glass at 1150°C resulted in a bending strength of 37.6 MPa [46]. However, even the highest densified HAP ceramics did not show as high mechanical strength as the human cortical bone [1]. For this reason, the use of glass-reinforced HAP ceramics remained to be limited to low and/or medium load-bearing biomedical applications.

2.1.3.2 Bioactive Glasses

In 1969, Hench and his colleagues [50] discovered that bone could bond chemically to certain glass compositions. Since then, this group of

glasses has become popular as bioactive glasses. The first and most widely studied bioactive glass, termed "*Bioglass® 45S5*", was produced by ordinary glass making method. The product had chemical composition in terms of 45 % SiO_2, 24.5 % Na_2O, 24.5 % CaO and 6 % P_2O_5. The reoson for selecting this specific composition was based on that it represented the neighborhood of the eutectic glass in the Na_2O-CaO-SiO_2 ternary system.

The work carried out by Hench and his co-workers [50] could be summarized on the base triangle of the Na_2O-CaO-SiO_2 system (with 6% P_2O_5) as shown in **Figure 2.2**. The region A demonstrated the glasses which were bioactive and bonded to natural bone. In the middle of this area a smaller region was indicated by broken lines, representing glasses which could develop bonds with the soft tissue as well.

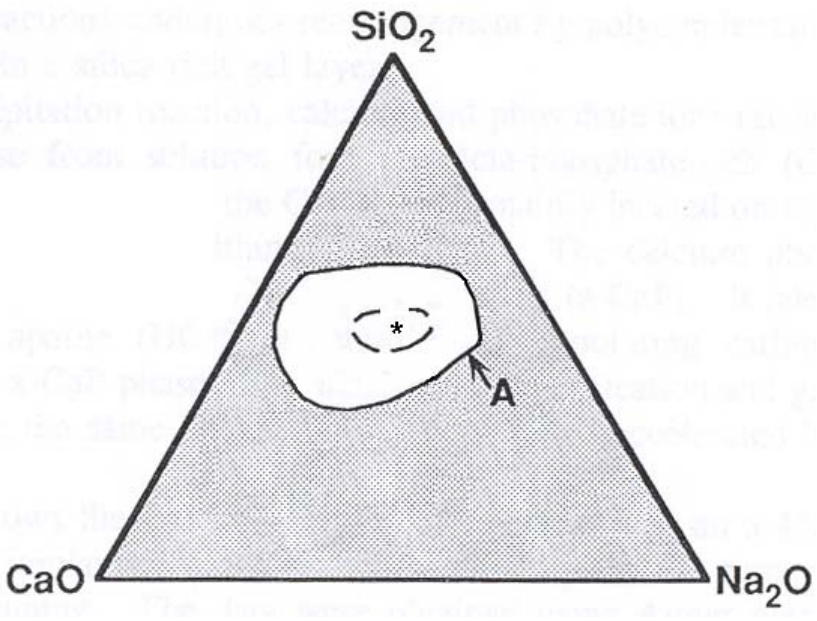

Figure 2.2 Compositional dependence, wt%, of bone bonding and soft-tissue bonding of bioactive glasses (* Bioglass® composition) [1].

The first clinical use of commercial bioactive glass, designated as 45S5 Bioglass®, was in the reconstruction of the bony ossicular chain of the middle ear for the treatment of conductive hearing loss [51]. When metal or plastic implant was used in the same place they would wear thoroughly and get lost through the hole. These problems were overcomed by the special properties of 45S5 Bioglass which bonded to both the hard and the soft tissue with a great success.

The use of bulk bioactive glasses for orthopedic applications has been somewhat limited because of the poor mechanical properties of these materials. For bone grafting purposes these materials are good candidates. Because, in these nonstructural graft sites, load bearing is not a requirement. The successful use of bioactive glass for filling bony defects was reported by Wilson et al. [52] in 1988. It was found that the bioactive glass granules not only allowed bone to fill into the periodontal defects, but also they encouraged the proliferation of bone. This phenomenon was termed "osteoproduction" and it clearly distinguished bioactive glasses from osteoconductive materials, such as sintered HAP.

The most beneficial property of bioactive glasses is their rapid rate of surface reaction which leads to fast tissue bonding [50]. Their primary disadvantage has been the mechanical weakness, specifically low fracture toughness, due to an amorphous two-dimensional glass network. Tensile strength of most of the bioactive glasses varies within the range of 40 to 60 MPa, which makes them unsuitable for load-bearing applications [50]. They may, however, serve as coatings on metal implants where the interfacial strength is a limiting factor, and low stiffness may be an advantage.

In order to overcome the mechanical reliability problems, recent studies were devoted to investigate new routes for production of bioactive glasses. For

example, glasses produced by sol–gel technique showed many advantageous properties such as lower processing temperature, improved homogeneity, and higher bioactivity over glasses produced by melting [53].

One method of improving the strength of material and thereby widening its suitability for load-bearing applications is to make composites from higher strength material and bioglass. stainless steel or titanium or Si_3N_4 reinforced–bioglass composites have been produced to combine the advantageous properties of Stainless steel / Ti / Si_3N_4-based materials, i.e. high strength , fracture toughness and wear resistivity with the high bioactivity of bioglasses [54, 55]. The novel Si_3N_4-bioglass composite was a highly dense material composed of 70 wt% Si_3N_4 ceramic phase and 30 wt% Bioglass®. This composite material had a bending strength of 383 ± 47 MPa and fracture toughness of 4.4 MPa $m^{1/2}$ [54]. Although, the mechanical properties of bioactive glasses have been improved by these new investigations, there is little information in literature concerning the biological performance of these new composites.

2.1.3.3 Bioactive Glass-Ceramics

Glass-ceramics are polycrystalline materials produced through controlled crystallization of glasses. Their microstructure can resemble those of fine sintered ceramics. Shortly after the discovery of Bioglass® by Hench et al [50], Brömer et al. [56] proposed a bioactive glass-ceramic material in the Na_2O-MgO-K_2O-CaO-SiO_2-P_2O_5 system. The product, called as “Ceravital”, actually designated a number of glass-ceramic materials having different compositions [1]. In the first enthusiasm, these new materials were optimistically considered to be applicable in high load bearing conditions, but it was soon realized that their mechanical properties fell rather short of achieving that aim.

Kokubo et al. [6] developed a glass-ceramic in the MgO-CaO-SiO_2-P_2O_5 system in 1982. This was a multiphase material containing apatite and wollastonite crystal phases in the MgO-CaO-SiO_2 glass matrix. Since then, this material has been called as apatite-wollastonite (A-W) glass-ceramic. In air environment the bending strength of the A-W glass-ceramics (215 MPa) was almost twice that of dense hydroxyapatite (113 MPa) and was even higher than that of the human cortical bone (160 MPa) [1, 57, 58]. Owing to its high strength and high bioactivity, A-W glass-ceramics played a crucial leading role for investigations into other glass-ceramic systems.

In the development of the A-W glass-ceramic, Kokubo et al. [6, 58] started with an intended glass composition, in terms of weight percentages 34.2 % SiO_2, 44.9 % CaO, 4.6 % MgO, 16.3 % P_2O_5, and 0.5 % CaF_2. A batch, consisting of a powdered mixture leading to this nominal composition, was melted in a platinum crucible at 1450°C for 2 hours. The melt was poured on to a stainless steel plate and pressed into plates. Cast plates were heated to 1050°C at a rate of 60°C/h, held at the peak temperature for 4 hours and then furnace cooled to room temperature. Microstructural analysis of the A-W glass ceramic revealed that the surface nucleation and rapid growth of wollastonite crystals caused internal cracks.

In a second attempt, Kokubo and his colleagues [58] crushed and ground the glass-ceramic plates into a fine powder, then, pressed the powder into desired form and finally subjected the compacts to the same heat treatment. The powder compact was fully densified at approximately 830°C. Oxyfluoroapatite, $Ca_{10}(PO_4)_6(O,F_2)$ and wollastonite, $CaSiO_3$, precipitated during successive heat treatments conducted at approximately 870°C and 900°C, respectively. The Differential Thermal Analysis (DTA) and thermal shrinkage curves reproduced in **Figure 2.3** demonstrates the precipitation temperatures of these phases.

The resultant A-W glass-ceramic was crack free and it did not contain any pore. Crystals were homogeneously distributed in the glassy matrix. According to X-ray diffraction data, it was possible to crystallize approximately 38 wt% apatite and 34 wt% wollastonite as solid phases. Hence the residual glassy matrix was approximately 28 wt%. A glass-ceramic with this type of phase constitution was characterized by a bending strength of 215 MPa, a compressive strength of 1080 MPa, and a fracture toughness of 2.0 $MPa.m^{1/2}$. Since 1983, the A-W glass-ceramics have been used successfully in clinical applications involving iliac crest prostheses, artificial vertebrae, spinous process spacer, intervertebral spacer, hip and spine surgery [1].

The basic chemical composition and the constitution of the A-W glass ceramic have remained essentially the same as in the original invention of Kokubo et al. [6, 58]. Newer studies on this material system showed that small additions of alumina could enhance the strength and also induce bioactivity [59, 60]. Additionally, Ohgushi et al. [61] showed that Al_2O_3 doped A-W glass ceramics provoked osteogenic differentiation so that they could possibly be used for bone reconstruction in orthopedic surgery, in craniomaxillofacial surgery, and in neurosurgery.

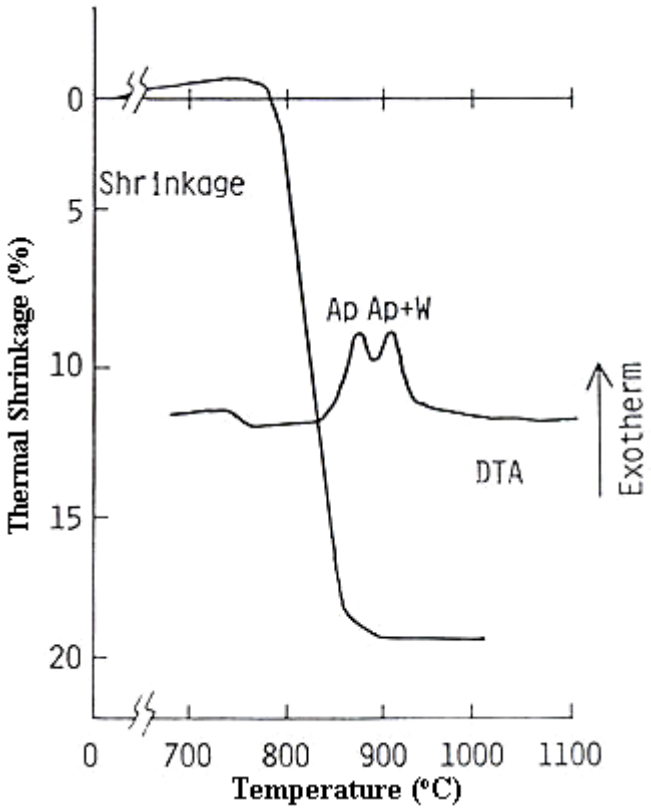

Figure 2.3 DTA and thermal shrinkage curves of glass powder compact [58].

Another multiphase bioactive phosphosilicate glass-ceramic, called Bioverit®, was developed by Höland et al. in the early 1980s [62]. In this material, apatite and mica phases, the latter as the curved phlogophite crystal $(Na,K)Mg_3(AlSi_3O_{10})(F)_2$, were precipitated after controlled crystallization in a fluorine containing glass. The composition of the glass, in terms of weight proportions, was in the range 29.5 to 50 % SiO_2, up to 19.5 % $A1_2O_3$, 6 to 28 % MgO, 5.5 to 9.5 % Na_2O/K_2O, 2.5 to 7 % F, 13 to 28 % CaO, 8 to18 % P_2O_5 and a trace amount of TiO_2 [62].

The most advantageous property of the apatite-mica glass-ceramics over A-W glass-ceramics was their ease of machinability. Mica crystals improved the mechanical machining characteristics of the formed glass-

ceramic. The formation of apatite was achieved by influencing the immiscibility of the glass to form a $CaO-P_2O_5$ rich glassy phase which later served as the nucleus. It was noted that the apatite precipitated within this droplet and that it grew up to the phase boundary in the typical hexagonal form. The resulting glass-ceramic demonstrated bending strength of 140 to 180 MPa, and fracture toughness range of 1.2 to 2.1 MPa $m^{1/2}$. Since 1988, these glass-ceramics have been used in low load bearing clinical applications in the field of head and neck surgery and stomatology [62].

The clinical success achieved by A-W glass ceramics prompted research on ceramic systems that would yield other useful materials in this family. The new glass-ceramics used in dental restorations was basically the outcome of this effort. Beall et al [63] succeeded in controlling the volume nucleation and crystallization of tetrasilicic mica, paving way for the production of castable or machinable mica glass ceramics. Moreover, leucite based glass-ceramics were developed by Höland et al. [64].

The formation of a glass-ceramic with leucite and needle-like apatite was possible in the composition range of 49-58 wt% SiO_2, 11-19 wt% $A1_2O_3$, 9-23 wt% K_2O, 1-10 wt% Na_2O, 0.2-2.5 wt% F, 2-12 wt% CaO, 0.5-6 wt% P_2O_5, 1-9 wt% ZrO_2, with up to 6 wt% additions of preferably CeO_2, B_2O_3, Li_2O [64]. This glass-ceramic demonstrated translucency as well as excellent chemical and wear resistance. The apatite phase improved the capacity of bonding chemically with glass-ionomer cements and thus crowns based on apatite phase could be readily bonded in place without further treatment. These glass-ceramics have been used in dental applications as inlays, crowns, veneers, etc. for 15 years [62].

One of the latest developments in dental glass ceramic materials is the apatite-mullite ceramics developed by Hill et al. [65-67] through heat treatment of glasses formed in the $SiO_2-CaO-Al_2O_3-P_2O_5-CaF_2$ system. The

high fluorine content of the glasses was found to influence strongly nucleation and crystallization behavior. In the fluorapatite containing glass-ceramics studied by Hill et al. [66] and Höland et al. [64], the apatite was formed as elongated needle-like crystals. This elongated nature of the fluorapatite crystals was thought to contribute to the strength and enhanced toughness of the glass-ceramic.

Mechanical properties of some common bioactive ceramics or glasses are tabulated in **Table 2.3**. As can be seen from the table A-W glass-ceramics have favorable mechanical properties than any other bioactive ceramic or bio-glass. Nevertheless, they were similarly prone to low fracture toughness and high elastic modulus. Therefore, in order to use them in high-load bearing biomedical applications, their properties need to be improved.

Table 2.3 Mechanical properties in bioactive ceramics/glasses and bone [1, 5, 68, 74, 111].

	Strength (MPa)		Young's Modulus (GPa)	Fracture Toughness, K_{IC}, (MPa $m^{1/2}$)
	Bending	**Compressive**		
Bioglass®	42	-	35	-
Sintered Hydroxyapatite	20-113	70-509	9-88	≤1,0
A-W Glass-ceramic	215	1080	118	2,0
Cancellous Bone[a]	-	2-12	0,05-0,5	-
Cortical Bone[a]	50-150	100-230	7-30	2-12

[a] Direction of measurements not specified

2.1.3.3.1. New directions in bioactive glass-ceramics

Current research and development on bioactive glass-ceramics is concentrated on development of materials with enhanced mechanical properties without sacrificing bioactivity. Three different strategies have been proposed [62]: (1) changing composition of parent glass, (2) modification of the production process of parent bioactive glass, and (3) composite approach like polymer addition to yield bioactive composites with more reliable mechanical properties.

Calcium phosphate glass-ceramics without silica have a high potential to be used as biomaterials since their chemical composition is similar to that of the natural bone. Actually, glass-ceramics with high CaO/P_2O_5 ratio, containing large amounts of calcium phosphate crystals, is believed to be one

of the best approaches to obtain bioceramic implants suitable for bone replacement [69]. Unfortunately the mechanisms of nucleation, which were successfully used in silicate and silicophosphate glasses, cannot be used in pure phosphate glasses to form glass-ceramic. Consequently, special attention should be given to achieve the controlled volume nucleation of crystals in the P_2O_5-CaO system. Kasuga et al. [70] reported the preparation of phosphate glasses in the pyrophosphate region (with high ratio of $CaO/P_2O_5 \approx 2$) by introducing 10 mole percent total of Na_2O and TiO_2 mixture, yet results obtained from this study were not successful enough. Later on, Zhang et al. [69] added small amount of MgO, Na_2O and TiO_2 to this parent glass and claimed that bulk calcium phosphate glass-ceramic could be successfully obtained by this approach.

Höland et al. [62] produced a silica-free glass-ceramic in CaO-P_2O_5-Al_2O_3 system by controlled volume nucleation of $AlPO_4$ phase. For this purpose, they added small amounts of iron oxide to the parent glass. Similarly, Pernot and Rogier [71] produced phosphate glass-ceramic for the development of glass-ceramic/metal composites with the composition of 69 wt% P_2O_5, 8.3 wt% $A1_2O_3$, 22.7 wt% CaO. A cobalt-chromium alloy or 316L stainless steel was used as a metallic addition [71, 72].

Although A-W glass-ceramics ceramics based on the SiO_2-CaO-P_2O_5 (MgO, Na_2O, Al_2O_3) system, have many desirable mechanical properties with high bioactivity, these glass-ceramics have high elastic modulus and they proved to be prone to low facture toughness. Recently, Juhasz et al. [7] studied the effect of polyethylene content on the fracture toughness and elastic modulus of A-W glass-ceramics. They claimed effective stiffening of the glass-ceramic. However, as yet, there is no information in literature on the biological performance of these composites.

The literature on bioceramics points to the fact that for enhanced mechanical properties and increased reliability, promising results can be obtained by the synthesis of multiphase bioactive composite ceramics consisting of a stiff matrix and a second phase dispersion in the form of fibers, whiskers, or particulates. However, despite the wealth of information and abundance of data on multiphase glass-ceramic type of biomaterials, relatively little is known about the outcome of process like liquid phase sintering of bioceramic powders which might result in a multiphase ceramic.

CHAPTER III

EXPERIMENTAL PROCEDURES

3.1. GENERAL

Apatite-wollastonite ceramics were manufactured by sintering the compacts prepared from powders of calcium hydroxyapatite (HAP), wollastonite, and a frit that would produce a liquid phase during firing. Calcium hydroxyapatite was either pure HAP with the molecular formula $Ca_{10}(PO_4)_6(OH)_2$ or was a siliconized apatite in which part of the phosphorus in pure HAP was replaced with silicon.

The apatite and wollastonite powders were produced in the laboratory through sequential steps involving blending of chemicals followed by thermal synthesis. The frits were obtained by melting the raw material mixtures into clear glass with subsequent granulation and fine communition.

During the firing process the flux component produced a glassy phase which served as the high temperature binder for the ceramic. In addition, the liquid glass was expected to act as a medium of reaction through which an apatite-wollastonite composite ceramic could form with special morphological features that would promote strength and bioactivity.

The ceramics manufactured were characterized by determining their mechanical properties and by examination of microstructures. Additionally, the structural features were determined by X-ray diffraction, XRD, and by spectral techniques. **Figure 3.1** demonstrates all those stages in detail.

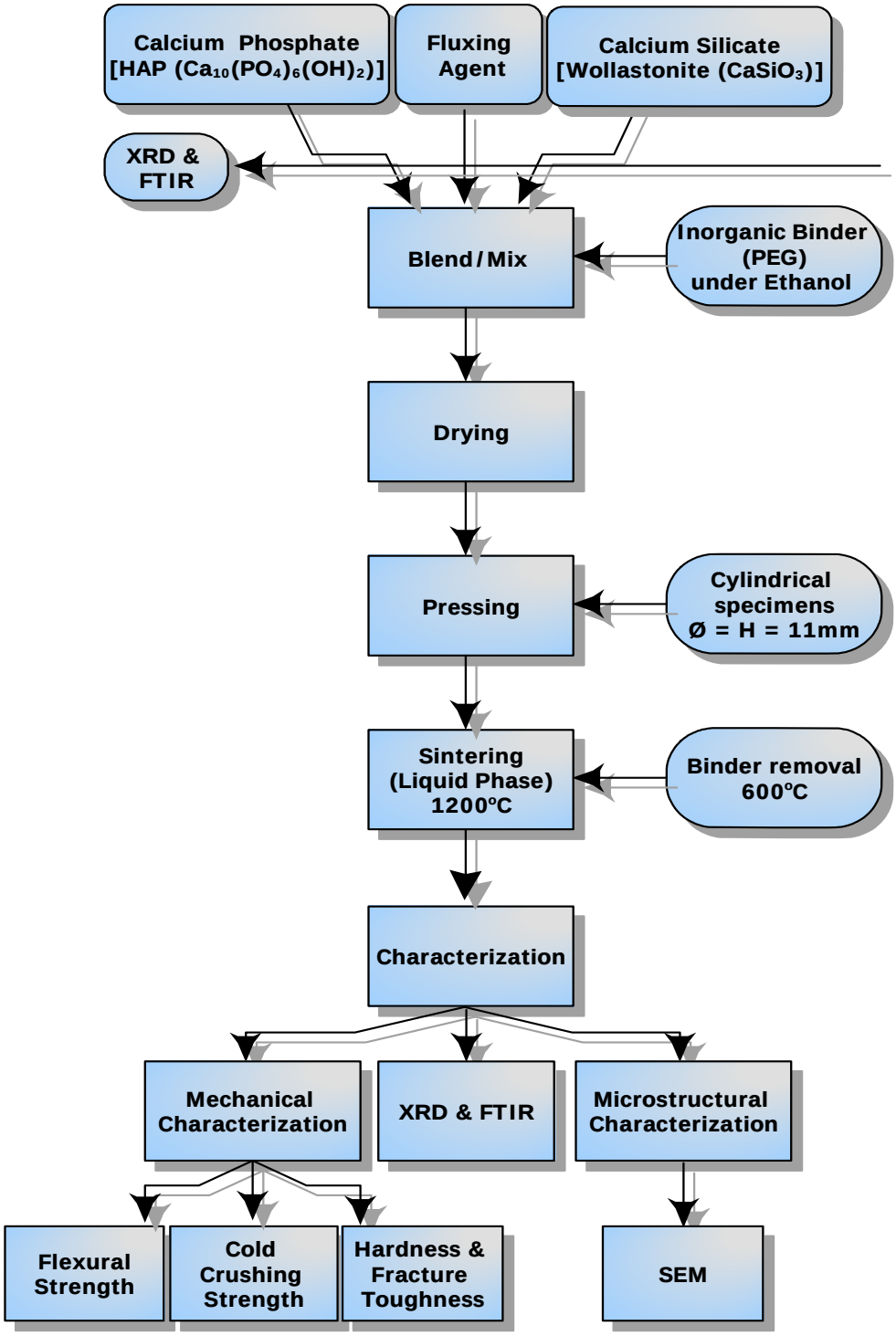

Figure 3.1 A simple flowchart of the experimental procedure carried out, in the present study.

3.2. DETAILS

3.2.1 Powder Synthesis

3.2.1.1 Production of Calcium Hydroxyapatite Powder

The calcium phosphate compound of basic interest for this study was the calcium hydroxyapatite, abbreviated as HAP. The molecular formula for this compound is generally written as $Ca_{10}(PO_4)_6(OH)_2$.

In the literature various techniques have been developed for the synthesis of biomedical grade HAP powders. Most of these depend on precipitation of solid precursors from aqueous solutions that contain the ions of calcium and phosphorus in the proportions required in the apatite powder. The process is called as “chemical route” of ceramic powder synthesis and has become preferable due to the perfect mixing of cations in the product.

The procedure developed by Hayek et al [73] constitutes the basis of the chemical route for the production of apatite powders. In this method, a solution of nitrate salt of calcium, $Ca(NO_3)_2$, is mixed with a solution of di-ammonium phosphate, $(NH_4)_2HPO_4$, in an aqueous environment maintained at about 80°C. When this aqueous mixture is buffered to an acidity level of pH = 5.5 to 6.0 a solid precursor of HAP precipitates homogeneously. The strengths of calcium nitrate and phosphoric acid solutions may be adjusted in such a manner that an atomic ratio of Ca to P equaling 1.67 can be achieved in the precipitate. The precursor is separated from the residual liquor through centrifuging. Several intermediate washings are necessary to ensure the phase purity of the product.

The preparation of HAP through the precipitation process described above has been found slow and cumbersome. The process needs great care to ensure reproducibility and chemical homogeneity which may be destroyed rather easily due to incomplete precipitation and stray losses of some cations during washings.

In 1981, Akao et al [74] developed a simplified approach to the production of HAP powders, which involved reacting a fine suspension of $Ca(OH)_2$ in water with phosphoric acid, H_3PO_4. The method was found to result in powders with fairly reproducible chemical composition and particle morphology that would be essential for biomedical applications.

HAP powders used in the experiments of the present thesis work were produced by following the method developed by Akao at al [74] with some modifications which enhanced chemical stability. The process was based on reacting an aqueous slurry of $Ca(OH)_2$ with a diluted phosphoric acid solution.

Orthophosphoric acid, H_3PO_4 (Merck, #100564, 89%, M=98.00 g/mol, 1ℓ=1.75kg), and $Ca(OH)_2$ (Merck, #102047) were the starting chemicals. The purity of each chemical was specified to be better than 99%. Initially, a stock solution of orthophosphoric acid with a strength of 0.1M H_3PO_4 was prepared by diluting the orthophosphoric acid with de-ionized (DI) water. Next, a weighed quantity of $Ca(OH)_2$ powder was placed in a 1 liter capacity flask and a suspension was formed by adding DI water on it. A solid to liquid ratio was adjusted to 1÷3 by weight. The beaker was placed on a hot plate equipped with a magnetic stirrer, the contents were mixed continuously for about 30 minutes. During this period, the beaker was heated to 85°C while the pH of the slurry shifted slowly towards the basic range owing to the partial dissolution of $Ca(OH)_2$ in water.

The 0.1M H_3PO_4 phosphoric acid solution was added to the $Ca(OH)_2$ slurry through a burette in a dropwise manner while the suspension was stirred vigorously. The rate of acid addition was adjusted in such a manner that the pH of the slurry was always maintained in the basic range. The experimental set-up used for HAP powder preparation is shown schematically in **Figure 3.2.** Akao et al [74] proposed following reaction for describing the formation of HAP in the slurry:

$$\mathbf{10Ca(OH)_2 + 6H_3PO_4 \rightarrow Ca_{10}(PO_4)_6(OH)_2 + 18H_2O} \qquad \mathbf{(a.1)}$$

The reacted mixture was stirred for about 6 hours to allow the completion of the above reaction and thickening of the slurry by evaporation of its water. The beaker was then transferred into a drying oven maintained at 90°C. The slurry was dried in the oven until lumps of HAP were formed. The dry HAP mass was ground in a porcelain mortar, 3 wt% Polyethylene glycol (PEG) was added and the powder was pressed uniaxially into cylindrical tablets (Ø=32mm) in a 2080 tool steel die under a pressure of 1250 kgf/cm^2.

Pressed tablets were calcined at temperatures of 700°C, 800°C and 1000°C for 6 hours at the peak calcination temperature. A binder removal step lasting 30 minutes at 600 °C was incorporated in the calcination schedule before reaching the peak treatment temperatures. The formation of HAP in the calcined product was monitored by XRD. The bond structure in the resulting product was identified by FTIR analysis.

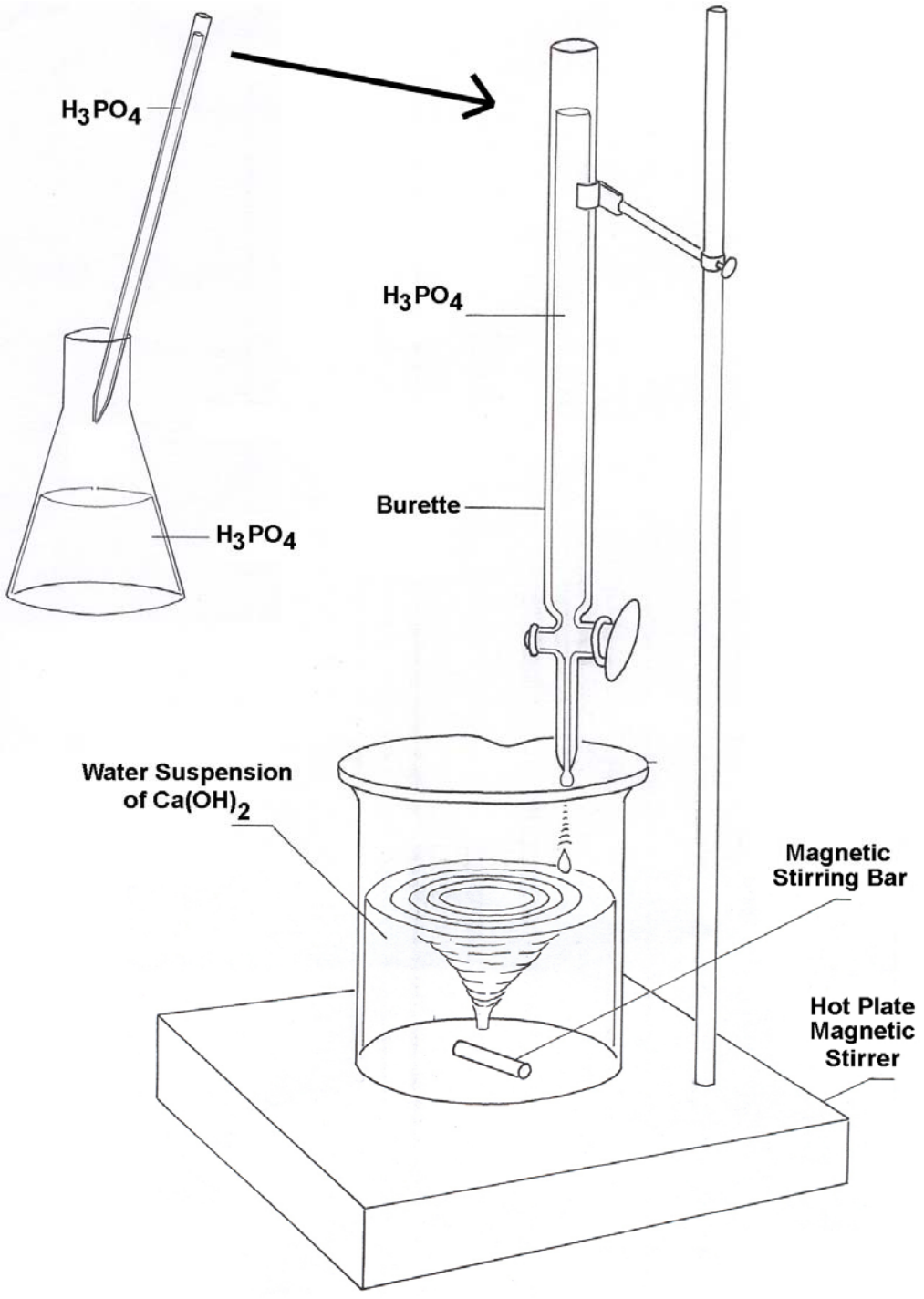

Figure 3.2 A Schematic view of the set-up used for HAP powder preparation.

3.2.1.2 Production of Siliconized Hydroxyapatite Powders

Calcium hydroxyapatite in which phosphate is partially replaced by silicon can be represented by the following molecular formula: [75]

$$Ca_{10}(PO_4)_{6-x}(SiO_4)_x(OH)_{2-x}$$

The formula indicates that for each atom of silicon entering the HAP structure an equivalent amount of $(OH)^-$ is lost to maintain the charge neutrality of the new compound. The formation of siliconized HAP can be described by the following reaction: [75]

$$10Ca(OH)_2 + (6-x)H_3PO_4 + xSiO_2 \rightarrow Ca_{10}(PO_4)_{6-x}(SiO_4)_x(OH)_{2-x} + (18-x)H_2O \quad \textbf{(a.2)}$$

The maximum amount of silicon that can be admitted into a molecule of HAP is governed by the minimum allowable level of $(OH)^-$ in the structure. The reaction given above indicates that this limit is exceeded when 2 atoms of silicon are introduced into HAP; at this stage the compound loses its "hydroxyl" characteristics by transforming into a calcium silico-phosphate compound, i.e. silicocarnotite.

In the present study, siliconized HAP powders were prepared with x values 1, 1.5 and 2.0 by using the reactor shown in **Figure 3.2.** As the source of SiO_2 a high surface area powder product of Sigma-Aldrich (#S5130, powder, particle size 0.007 μm), marketed as "fumed silica" was used together with $Ca(OH)_2$ and H_3PO_4 obtained from Merck. Powders of $Ca(OH)_2$ and SiO_2, weighed in proportions in accordance with the stoichiometry of the reaction in Equation (a.2), were placed in the 1 liter capacity flask and then brought into suspension in DI water while being heated to 85°C. The

remainder of the process involved essentially the same steps described for the preparation and characterization of pure HAP powder.

3.2.1.3 Production of Wollastonite Powder

Wollastonite is a compound that forms in the CaO-SiO_2 binary system with the molecular formula $CaSiO_3$. In wollastonite, CaO and SiO_2 are combined in equimolar proportions. Natural wollastonite, which has a fibrous structure, may not be used in the production of biomedical ceramics due to the presence of impurities, notably iron, in the material.

Synthetic wollastonite is manufactured commonly by reacting an intimate mixture of $CaCO_3$ with SiO_2 at high temperatures. The reaction which describes the formation of $CaSiO_3$ can be written as:

$$\mathbf{CaCO_3 + SiO_2 \rightarrow CaSiO_3 + CO_2} \qquad \textbf{(a.3)}$$

Reagent grade powders of $CaCO_3$ (Merck, #102076, 99.5% pure) and SiO_2 (Sigma-Aldrich, #342890, 99.6% pure) were used to prepare the wollastonite needed in the present thesis. The individual powders of calcium carbonate and silica fume were weighed to obtain a 100 gram wollastonite product. The powder mixture was blended in a porcelain mortar and pestle for 30 minutes under ethyl alcohol and then this slurry was transferred to an alumina porcelain jar for further blending by ball milling for 12 hours. DI water was added to the slurry so that an efficient mixing could be obtained.

When blending and grinding in the ball mill was completed, the slurry was poured into a Pyrex dish and was dried completely in an oven by raising the temperature gradually to 110 °C. The dry powder mixture was pressed into 32 mm diameter cylindrical tablets. The tablets were placed in a muffle

furnace and heated there to 1250°C for thermal synthesis of wollastonite produced by means of the reaction shown in Equation (a.3). The synthesis, which is also called calcination, was conducted in two stages. The first calcination lasted 24 hours. Because of sluggishness of the formation reaction the wollastonite yield in this first step was around 90 percent. The second calcination step was necessary to ensure complete conversion.

For the second calcination stage, the tablets from the first step were cooled, crushed and ground, and then ball milled in the alumina porcelain jar for 12 hours with deionized water serving as the grinding medium. The slurry was dried, the new tablets were pressed and they were reacted again in the muffle furnace at 1250°C for an additional 24 hours. The product of the second calcination step was subjected to communition consisting of crushing and grinding followed by ball milling in DI water for 12 hours. The formation of wollastonite in the calcination steps was followed and verified by X-ray diffraction analysis on the products.

3.2.1.4 Production of Fluxing Agents

Three distinct fluxing agents were prepared to act as additives for generating the liquid phase during sintering of the ceramic compacts of this study. The first flux was chosen from the system MgO-CaO-Al_2O_3-SiO_2. The projection of the liquidus surface of this system is shown in **Figure 3.3**. The flux was selected to have the composition of the eutectic indicated on the diagram as point A. The temperature of the invariant was approximately 1300°C. This flux was labeled as "MCAS" taking its name from the initials of the oxides involved in its structure.

Raw materials used in making the flux were reagent grade chemicals of $CaCO_3$, $MgCO_3$ (Merck, #105828, 40-50% MgO), Al_2O_3 (Merck, #101095,

99% pure) and SiO_2. The purity of all powders, specified by the supplier, was 99% or better. The powders were weighed in the proportions required, taking the invariant point as the target. The powder constituents were blended in a porcelain mortar and pestle, plasticized with 3 wt% addition of DI water, and then compacted as cylindrical tablets (Ø=20mm) under a pressure of 500 kg/cm^2. The tablets were placed in an impervious alumina crucible and melted in a muffle furnace by raising the temperature gradually to 1400°C. The melt was homogenized for 3 hours at the peak temperature and then cast by pouring into a bucket of distilled water. The beads were crushed and ground. In order to produce micron size flux powder, the fraction passing 100 mesh sieve was ball milled in an alumina porcelain jar for 16 hours. DI water served as the grinding medium.

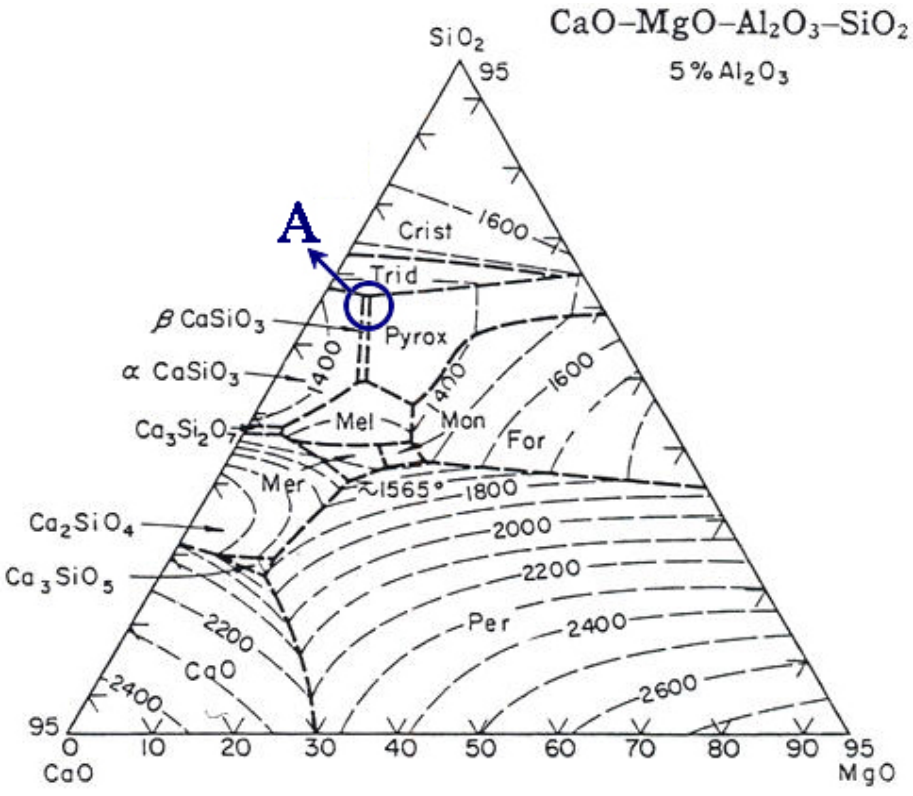

Figure 3.3 The projection of the liquidus surface of the system CaO-MgO-SiO_2 with 5 wt% Al_2O_3 [76].

The chemical analysis of the flux, obtained from the Energy Dispersive Spectrometry (EDS) unit attached to of the Scanning Electron Microscope (SEM), in terms of weight percentages was approximately as follows:

$$CaO = 33\ \%,\ MgO = 12\ \%,\ Al_2O_3 = 5\%,\ SiO_2 = 50\%.$$

This composition was close to the target product. While weighing the raw materials, allowance was made to compensate for the probable Al_2O_3 pick up from the alumina melting crucible.

The second flux was sodium feldspar which finds widespread use in glass-making. Due to its Na_2O component this flux was considerably more reactive than the MCAS mentioned above. Sodium feldspar was received from the Bozüyük facilities of Eczacıbaşı Seramik Company. The flux had the following molecular formula:

$$1.00\ Na_2O\text{-}0.91\ Al_2O_3\text{-}5.99\ SiO_2$$

The chemical analysis obtained from the EDS spectrum of it in SEM verified this composition. The weight percentage analysis of the feldspar was 12.05 % Na_2O, 18.10 % Al_2O_3, and 69.85 % SiO_2. The as-received feldspar was already in powder form, it was ball milled in an alumina jar to fineness below 3 micron size.

The third flux was a frit belonging to the system Na_2O-CaO-Al_2O_3-SiO_2. Throughout this thesis study it has been named as “NCAS frit” due to the initials of the oxides involved in its structure. The modifiers CaO and Na_2O made the frit more reactive than the MCAS flux mentioned above. The frit was produced in the Bozüyük facilities of the Toprak Seramik Company in accordance with the following molecular formula:

0.29 Na_2O-0.38 Al_2O_3-3.32 SiO_2-0.71 CaO

This composition was verified by taking the EDS spectrum. In terms of weight percentages of the constituent oxides it contained 5.5 % Na_2O, 12.1 % CaO, 11.8 % Al_2O_3, and 60.6 % SiO_2. The as-received frit beads were crushed and ground by a porcelain mortar and pestle and then ball milled in an alumina jar to a fineness below 3 micron size.

The powder X-ray diffraction analyses of the two fluxes mentioned above revealed that the "$NCAS_{frit}$" was essentially amorphous while "MCAS" had some residual crystallinity. The XRD charts associated with the fluxes are shown in **Figure 3.4**.

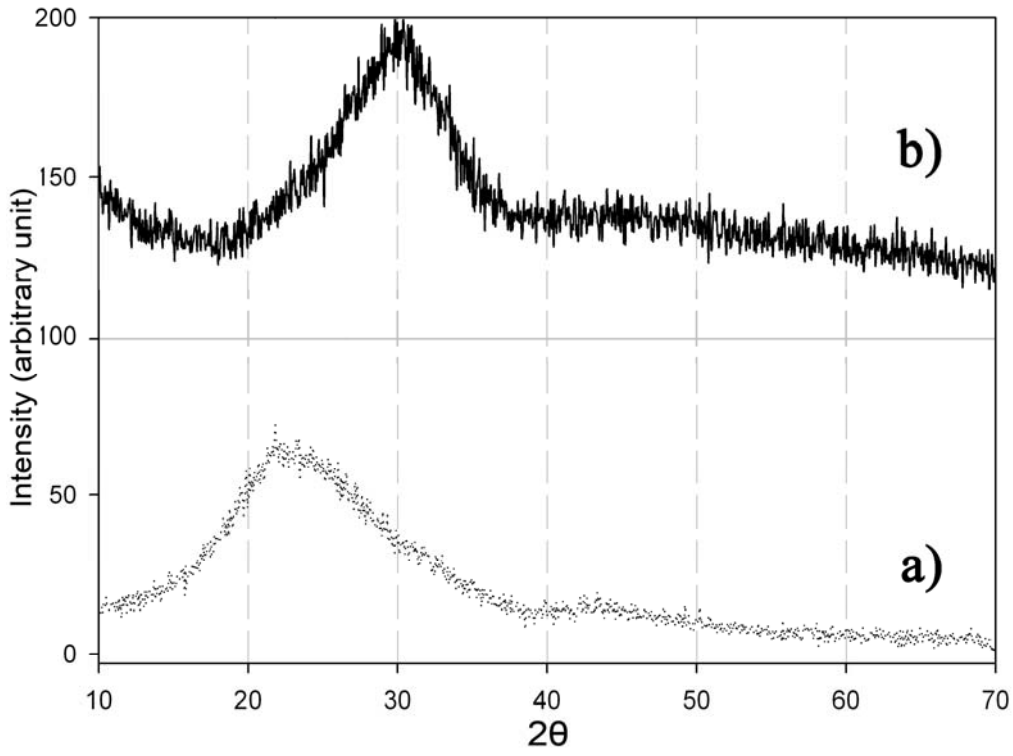

Figure 3.4 X-ray diffraction patterns of the fluxing agents:
a) $NCAS_{frit}$, b) $MCAS_{flux}$.

3.2.2. Preparation of Ceramic Samples

The ceramic samples used for a variety of purposes in the present thesis work were prepared by compaction of the powders into selected shapes followed by sintering at high temperature to gain strength. The ceramic samples produced by sintering would be useful for following purposes:

1) Study of microstructure
2) Determination of flexural and compressive strength
3) Determination of hardness and fracture toughness.

Although the shape and dimension of the ceramics used in each of these determinations were different, the preparation of the ceramic samples shared some common features; i.e., the green ceramic was shaped by compaction of the powder mixture through a pressing process in a suitable die and then the compact was densified by sintering the green shape at a temperature of 1200 °C, 4 hours.

In order to prepare the pressing powders, the powders of the constituents hydroxyapatite, wollastonite or flux were weighed in desired quantities and placed in an agate mortar for blending under ethyl alcohol by a rotary grinding action of the pestle. The mixing of each batch lasted at least 30 minutes. 3 wt% of PEG was added to the mixture to serve as an aid in the subsequent shaping pressing process. PEG was prepared in the form of a wax solution in ethanol. The mixing process was extended until the alcohol of the slurry evaporated substantially and then the mix was allowed to stand in air for 12 hours so that the powder mixture became ready for pressing.

The green ceramic samples for the study of microstructure development during sintering were pressed as 11mm long cylinders with 11mm diameter. The quantity of powder needed for producing such a sample

was about 1.5 grams. The plasticized powder was poured into the die cavity and then pressed under a load of 150 kg/cm^2. The die itself was manufactured from 2080 steel, hardened and polished properly. Working parts of the die were lubricated with a 4 wt% solution of stearic acid in acetone, prior to each pressing.

For the sintering process the green cylindrical pellets were placed on a platinum sheet supported with a cordierite ceramic substrate serving as the saggar. This assembly was placed into a muffle furnace which could perform sintering runs with the help of a programmable Proportion Integration Differentiation (PID) unit. The sintering program applied to the green ceramic cylinders is shown in **Figure 3.5**. The rates in the heating or cooling sections of the sintering schedule were adjusted to 4°C per minutes. The isothermal hold duration was 30 minutes at 600 °C for the removal of PEG and the second one at 1200 °C, which lasted 4 hours, represented the soak period of the sintering process.

The atmosphere during sintering was always air. The sintered sample was left inside the furnace until the cooling subsided when the program reached room temperature.

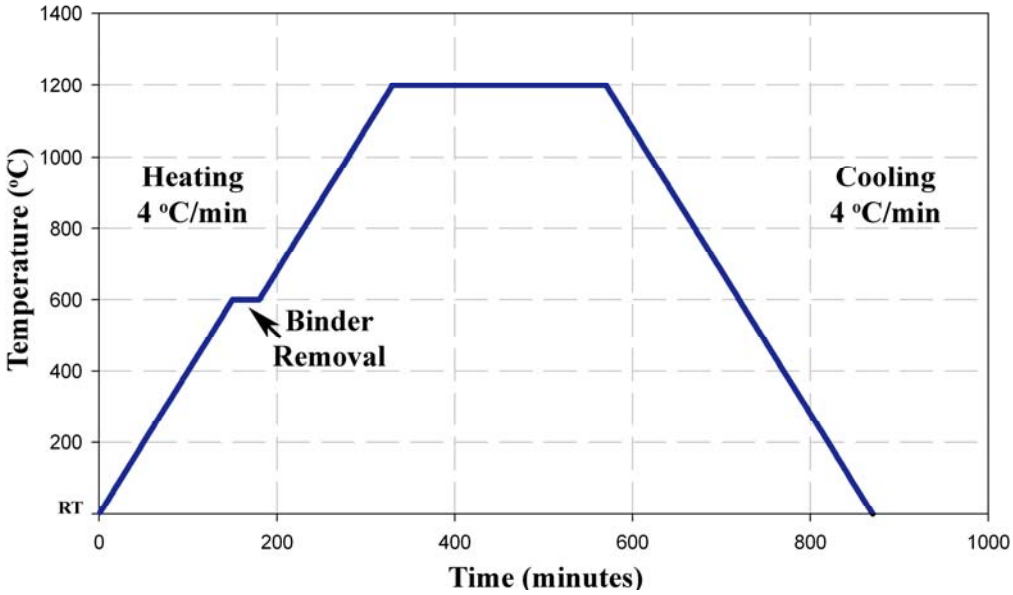

Figure 3.5 Diagram showing the sintering schedule in terms of temperature and time.

The samples used in bending tests for flexural strength and compression test for compressive strength measurements and those used in hardness or fracture toughness determination were prepared by following the same procedure for the samples used in microstructural study described above with the exception that the shapes of the samples were different. For bending tests rectangular bars were prepared whereas compressive strength, hardness and fracture toughness determinations were made on disc shaped tablets.

3.2.3. Characterization

3.2.3.1. Microstructural Characterization

The primary tool used for microstructural characterization was the JEOL - JSM6400 Scanning Electron Microscope, (SEM), equipped with NORAN X-ray Microanalysis System and Semafore Digitizer. SEM examinations were conducted on cut or freshly broken surfaces. Prior to SEM

investigation all surfaces were sputter-coated by a 250 Angströms, A°, thick layer of an Au-Pd alloy.

The EDS attachment on the scanning electron microscope facilitated to make records of the spectra and to obtain in-situ chemical analysis of the samples. These features helped greatly in identification of chemical nature of crystalline and glassy phases which exhibited different morphological characteristics.

3.2.3.2. X-Ray Diffraction and FTIR Studies

The constitution of ceramic powders and the nature of phases in the sintered ceramics were investigated with powder X-ray diffraction, (XRD), methods using a Rigaku DMAX-B unit. XRD work was carried out primarily as a qualitative study directed towards identification of the crystalline phases. In sintered ceramics, fragments were crushed and ground to obtain the powders necessary for phase identification.

2θ-values, peak heights and phase analysis on the collected data were made by the automated built-in computer software of the XRD unit. The details related to the XRD procedures employed in the present study were summarized in **Table 3.1**.

Table 3.1 The variables used in XRD analyses.

Radiation type	X-Ray, Cu, 40kV, 20mA
λ value used	1.542 A° $K_{\alpha 1}$
λ discrim.	Diffracted beam, graphite mono
λ detector	Scintillation
Temperature	22±2 °C
Range of 2θ	10 to 70
Step size	0.05°2θ
Count time	3 sec

A Fourier Transform Infrared Spectroscopy (FTIR) unit was used to characterize the functional groups in powders and ceramics containing HAP. FTIR samples were prepared by freeze drying the powders in the laboratory freeze drier, Freezone 6, produced by Labconco Corporation, USA. The duration of freeze drying was 24 hours. Dried powders were ground and mixed with potassium bromide (KBr) in 1:100 ratio by weight, and then pressed into a pellet form. The infrared analyses of pellets were performed in a Perkin-Elmer "Spectrum One" model FTIR spectrophotometer at a resolution of 4 cm^{-1} over the 4000-450 cm^{-1} spectral region. IR Spectroscopy Version 5.0.1 software was used to collect the data from an average of 50 scans on each sample.

3.2.3.3 Mechanical Characterization

The mechanical properties of selected sintered ceramics were evaluated in terms of three-point bending strength, cold crushing strength,

hardness, and fracture toughness. The details of these tests are described in the following subsections:

3.2.3.3.1. Three Point Bending

Three-point bending tests were carried out at ambient temperature to measure the flexural strength and to determine extent of deformation. The tests were made according to ASTM-C 1161–90 procedures using the size B code [77]. The ceramic samples used in the three point bending test were in the form of rectangular prisms prepared in dimensions required by the size B code. Prior to the application of the test, the sintered ceramic bars were lapped on a polishing machine in order to produce flat and scratch-free surfaces. The rectangular ceramic bars used in three point bending test had the following dimensions:

Length (L_T) = 40 mm, Width (b) = 4.0 mm and Height (d) = 3.0 mm.

The three point bending test was performed in a Shimadzu AGS (Japan) tensile testing machine with 10kN capacity. The breaking load on the sample was applied at a crosshead speed of 0.5 mm per minute. **Figure 3.6** demonstrates the test configuration and sample geometry.

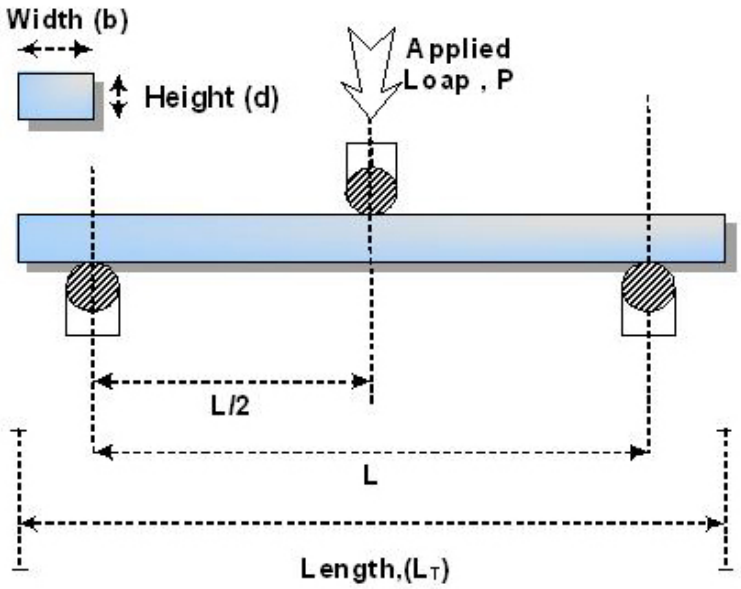

Figure 3.6 Three-Point bending test configuration.

The test yielded the fracture load, P_f, and the maximum deformation at fracture, δ. From these data the bending strength, σ_b, and the Young's modulus, E, were calculated by using following expressions [78]:

Bending strength:

$$\sigma_b = \frac{3P_f\ L}{2bd^2} \qquad \textbf{(3.1)}$$

The value of E could be calculated from the slope (dP/dδ) of the initial linear portion of the load versus deflection curve.

Young's modulus:

$$E = \frac{\sigma}{\varepsilon} \tag{3.2}$$

where

$$\varepsilon = \frac{6\mathrm{d}\delta}{\mathrm{L}^2} \tag{3.3}$$

therefore;

$$E = \frac{\mathrm{L}^3}{4\mathrm{bd}^3}\left(\frac{dP}{d\delta}\right) \tag{3.4}$$

3.2.3.3.2. Cold Crushing Strength

Cold Crushing Strength (CCS) or compressive strength of the sintered ceramics was determined by means of the cold crushing test procedure specified in ASTM Standard C773-88 [79]. The test was carried out in a 60 ton capacity ALŞA machine (Turkey). The ceramic samples used in the test were cylinders 9 mm in diameter and 9 mm in height. The cylinders were subject to compression along their axes by placing them in between the platens of the machine. The cross-head speed was 1 mm per minute. **Figure 3.8** demonstrates the test set-up.

The compressive strength of the ceramic was calculated from the breaking load, P_f, and the original cross sectional area, A_0, of the cylinder sample:

Cold Crushing Strength :

$$CCS = \frac{P_f}{A_o} \tag{3.5}$$

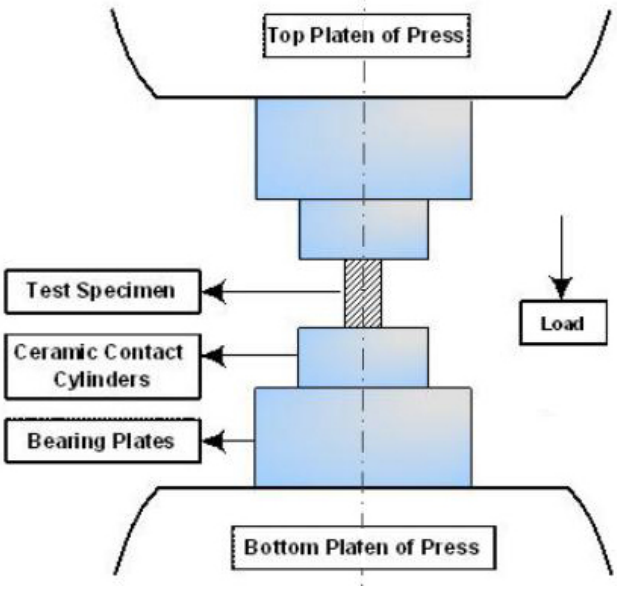

Figure 3.7 Test configuration for the determination of compressive strength.

3.2.3.3.3. Determination of Hardness and Fracture Toughness

a) Hardness

The hardness measurements of the sintered ceramic samples were done by the Vickers indentation method in accordance with ASTM standard C1327-99 [80]. A Hardness Tester (Zwick GmbH & Co., Ulm, Germany) with a square based pyramidal indenter having face angles of 136° was used for indentation. The applied indentation load, P, was 10 kgf; except in case of pure calcium hydroxyapatite ceramic a 2 kgf load was found to be sufficient to develop well-defined cracks. The dwell time was kept at 15 seconds during each indentation.

The ceramic samples used in the hardness measurements were discs with 20 mm in diameter and 5 mm in height. Prior to the test, the flat surfaces of sintered discs were ground on alumina plate to 15 μm and then polished with diamond suspensions of 6 μm, 1 μm and 0.25 μm in order to produce

scratch-free surfaces. Indentations were made on the polished surfaces. The following equation was used for calculating the values of the Vickers hardness from the measured indent diagonal of "2a" [78]:

$$H_V = 463.6(\frac{P}{a^2}) \quad \textbf{(3.6)}$$

Where; Hv: Vickers hardness (GPa), P: applied load (N), and a: half diagonal of the indentation (μm). At least 10 indentations were made on each specimen to obtain reliable data on "a".

b) Fracture Toughness

The fracture toughness (K_{1C}: MPa. $m^{1/2}$) calculations were based on the crack length measurements of the crack pattern produced by Vickers (Hv) indentations. Following equations were used for converting the crack length data to fracture toughness:

$$K_{1C} = (H)^{0,6} \times (E)^{0,4} \times \sqrt{a} \times (10)^{y} \quad \textbf{(3.7)}$$

where,

$$y = -1.59 - (0.34x) - (2.02x^2) + (11.23x^3) - (24.97x^4) + (15.32x^5) \quad \textbf{(3.8)}$$

and

$$x = \log(\frac{c}{a}) \quad \textbf{(3.9)}$$

$$K_{1C} = 0.018 \times \left(\frac{c-a}{a}\right)^{-0.5} \times (\frac{E}{H})^{0.4} \times H \times \sqrt{a} \quad \textbf{(3.10)}$$

Equation (3.7-3.9) was proposed by Evans [81] and Equation (3.10) was suggested by Niihara et al [82].

In the K_{1c} expressions given above c is the distance from the center of the indentation to the extremity of the crack expressed in μm. A traveling microscope attached to the Zwick hardness tester was used for the measurement of "a" and "c" values. The elastic modulus (E) for each specimen group was found from the stress-strain curves obtained from the three point bending tests.

3.2.3.4 Density Measurements

The density of fired ceramics were determined by Archimedes' technique employing xylene (extra pure >99.9%) supplied from Merck as the buoyant liquid. The density of xylene is 0.84 g/cm^3. Sintered pellets were weighed dry, and then immersed in xylene under vacuum for 24 hours until the ceramic was fully saturated with xylene. The suspended weight was measured by hanging a saturated pellet from the balance into a beaker of xylene. Next, the saturated weight was measured by removing the pellet from xylene, lightly wiping it to remove excess liquid from the surface, then quickly transferring it to the balance. The bulk density was calculated using following relation;

$$\rho_b = \frac{W_{dry}}{(W_{sat} - W_{sus})} \rho_{Xylene} \qquad \textbf{(3.11)}$$

where; W_{dry}: Dry weight, W_{sat}: Saturated weight,
W_{sus}: Suspended weight, ρ_b: bulk density.

All weight measurements were made on an analytical balance Sartorius type 2842 (Germany). The overall accuracy in the density measurements was estimated as ± 0.0001 g/cm^3 and hence, the percentage error in the measured density was ± 0.01%.

The extent of densification, expressed as percentage of the theoretical density, %TD, of the sintered ceramic was evaluated by the following relationship:

$$\%TD = \frac{\rho_b}{\rho_{th}} \times 100 \qquad \textbf{(3.12)}$$

where; ρ_{th} was the theoretical density and ρ_b was found by using the expression given above.

CHAPTER IV

EXPERIMENTAL DATA AND RESULTS

The data obtained throughout the experiments are presented in this chapter following the sequence of operations related to the production of apatite-wollastonite ceramics and to the determination of their properties.

4.1. SYNTHESIS OF BIOCERAMIC POWDERS

4.1.1. Calcium Hydroxyapatite Powder

The powders of HAP were produced in accordance with the procedure as described in Chapter III. The quantities of starting materials, $Ca(OH)_2$ and H_3PO_4, were adjusted in such a manner that a molar ratio of Ca÷P=1.667 was maintained in the slurry of the following reaction mixture:

$$\mathbf{10Ca(OH)_2 + 6H_3PO_4 \rightarrow HAP\ precursor + 18H_2O} \qquad \mathbf{(b.1)}$$

The HAP precursor obtained upon drying the reacted mass at 120 °C was subjected to XRD analysis. The pattern shown in **Figure 4.1.a** revealed that the reaction product was partially crystalline and could not yet be identified as HAP. In order to determine the proper treatment temperature for conversion into full HAP, small pellets of the precursor were calcined at temperatures ranging from 700 to 1000°C. The duration for calcination at each peak treatment temperature was fixed as 6 hours. The XRD patterns of the products of calcination at 700 and 800°C showed some unreacted CaO, whereas the product obtained after 1000°C treatment was identified as virtually phase-pure HAP.

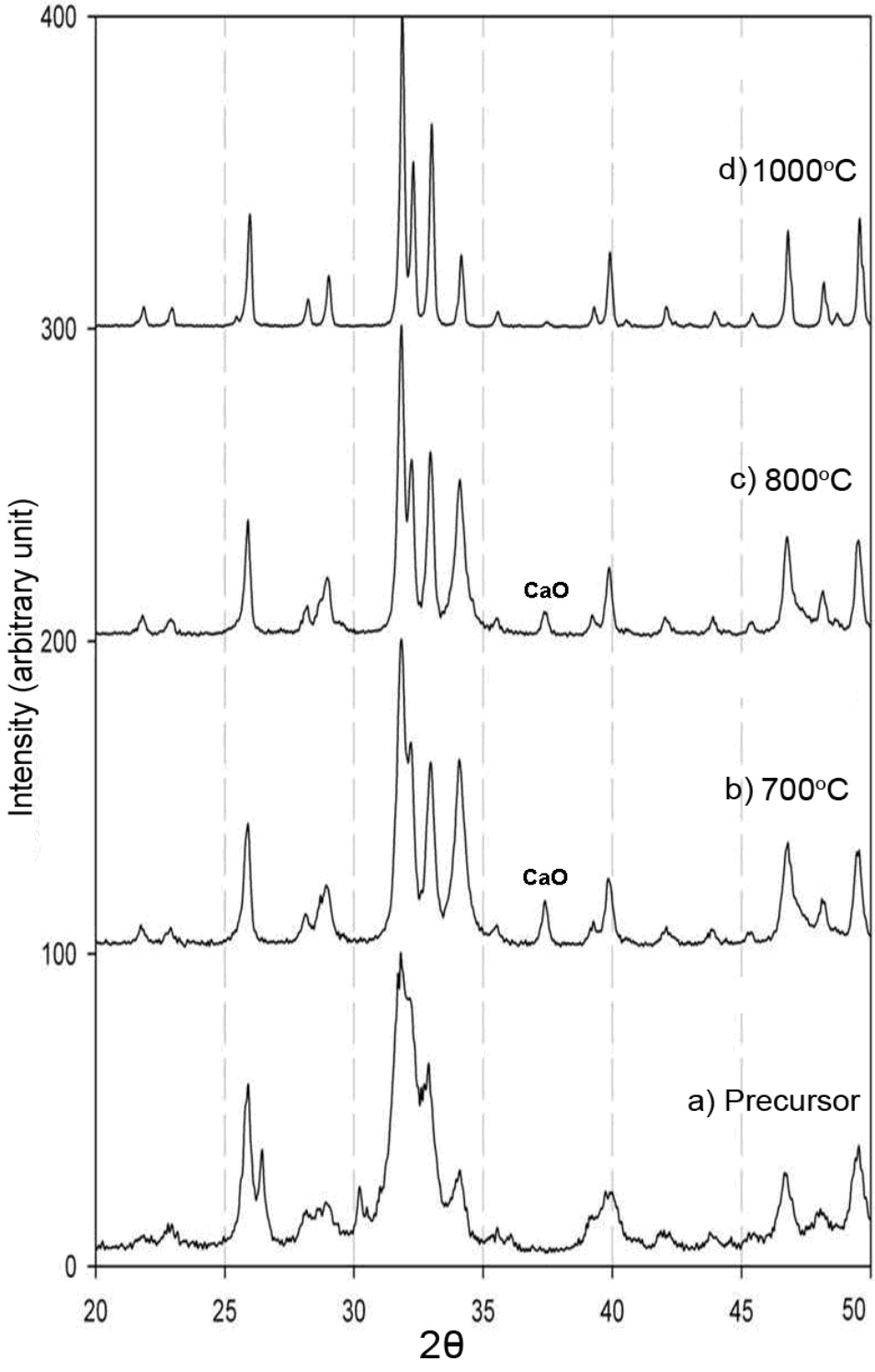

Figure 4.1 Crystallization scheme (XRD patterns) of apatite with respect to calcination temperature. a) As synthesized, b) 700°C calcined (HAP+CaO), c) 800°C calcined (HAP+CaO) and d) 1000°C calcined (HAP).

The XRD pattern of the HAP obtained after calcination confirmed perfectly to the one registered for calcium hydroxyapatite in JCPDS standards, see **Figure 4.1.d** [83]. The ASTM Standard F1185-85 [84] specifies that the surgical quality HAP should contain less than 5 wt% of either CaO or TCP as impurity phase. The HAP obtained in the present study was definitely a quality product acceptable for medical applications.

4.1.2. Wollastonite Powder

The wollastonite powder was produced by the solid state reaction route as described in Chapter III. At the end of the second stage of successive calcinations the product turned fully into $CaSiO_3$ as evidenced by the XRD pattern shown in **Figure 4.2**. The JCPDS file [85] confirmed that the material produced by thermal synthesis was α-wollastonite.

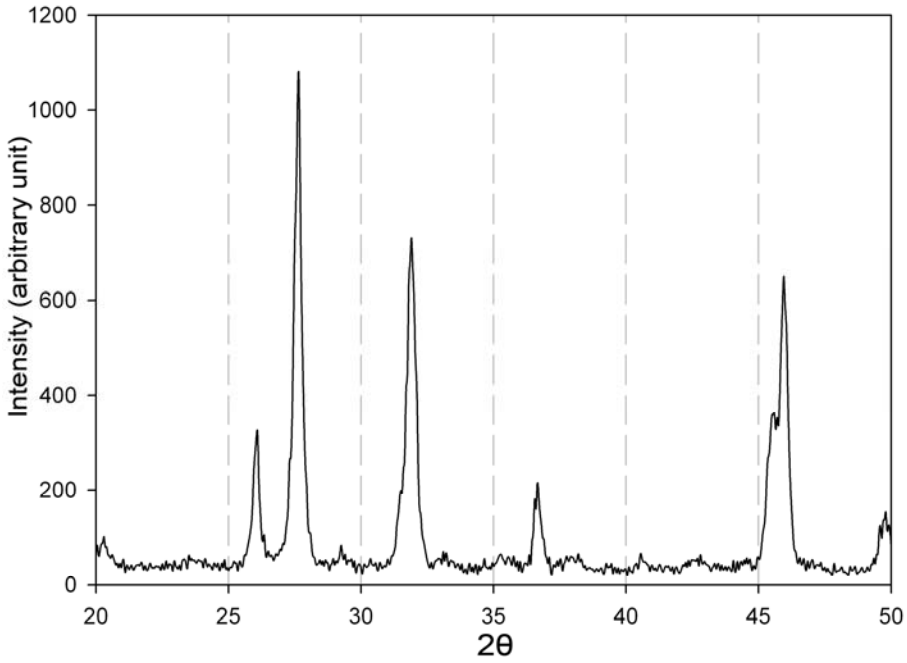

Figure 4.2 XRD pattern of α-Wollastonite

4.1.3. HAP Powders with Silicon Substitution

The powders of silicon-substituted hydroxyapatite or siliconized HAP, abbreviated as Si-HAP hereafter, were produced by the partial chemical route as described in Chapter III. The reactants $Ca(OH)_2$, H_3PO_4, and SiO_2 were mixed in accordance with the following stoichiometry:

$$\mathbf{10Ca(OH)_2 + (6\text{-}x)H_3PO_4 + xSiO_2} \qquad \mathbf{(b.2)}$$

Three types of HAP powders, designated as $Si\text{-}HAP_1$, $Si\text{-}HAP_2$, and $Si\text{-}HAP_3$ were prepared with x values of 1, 1.5 and 2 as shown in **Table 4.1**.

Table 4.1 Compositions of Si-HAP powders.

Powder	**x**	**Moles of $Ca(OH)_2$**	**Moles of $H_3(PO)_4$**	**Moles of SiO_2 fume**
$Si\text{-}HAP_1$	1.0	10	5.0	1.0
$Si\text{-}HAP_2$	1.5	10	4.5	1.5
$Si\text{-}HAP_3$	2.0	10	4.0	2.0

The precursors of Si-HAP, obtained by taking the reaction slurry to dryness, were calcined at 1000 °C for 6 hours in order to convert them fully into crystalline form. The XRD patterns given in **Figure 4.3** verified the formation of apatite structure in all powders with x values lower than 2. The XRD pattern of pure HAP is included in the diagram in order to compare the major peaks of Si-HAP with those of pure HAP.

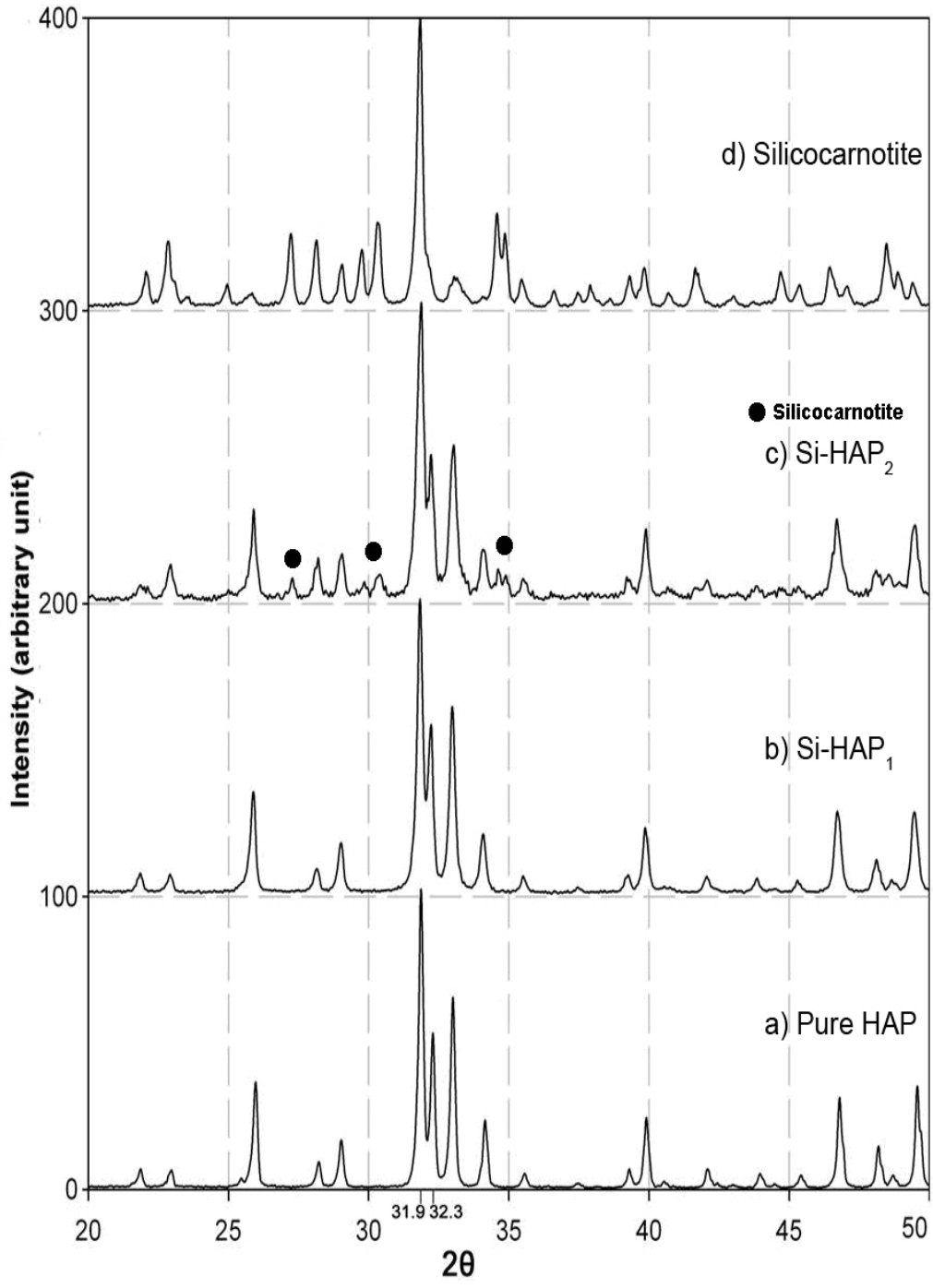

Figure 4.3 XRD patterns of (a) Pure HAP, (b) Si-HAP_1, (c) Si-HAP_2, and (d) Si-HAP_3: silicocarnotite.

The XRD pattern of Si-HAP_1 was identical to that of pure HAP, which meant that the crystal structure of HAP was retained at the substitution level of x=1. When x was raised to 1.5 silicocarnotite mineral started to appear as a second phase. This could be attributed to local compositional fluctuations. The diffraction pattern of the material contained the same features that Kim et al [86] observed in their recent work on the synthesis of silicon substituted hydroxyapatites. The latter used liquid tetraethyl orthosilicate as the source of silicon, despite the favorable mixing conditions at atomic level some silicocarnotite was also produced in their Si-HAP with x=1.5.

At the substitution level of x=2, the HAP was destroyed completely as observed from the XRD pattern. This was expected, because at this stage all hydroxyls of HAP were removed and the material turned into the compound $Ca_{10}(PO_4)_4(SiO_4)_2$, known as the silicocarnotite mineral [87].

The changes that occur in the bond structure of HAP due to silicon substitution were examined by FTIR spectroscopy. This was considered necessary because no major differences between the XRD patterns of pure HAP and the siliconized versions could be detected that would substantiate the formation of Si-HAP. **Figure 4.4** is a replicate of the FTIR spectra obtained for HAP and Si-HAP_1.

The spectra exhibited the features reported in the literature [86, 88-91] characteristic to HAP and Si-HAP. The peaks at the characteristic bands around ν=3570 cm^{-1} and ν=631.8 cm^{-1} represented the stretching and vibrational frequencies owing to the presence of hydroxyl bonds. It was evident that in going from HAP to Si-HAP there was a definite reduction in the intensity of the peak at ν=631.8 cm^{-1}. This showed that the charge deficiency created by introduction of silicon into HAP was compensated by a

decrease in the amount of hydroxylation in the framework. Furthermore, the additional peaks detected in Si-HAP_1 at $\nu \approx 890$ cm^{-1} and $\nu \approx 752$ cm^{-1} could be assigned to the $(SiO_4)^{4-}$ group [90]. These peaks strengthened the evidence of silicon substitution in the HAP structure. The peaks around $\nu = 1089$ cm^{-1}, $\nu = 1047$ cm^{-1}, $\nu = 961$ cm^{-1}, $\nu = 570$ cm^{-1}, and $\nu = 603$ cm^{-1} were characteristic phosphate bands [90, 91]. As expected, the intensities of these peaks were reduced in Si-HAP_1 due to the replacement of $(PO_4)^{3-}$ tetrahedra by $(SiO_4)^{4-}$ in the HAP structure.

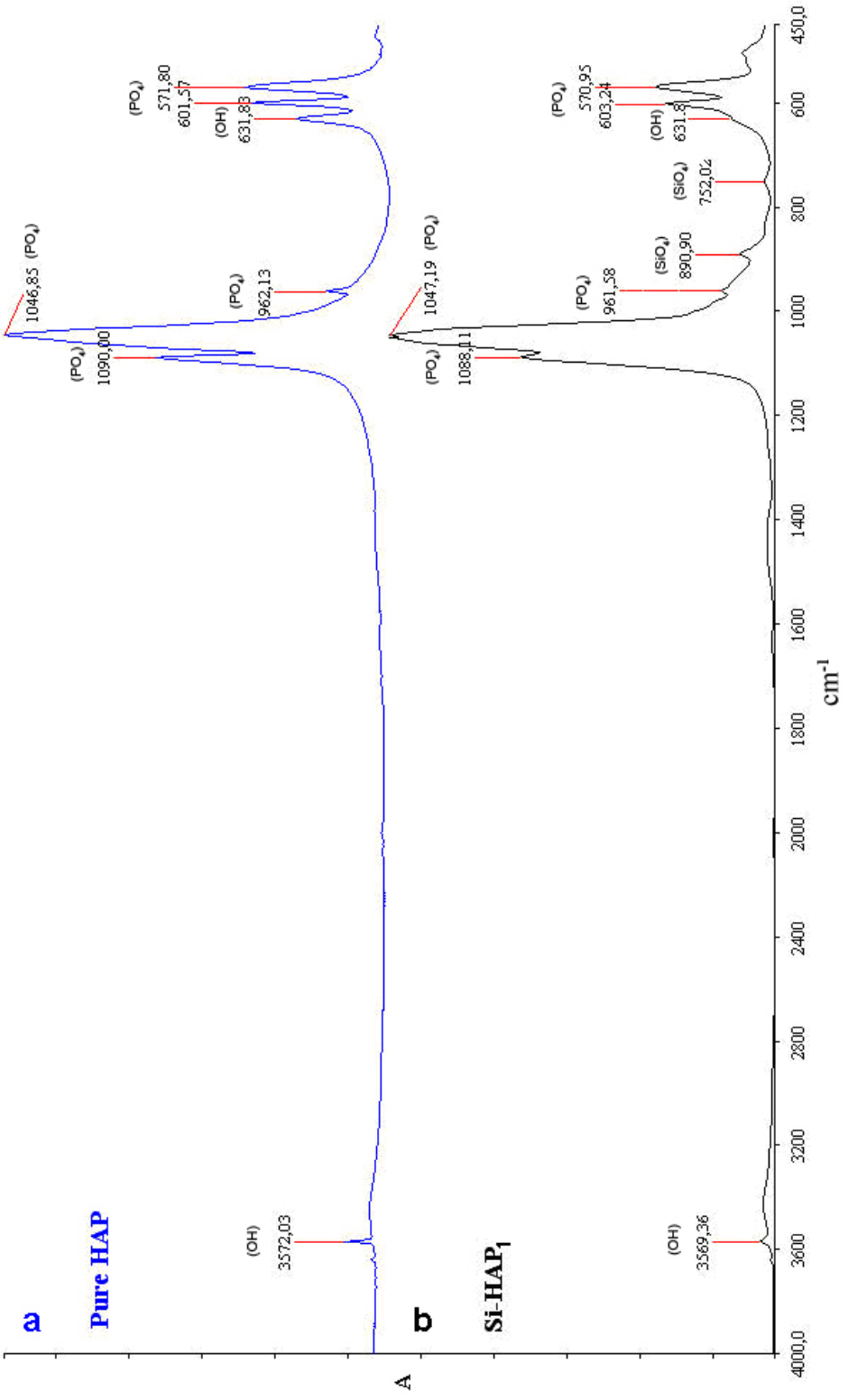

Figure 4.4 FTIR spectra for (a) Pure HAP and (b) Si-HAP$_1$.

4.2. PRODUCTION OF CERAMICS

During the past two decades liquid phase sintering techniques have been developed for SiC and Si_3N_4 based ceramics which allowed to obtain materials with a distinct bimodal grain size distribution composed of large elongated grains embedded in a fine grained matrix [92-95]. This type of microstructure was found to be the key to the production of self-reinforced ceramics with enhanced strength and improved toughness.

4.2.1. Microstructure Development

The central objective of the sintering studies conducted during this thesis study was to come up with a liquid phase sintering process leading to a ceramic with a bimodal microstructural assembly in which rod-like grains would be distributed homogeneously and be bonded to equiaxed micro grains by the help of a properly selected fluxing agent. The results of the sintering experiments conducted with different kinds of fluxing agents are provided in the following subsections.

4.2.1.1. Sintering with the MCAS Flux

The samples for sintering were prepared by mixing the powdered MCAS flux with HAP, wollastonite or both in the proportions as shown in **Table 4.2**. The tablets pressed from these mixtures were fired at 1200 °C for 4 hours.

Table 4.2 Compositions of the ceramics prepared from HAP and wollastonite powders with MCAS flux addition.

Sample Number	HAP (wt%)	Wollastonite (wt%)	$MCAS_{flux}$ (wt%)
1	100	-	-
2	90	-	10
3	80	-	20
4	-	100	-
5	-	90	10
6	-	80	20
7	50	50	-
8	45	45	10
9	40	40	20

Hereafter, the samples which have gone through the microstructural examinations will be identified as the sample number given in **Table 4.2**.

4.2.1.1.1. HAP + MCAS Ceramics

The microstructure of the sintered tablet made from pure HAP, sample 1 is seen in **Figure 4.5**. The micrograph was taken from a freshly broken surface. Apparently, the tablet acquired a high degree of densification; all open pores were eliminated and the closed pores were limited in number.

Sample 2 and Sample 3 were HAP tablets sintered in the presence of increasing amounts of MCAS. The presence of MCAS in these samples deteriorated the microstructure as seen in **Figure 4.6**. The coherency observed in the sintered pure HAP ceramic was lost; the structure consisted of discrete apatite grains separated with plate-like inserts. These platelets might have

been the remnant of a liquid phase which probably existed temporarily before turning into solid.

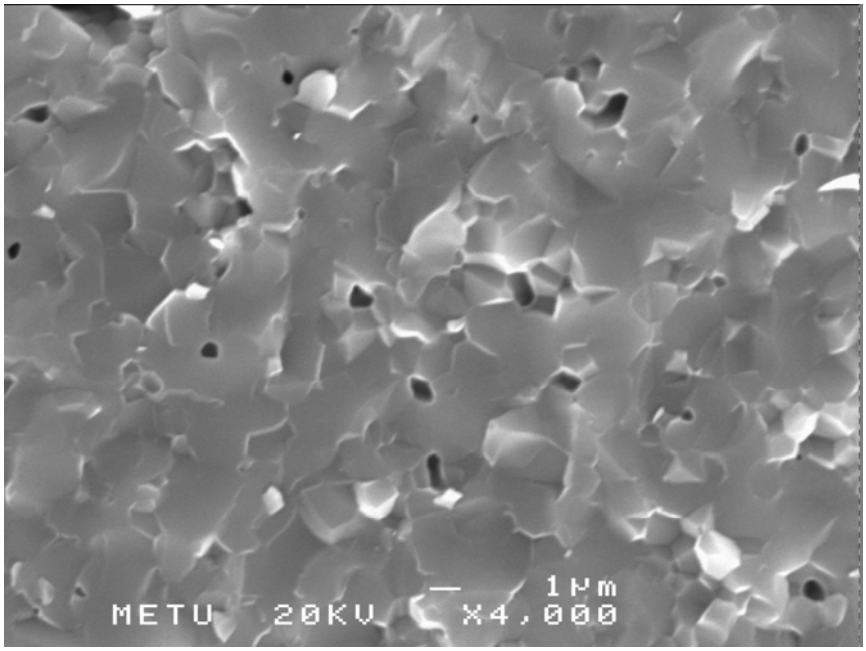

Figure 4.5 SEM micrograph taken from the fracture surface of phase pure HAP tablet sintered at 1200 °C for 4 hours.

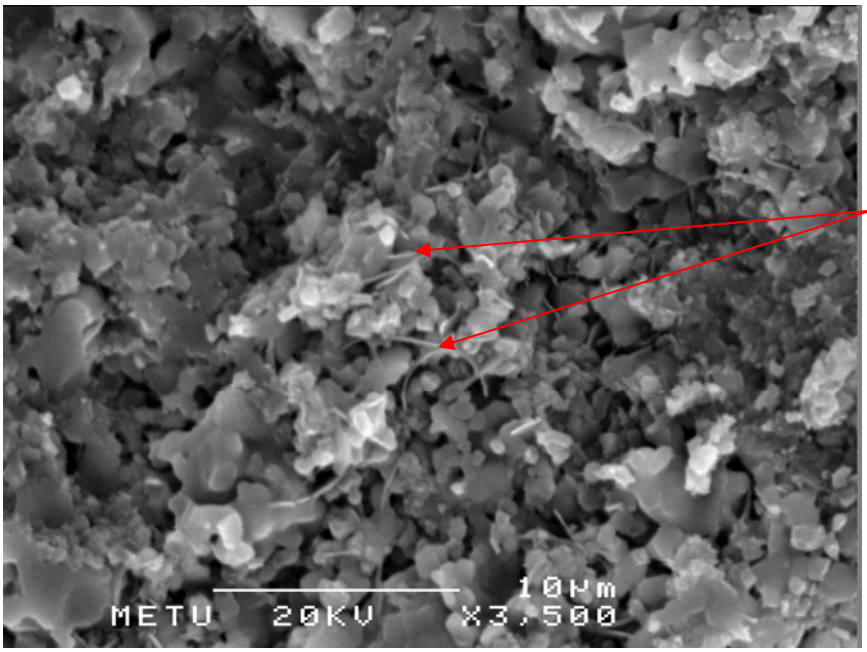

Figure 4.6 SEM micrograph taken from the fracture surface of the sample with 90 wt% HAP + 10 wt% MCAS.

The reason why the platelets appear as discrete occurrences in the microstructure may be due the improper wetting. The platelets seen in the micrograph of **Figure 4.6** were analyzed with EDS and shown in **Figure 4.7**. The EDS spectrum revealed that the major constituents in the platelets were CaO and P_2O_5 with MgO, SiO_2, and Al_2O_3 entering as minor constituents. This would indicate that part of the HAP reacted with MCAS to form a transient liquid. The liquid dissolved some HAP in it but did not have any contribution to the liquid phase sintering process, due perhaps to the fact that it lacked proper wetting conditions.

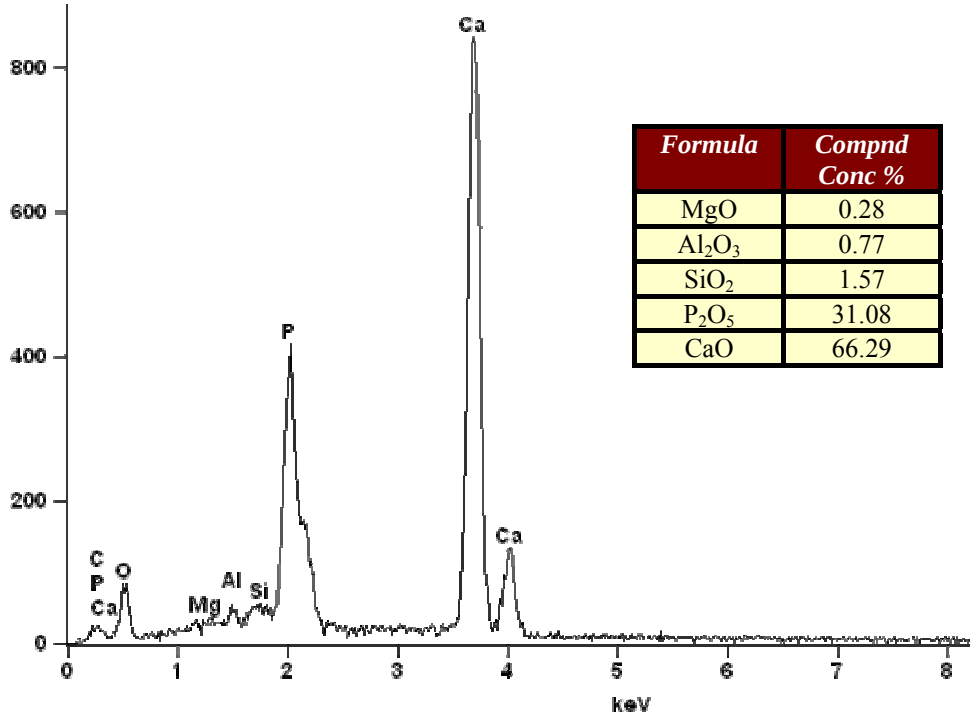

Formula	*Compnd Conc %*
MgO	0.28
Al_2O_3	0.77
SiO_2	1.57
P_2O_5	31.08
CaO	66.29

Figure 4.7 The EDS spectrum for the platelets in the microstructure of the ceramic 90 wt% HAP + 10 wt% MCAS.

Sample 3 was sintered with double the quantity of MCAS contained in Sample 1. The increase in the flux content did not improve the sinterability of the HAP + MCAS assembly. In addition there was no alteration in the morphology of HAP grains as shown in **Figure 4.8**.

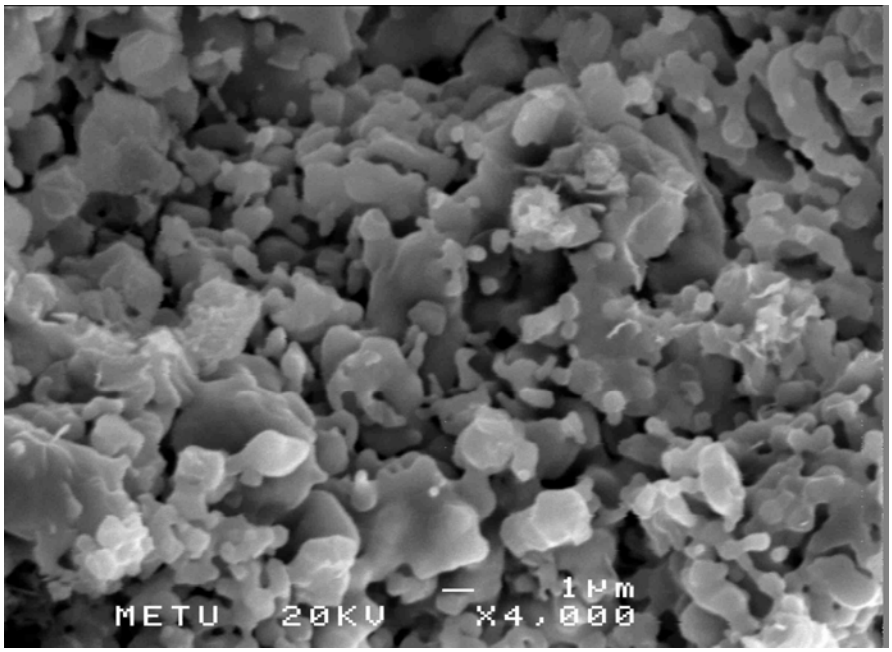

Figure 4.8 SEM micrograph of the sample containing 80 wt% HAP + 20 wt% MCAS.

4.2.1.1.2. Wollastonite + MCAS Ceramics

By reference to the phase diagram of the system MgO-CaO-SiO_2-Al_2O_3 shown in **Figure 3.3** the stability area of the wollastonite phase deserved some attention. The diagram shows that when α-wollastonite is equilibrated with liquid MCAS it has the potential of transforming into β modification. The same effect might also be attained in solid state when the system could be reacted under favorable kinetic conditions.

β-wollastonite is known to crystallize in fiber morphology [97, 98]. Therefore, sintering of wollastonite in the presence of MCAS flux was of interest not only for examining the effects of MCAS on the sintering process but also for evaluation of fiber formation possibility.

Sample 4 was pure α-wollastonite. The resulting microstructure of this ceramic is shown in **Figure 4.9**. The ceramic contained considerable amount of porosity. When MCAS flux was added into wollastonite, there was no substantial change in densification, as could be seen in **Figure 4.10** and **Figure 4.11**. MCAS flux was not instrumental in changing the morphology of the wollastonite either. In fact, when a comparison was made, the porosity in Sample 6 was even higher than that of the samples contained lower MCAS.

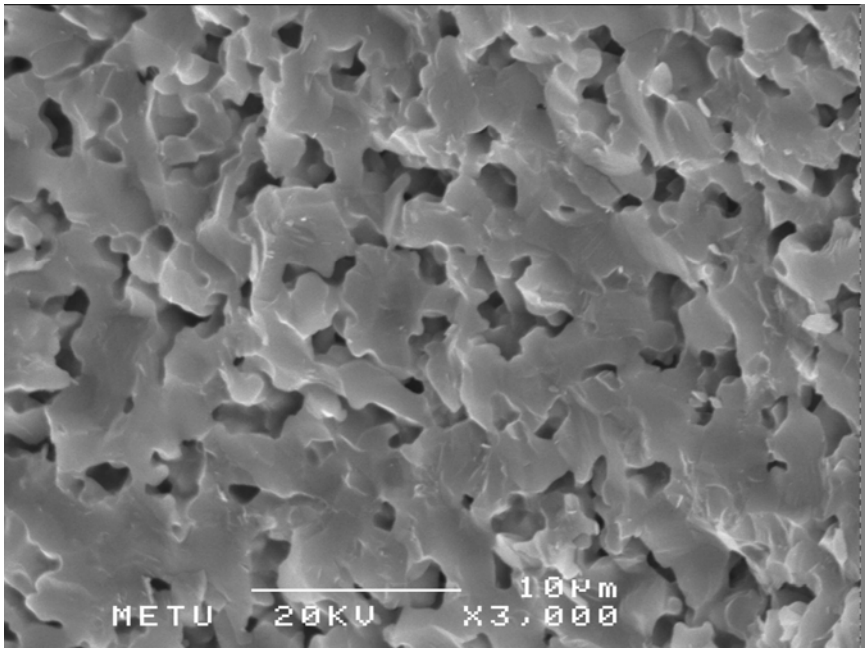

Figure 4.9 SEM micrograph of the phase pure α-wollastonite ceramic.

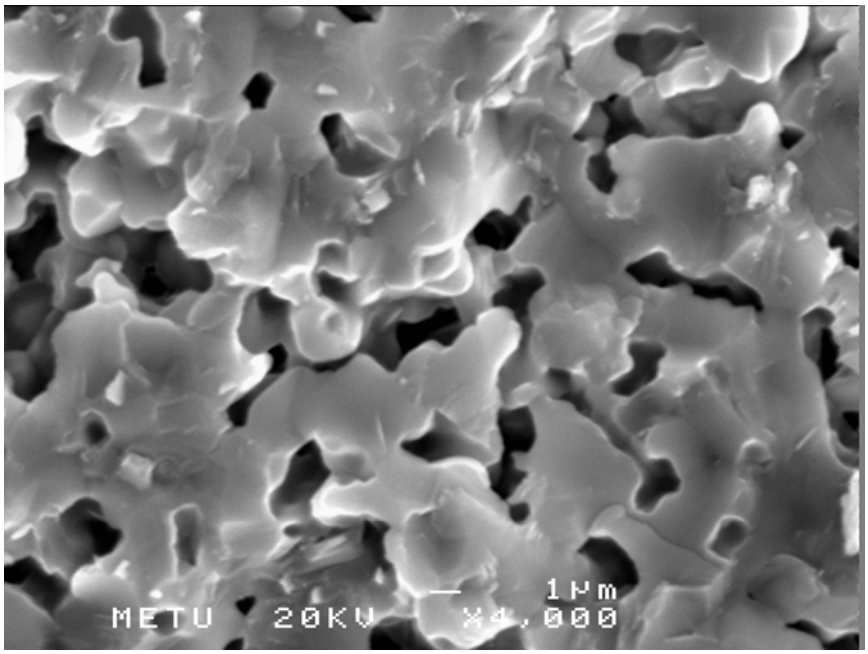

Figure 4.10 SEM micrograph of the sample containing 90 wt% Wollastonite + 10 wt% MCAS.

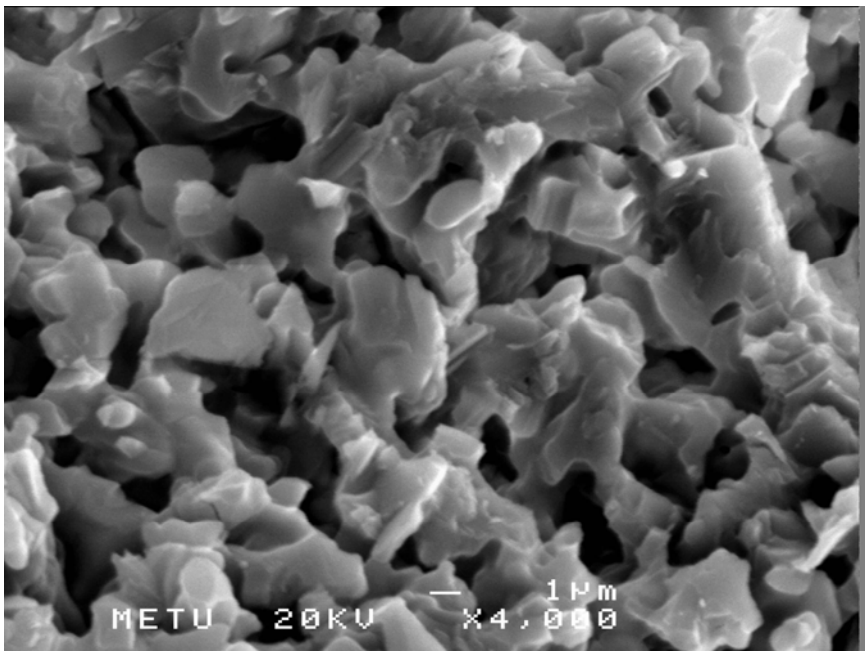

Figure 4.11 SEM micrograph of the sample containing 80 wt% Wollastonite + 20 wt% MCAS.

4.2.1.1.3. HAP + Wollastonite + MCAS Ceramics

The last three samples in **Table 4.2** were ceramics produced from mixtures of HAP and wollastonite. These were sintered with the aim of examining if any synergic effect could be obtained from the combination of three components. **Figure 4.12** shows the microstructure of the sample containing equal parts by weight of HAP and wollastonite.

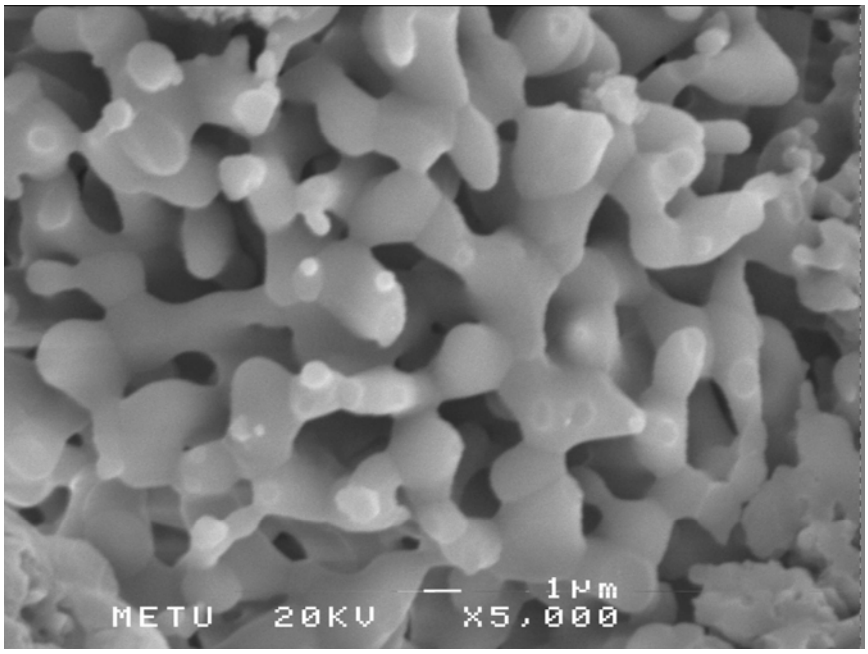

Figure 4.12 SEM micrograph of the sample containing
50 wt% HAP + 50 wt% Wollastonite

Well-developed necks were formed between dissimilar grains. The material had a spongy outlook with uniform distribution of porosity connected through micropore channels.

The second and third ceramics in this group were made by sintering tablets which contained 10 and 20 wt% MCAS, respectively, in mixtures with equal parts of HAP and wollastonite. The microstructures shown in **Figure 4.13** and **Figure 4.14** revealed enhanced densification as compared to the ceramic without flux, but the grains preserved their equiaxed morphology.

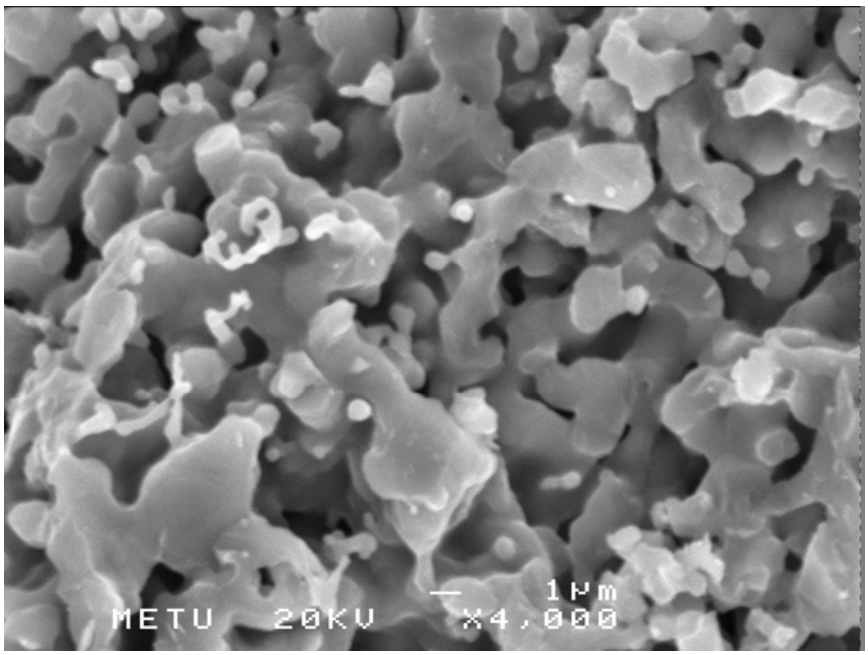

Figure 4.13 SEM micrograph of the sample containing 45 wt% HAP + 45 wt% W and 10 wt% MCAS.

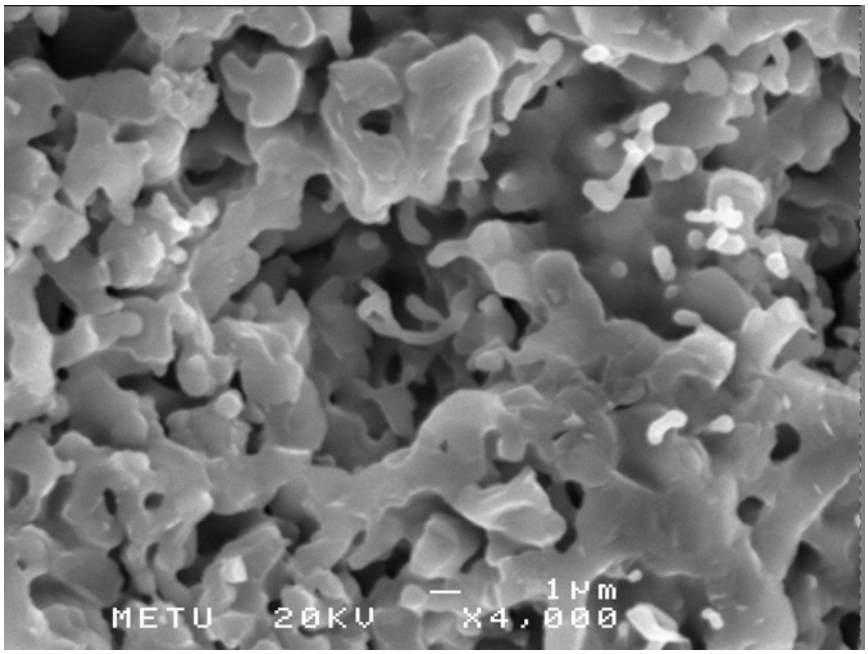

Figure 4.14 SEM micrograph of the sample containing 40 wt% HAP + 40 wt% W and 20 wt% MCAS.

4.2.1.2. Sintering with Sodium Feldspar

Sintering studies on samples that contained MCAS flux revealed that the flux was inadequate in achieving the goals of the thesis study. Therefore, attention was turned into a feldspatic type fluxing agent. The new candidate was sodium feldspar which finds widespread use in glass-making. A limited number of sintering experiments were conducted by incorporating small quantities of feldspar into HAP + Wollastonite composites having compositions specified in **Table 4.3**.

Table 4.3 Compositions of the ceramics prepared from HAP and wollastonite powders with feldspar addition.

Sample Number	HAP (wt%)	Wollastonite (wt%)	Na-Feldspar (wt%)
10	49	49	2
11	47.5	47.5	5

The microstructure of the ceramic which contained 2 wt% of feldspar is shown in **Figure 4.15**. The flux had a wholesome effect on densification. Despite this positive effect, however, there seemed to be a tendency of flux segregation leading to heterogeneities in the distribution of porosity throughout the bulk of the ceramic. This could be due to the high surface tension of the liquid phase which might have inhibited uniform spreading of the flux throughout the entire cross section.

Increasing the flux content in the ceramic from 2 wt% to 5 wt%, caused a very high degree of densification as could be seen in **Figure 4.16**. The sintered material displayed a choncoidal fracture. In addition, when the microstructure was examined carefully, especially through the holes like the one displayed on the micrograph, the first glimpses of the morphological changes became visible.

The EDS scan over the rod-like solids in the microstructure revealed that these were essentially HAP containing structures. On account of this, hereafter attention on sintering studies was turned to the transformation of granular HAP grains into rod-like grains.

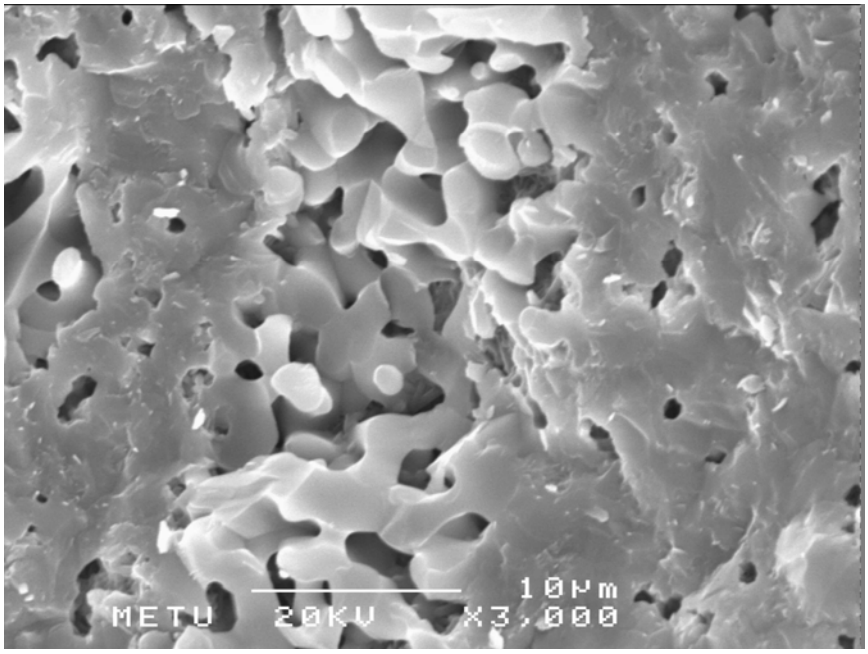

Figure 4.15 SEM micrograph of the sample containing 49 wt% HAP + 49 wt% W and 2 wt% sodium feldspar.

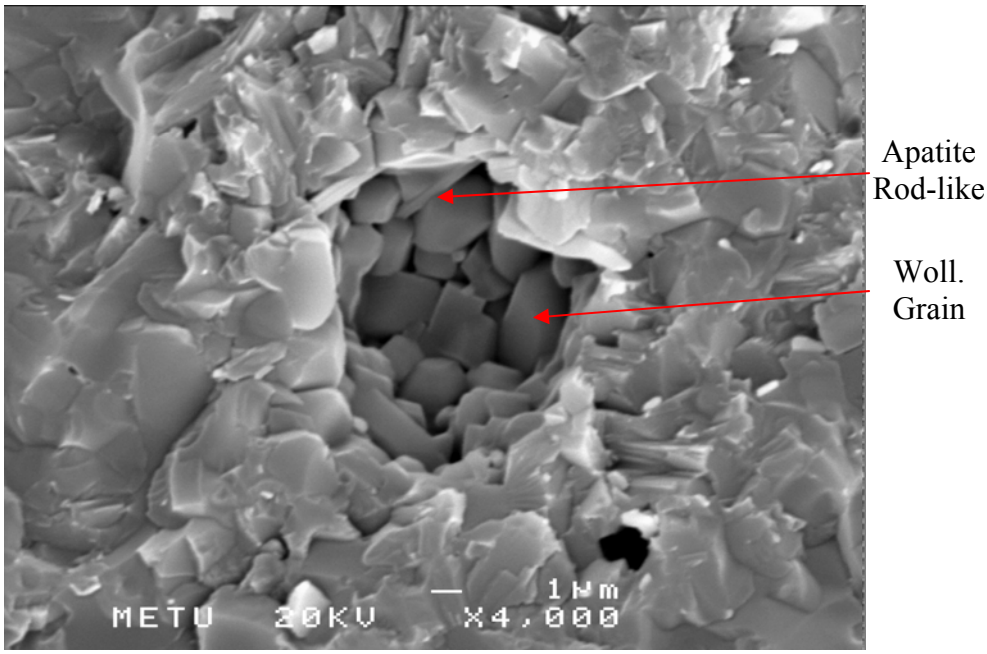

Figure 4.16 SEM micrograph of the sample containing 47.5 wt% HAP + 47.5 wt% W and 5 wt% sodium feldspar.

Despite all positive points outlined above, the amount of sodium feldspar that could be admitted into HAP + Wollastonite composites was rather limited. Even at 5 wt% feldspar level, a high amount of glassy phase was developed which seeped to the bottom of the sintering ceramic sticking it to the platinum substrate used as the container. Hence, a frit produced in Na_2O-CaO-Al_2O_3-SiO_2 system was used instead of sodium feldspar for the following sintering studies.

4.2.1.3. Sintering with the NCAS Frit

The third flux used as a sintering additive was the NCAS frit. Its choice was inspired by the high bioactivity exhibited by Bioverit® belonging to the Na_2O-CaO-Al_2O_3-SiO_2 glass-ceramic system. The frit was more reactive than the MCAS flux due to its Na_2O component and had a lower melting temperature so that a liquid phase could be developed rather easily at the sintering temperature of the present study.

Compositions of the ceramics prepared by sintering HAP and/or wollastonite in the presence of the NCAS frit are tabulated in **Table 4.4**.

Table 4.4 Compositions of the ceramics prepared from HAP and Wollastonite powders with NCAS frit addition.

Sample Number	HAP (wt%)	Wollastonite (wt%)	$NCAS_{frit}$ (wt%)
12	90	-	10
13	-	90	10
14	47.7	47.5	5
15	45	45	10
16	42.5	42.5	15

4.2.1.3.1. HAP + NCAS Ceramics

The SEM micrograph of HAP ceramic sintered with the addition of 10 wt% NCAS frit is shown in **Figure 4.17**. The frit melted during firing of the ceramic, disrupting the sintered microstructure considerably. The formation of some platelets could be observed, but a massive transformation of HAP from granular to rod-like morphology was still absent.

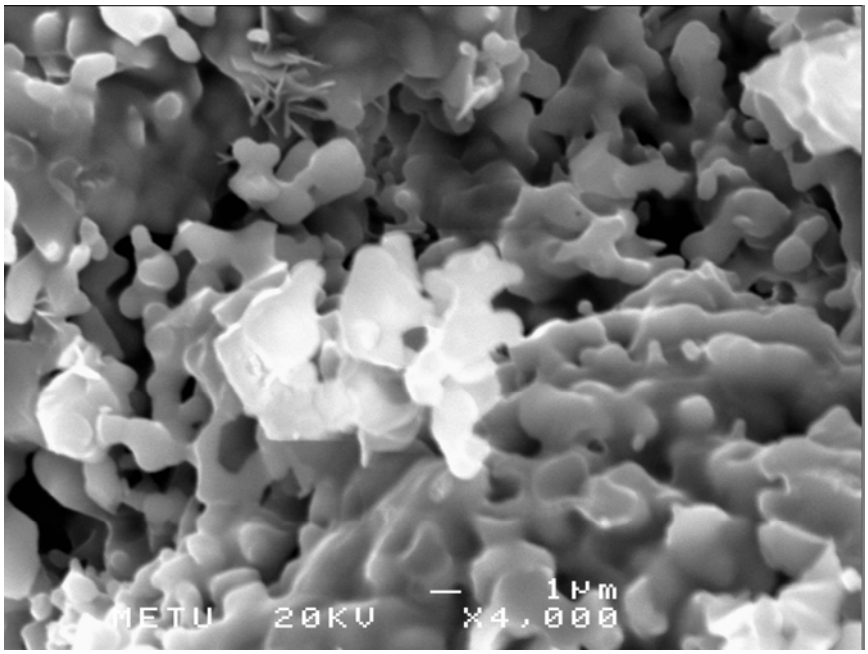

Figure 4.17 SEM micrograph of HAP ceramic sintered in the presence of 10 wt% NCAS frit.

4.2.1.3.2. Wollastonite + NCAS Ceramics

Addition of 10 wt% NCAS frit to wollastonite produced a high amount of liquid phase as seen in **Figure 4.18**. The proportion of the liquid probably induced a viscous sintering mechanism. In the enlarged view of SEM

micrograph, shown in **Figure 4.19**, the liquid seems to fill the entire intergranular space. The EDS scan over the liquid phase, displayed in **Figure 4.20**, revealed that during sintering, the grains of wollastonite dissolved partially in the molten frit. Apparently, however, the liquid phase was away from its limit of saturation. The conditions present in the sintering environment did not produce any change in the morphology of wollastonite grains.

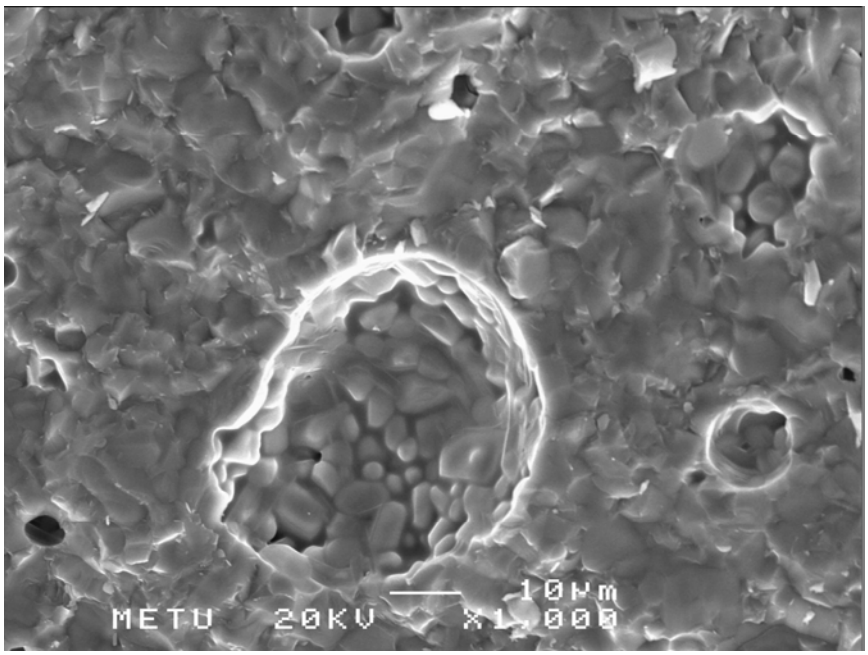

Figure 4.18 SEM micrograph of the wollastonite ceramic sintered in the presence of 10 wt% NCAS frit.

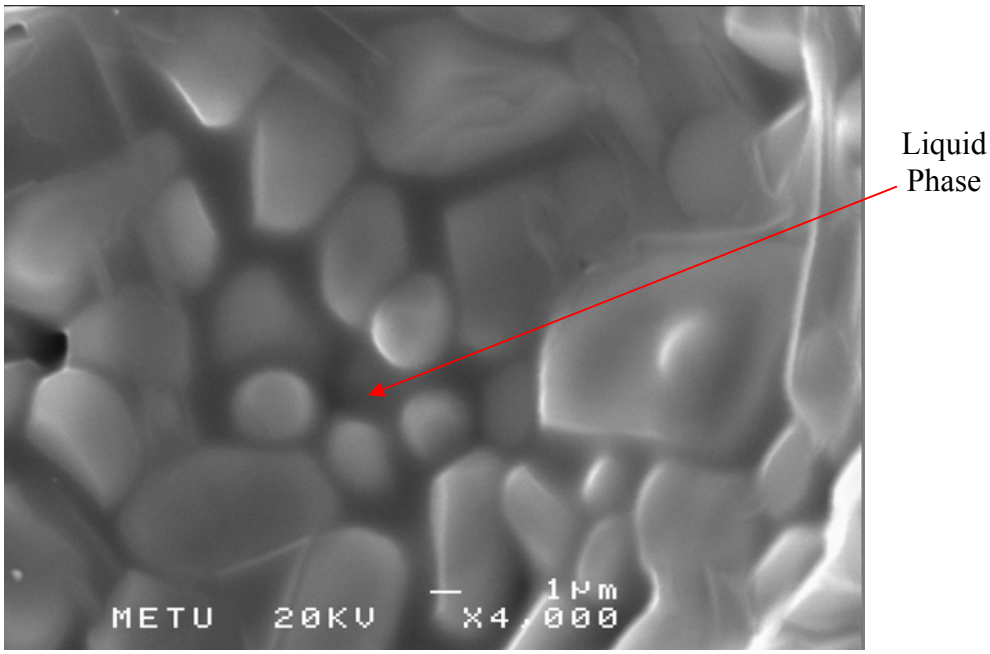

Figure 4.19 Enlarged view of the microstructure of the ceramic with 90 wt% wollastonite + 10 wt% NCAS frit, showing the presence of excessive liquid.

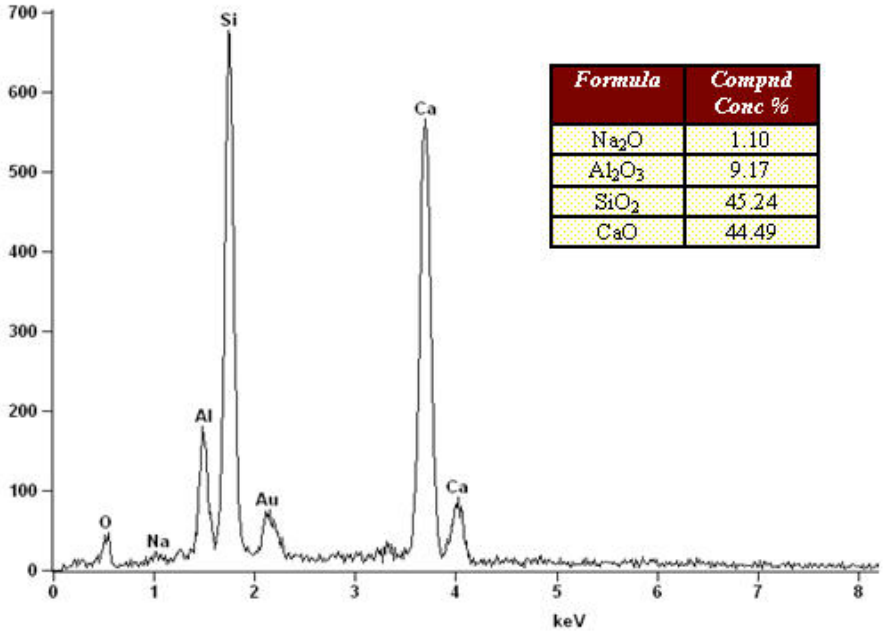

Figure 4.20 The EDS scan taken over the liquid phase in the wollastonite ceramic sintered in the presence of 10 wt% NCAS frit.

4.2.1.3.3 HAP + Wollastonite + NCAS Ceramics

The last three samples in **Table 4.4** represented ceramics produced by sintering mixtures of HAP and wollastonite with NCAS frit. In all these samples HAP and wollastonite were introduced in equivalent proportions by weight while the quantity of the NCAS frit was raised in a stepwise manner.

The SEM micrograph of the ceramic sintered with 5 wt% of NCAS frit addition is seen in **Figure 4.21**. The formation of a bimodal microstructure composed of equiaxed grains and elongated rods could be viewed easily. For the first time, in all samples studied until this point, the fibrous rod-like grains were formed unambiguously in the structure.

The EDS scan over the areas populated with rod-like solids in the microstructure revealed that these were essentially HAP containing perhaps with some silicon as seen in **Figure 4.22**.

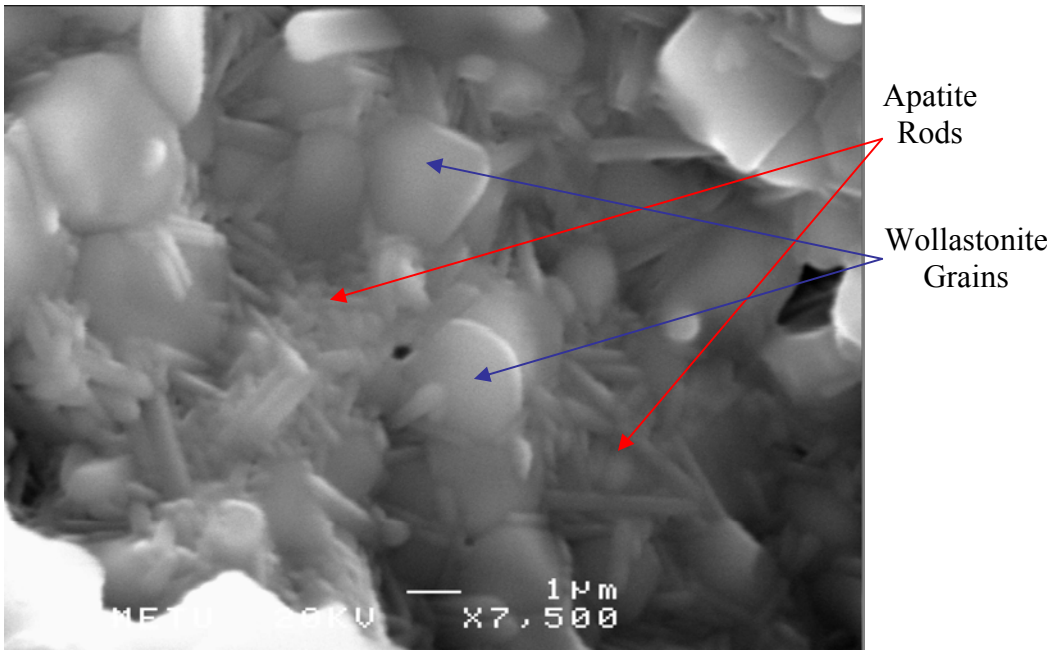

Figure 4.21 The formation of the bimodal microstructure containing equiaxed grains of wollastonite and rod-like grains of apatite.

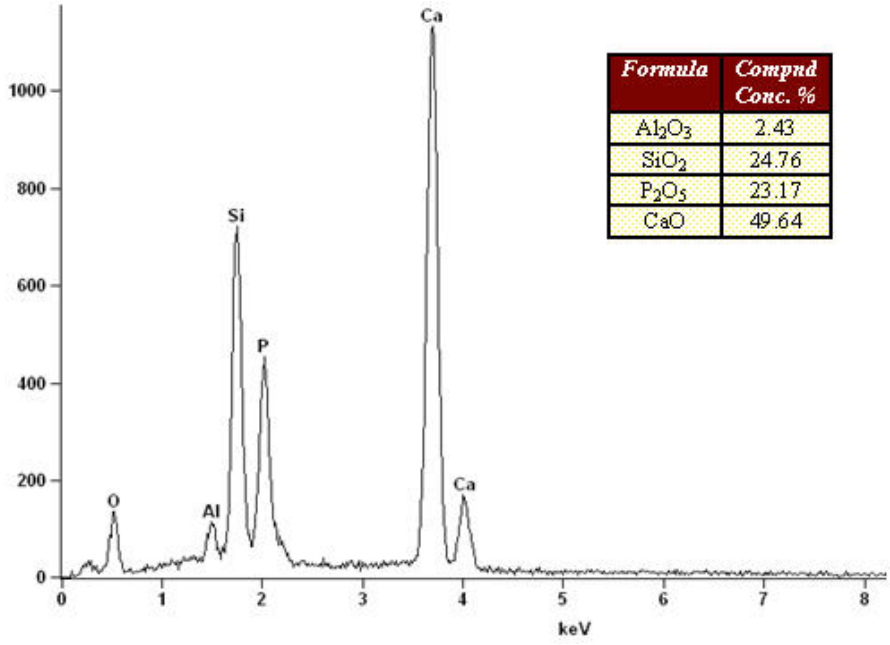

Figure 4.22 EDS scan taken over the rod-like grains in the microstructure of HAP + wollastonite ceramic sintered with 5 wt% NCAS frit.

The Si peak in the EDS of apatite rods was perhaps too intense due to interaction of the analyzing beam with neighboring wollastonite grains. The EDS scan taken over the equiaxed grains, given in **Figure 4.23**, showed that these were in essence wollastonite, contamination with phosphorus was probably a physical one rather than chemical, it could come from the neighboring apatite rods.

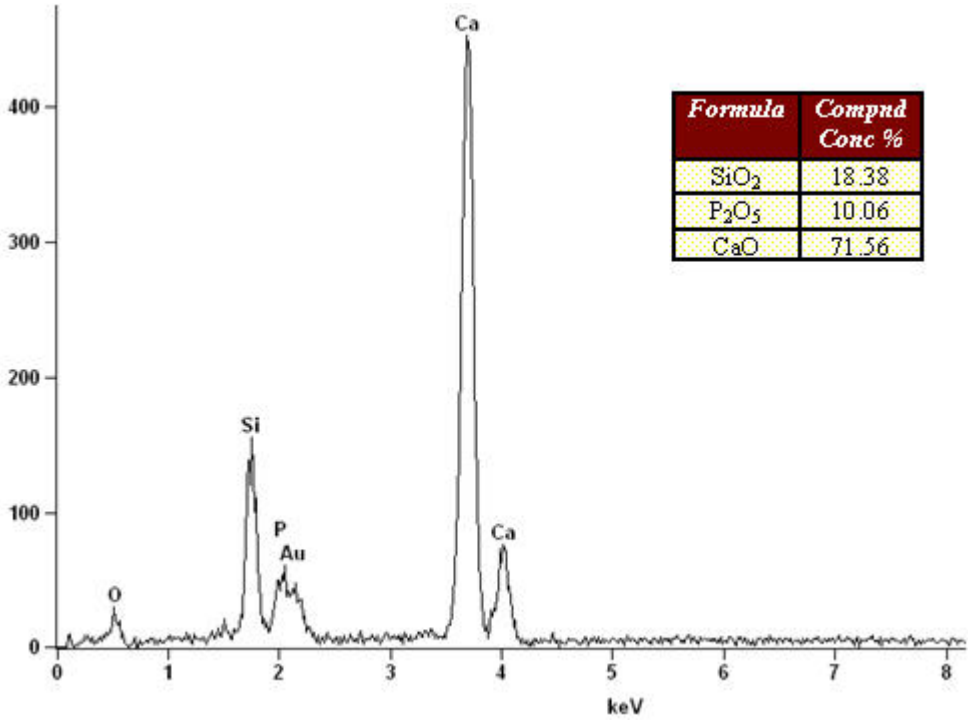

Figure 4.23 EDS scan taken over equiaxed grains in the microstructure of HAP + wollastonite ceramic sintered with 5 wt% NCAS frit.

In order to identify the solid phases present in the ceramic the powder XRD pattern, shown in **Figure 4.24**, was produced. The indexing of this pattern revealed that the major solid phases were HAP and wollastonite. There was a small amount of silicocarnotite phase as well. The peaks of HAP were somehow distorted, the distortion implied that HAP was not pure but a

modified version was formed. This indicated that the sintering process was a reactive one so that some of the (PO_4) in pure HAP was substituted with (SiO_4) through the aid of the NCAS frit.

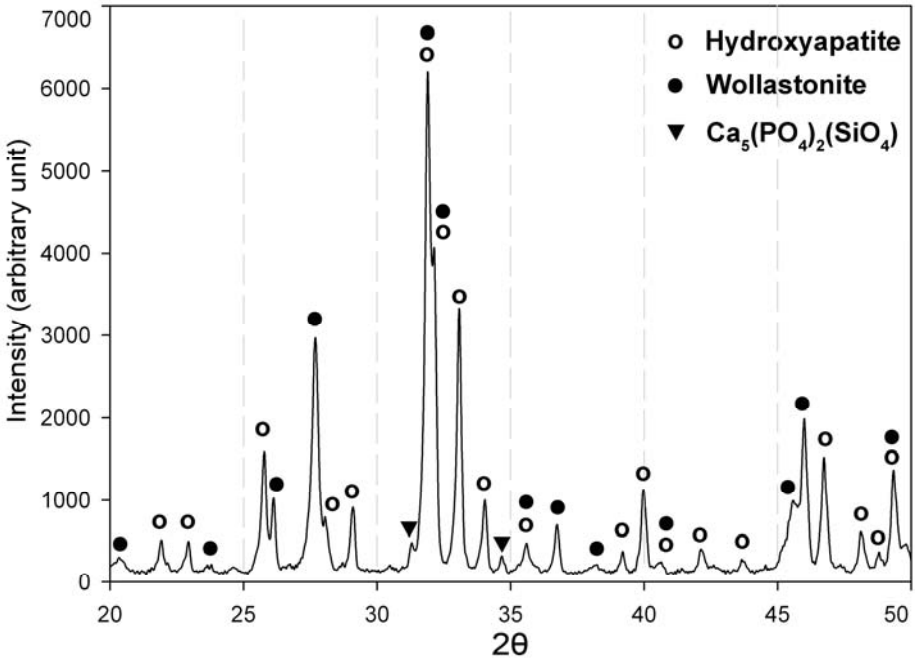

Figure 4.24 The powder XRD pattern of the HAP + wollastonite ceramic sintered with 5 wt% NCAS frit.

When the amount of NCAS frit was raised to 10 wt% level the rod-like HAP grains grew bigger in size with substantial increase in their aspect ratio. The micrograph shown in **Figure 4.25** proved that the NCAS frit had served as a suitable medium for ion-exchange reactions between the constituents of the ceramic.

The XRD pattern of this ceramic, displayed in **Figure 4.26**, had the same features observed in the XRD of the ceramic with 5 wt% NCAS frit, except that some peaks of the hydroxyapatite phase were depressed

considerably and the silicocarnotite phase became more pronounced. These changes indicated that the reactions during sintering became intense. In relation to the microstructure of the ceramic, it could be inferred that the liquid phase dissolved some HAP until it became saturated with respect to calcium and phosphorus and then reprecipitated the apatite of a modified chemical composition which led to the formation of rod-like elongated grains.

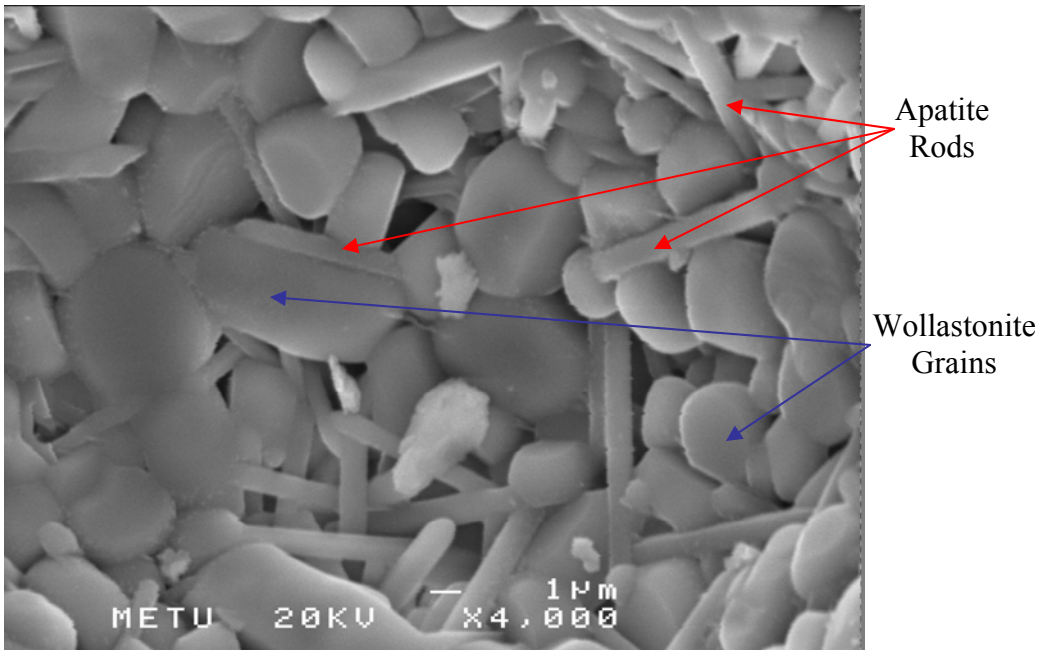

Figure 4.25 SEM micrograph of the sample containing 45 wt% HAP + 45 wt% W + 10 wt% NCAS frit.

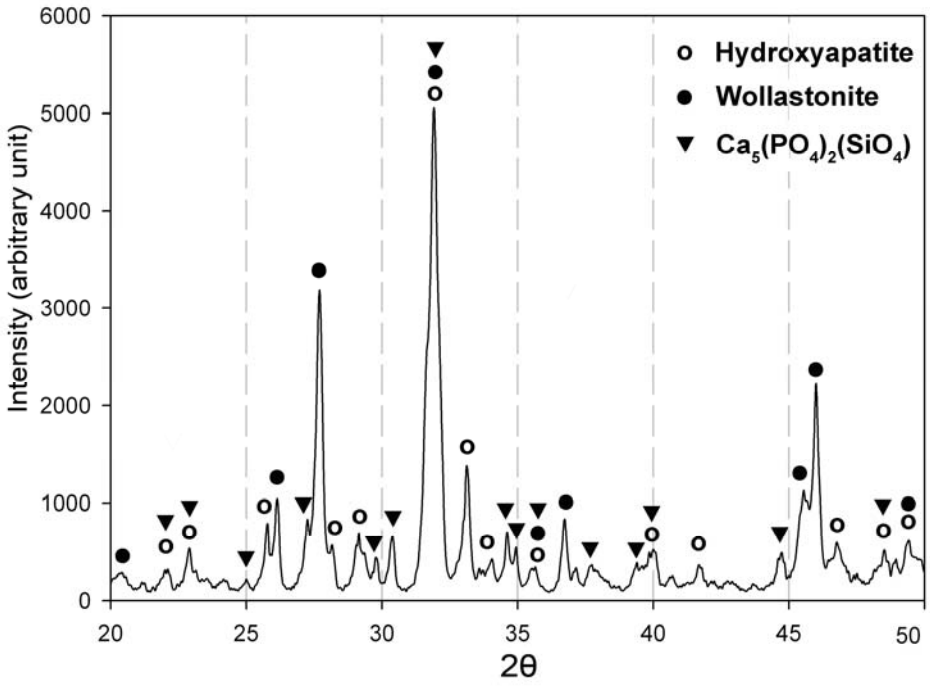

Figure 4.26 The XRD pattern of the HAP + wollastonite ceramic sintered with 10 wt% NCAS frit.

The EDS scan taken over the apatite rods revealed that the apatite phase contained considerable amount of silicon, as seen from the EDS spectra in **Figure 4.27**. The chemical composition of the apatite could be approximated by the molecular formula $Ca_{10}(PO_4)_{5.2}(SiO_4)_{0.8}(OH)_{1.2}$.

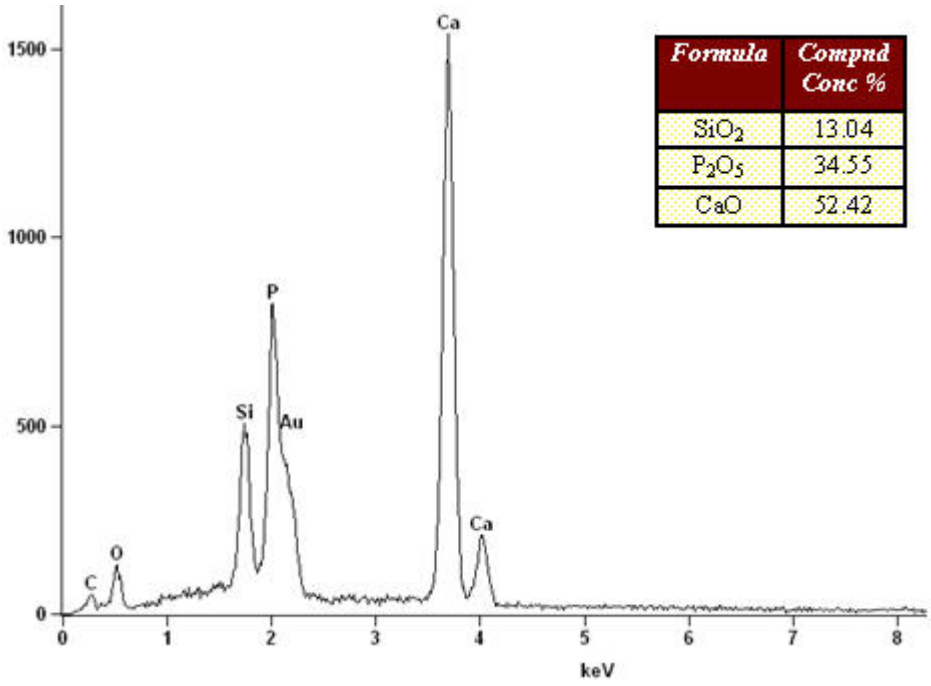

Figure 4.27 The EDS spectra for the apatite phase in the HAP + wollastonite ceramic sintered with 10 wt% NCAS frit.

The EDS scan taken over the silicate phase grains of the ceramic is displayed in **Figure 4.28**. The analysis inscribed on the spectrum showed that the phase was wollastonite of approximate composition $(CaO)_{1.07}SiO_2$. The defect structure in wollastonite is still unknown, but the composition given above would mean that in the ceramic under consideration, the liquid phase had dissolved some silica from the wollastonite until its composition approached that of the silicocarnotite. The round grains of wollastonite observed in the microstructure of **Figure 4.25** substantiated this interpretation.

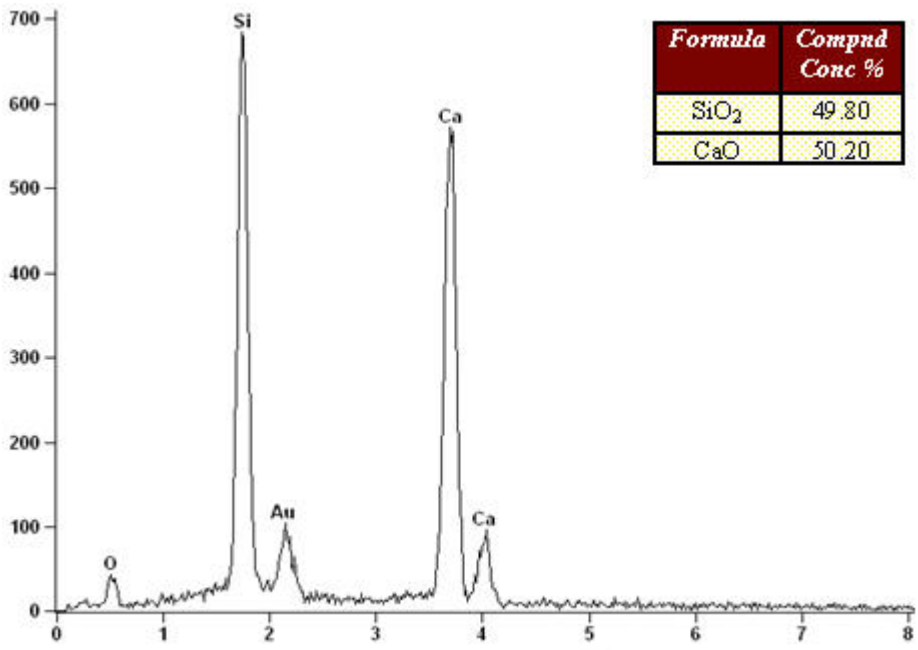

Figure 4.28 The EDS spectra for the silicate phase in the HAP + wollastonite ceramic sintered with 10 wt% NCAS frit.

The microstructure of the HAP + Wollastonite sample sintered with the aid of 15 wt% of the NCAS frit is shown in **Figure 4.29**. The presence of the liquid phase was obvious. Because of the high liquid volume no porosity was left in the ceramic. The excess liquid was solidified as glass, resulting in a final microstructure in which rod-like apatite and the equiaxed silicate phases were dispersed in the glass matrix.

As compared to the apatite fibers shown in **Figure 4.25**, the apatite phase in the ceramic made with increased flux was quite finer and lesser in population. This indicated that the amount of the reactive sintering aid was important in the development of microstructure. As expected, the presence of higher flux necessitated the dissolution of larger quantity of HAP in the liquid to attain saturation. As the result, the reprecipitation of apatite was hindered.

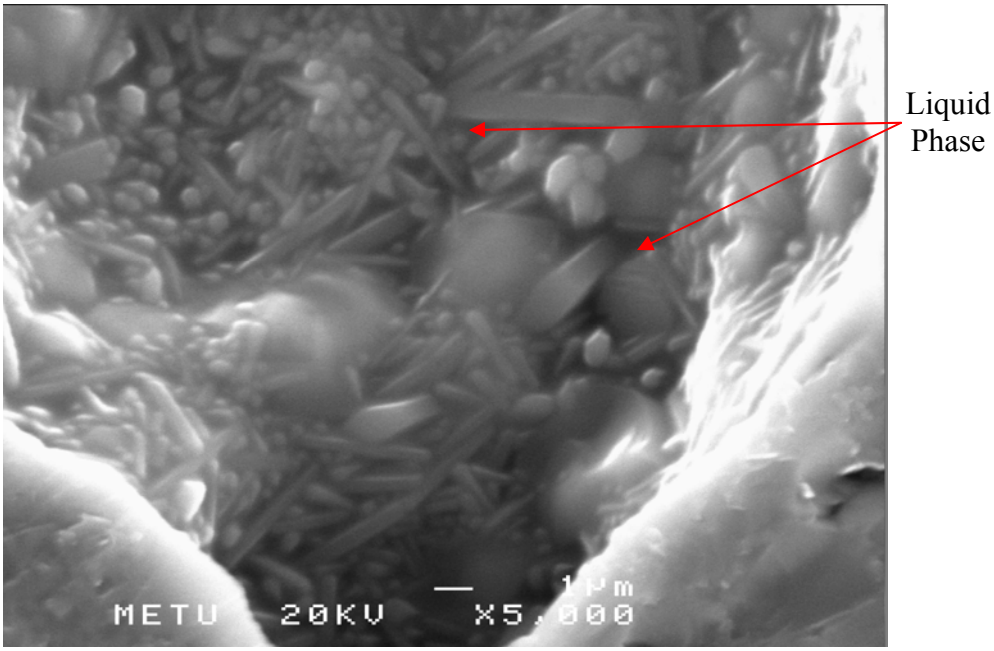

Figure 4.29 The SEM micrograph of the HAP + wollastonite ceramic sintered with 15 wt% NCAS frit.

4.2.1.3.4 Ceramics made from Siliconized HAP + Wollastonite Mixtures

The sintering experiments conducted on HAP + Wollastonite mixtures in the presence of NCAS frit indicated that a reactive liquid phase sintering process was effective in obtaining the microstructural features aimed in this study. Comparison of the microstructures revealed that the presence of 5 to 10 wt% of the NCAS frit would be sufficient to obtain well-developed rod-like apatite grains. Also, it was evident that dissolution of HAP in the liquid phase was an essential first step in the process.

In order to examine the effect of the starting HAP constitution on the formation of the ceramic, additional experiments were designed in which the ceramic samples were prepared by using siliconized HAP powders instead of

pure HAP. The compositions of the powder mixtures for these samples are given in **Table 4.5**.

Table 4.5 The compositions of the ceramic bodies prepared by using siliconized HAP powders.

Sample Number	Siliconized HAP (wt%)	Wollastonite (wt%)	$NCAS_{frit}$ (wt%)
17	47.5 Si-HAP_1, $Ca_{10}(PO_4)_5(SiO_4)_1(OH)_1$	47.5	5
18	47.5 Si-HAP_2, $Ca_{10}(PO_4)_{4.5}(SiO_4)_{1.5}(OH)_{0.5}$	47.5	5
19	47.5 Si-HAP_3, $Ca_{10}(PO_4)_4(SiO_4)_2$	47.5	5

(a) Ceramic made by using siliconized HAP with x=1;

The microstructure of the first ceramic in the above table is shown in **Figure 4.30**. The structure was occupied by rod-like grains of apatite and hexagonal grains of wollastonite. The XRD pattern of the ceramic, shown in **Figure 4.31**, revealed that α-wollastonite and hydroxyapatite were the only solid phases present. The absence of silicocarnotite indicated that the chemical changes during sintering did not cause any decomposition in the siliconized version of HAP used in making this ceramic.

(b) Ceramic made by using siliconized HAP with x=1.5

This ceramic was produced by using siliconized HAP powder with 1.5 mole SiO_2 substitution. The microstructure of the ceramic was as shown in

Figure 4.32. Rod-like grains of apatite were distributed uniformly among the equiaxed wollastonite grains.

(c) Ceramic made by using silicocarnotite, i.e., HAP with x=2

This ceramic was characterized as a mixture of equiaxed grains of wollastonite and silicocarnotite, as seen in **Figure 4.33**. Apparently, the flux had served as a powerful sintering aid. No rod-like grains were observed, indicating that a certain degree of hydroxylation is the necessary condition for the formation of apatite in fiber morphology.

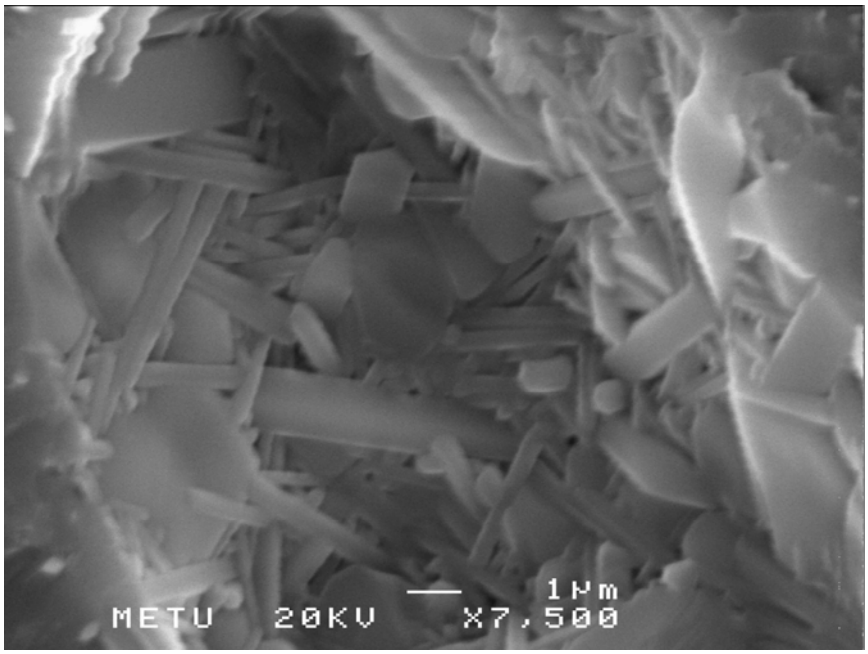

Figure 4.30 SEM micrograph of the sample containing 47.5 wt% Si-HAP_I + 47.5 wt% W + 5 wt% NCAS frit.

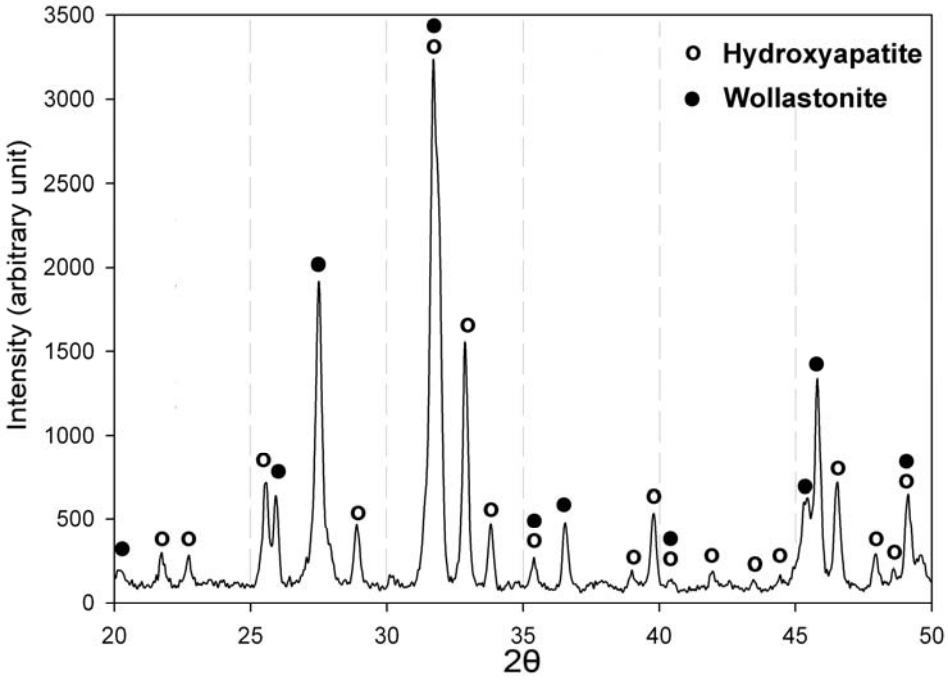

Figure 4.31 XRD pattern of the sample containing 47.5 wt% Si-HAP_1 + 47.5 wt% W + 5 wt% NCAS frit.

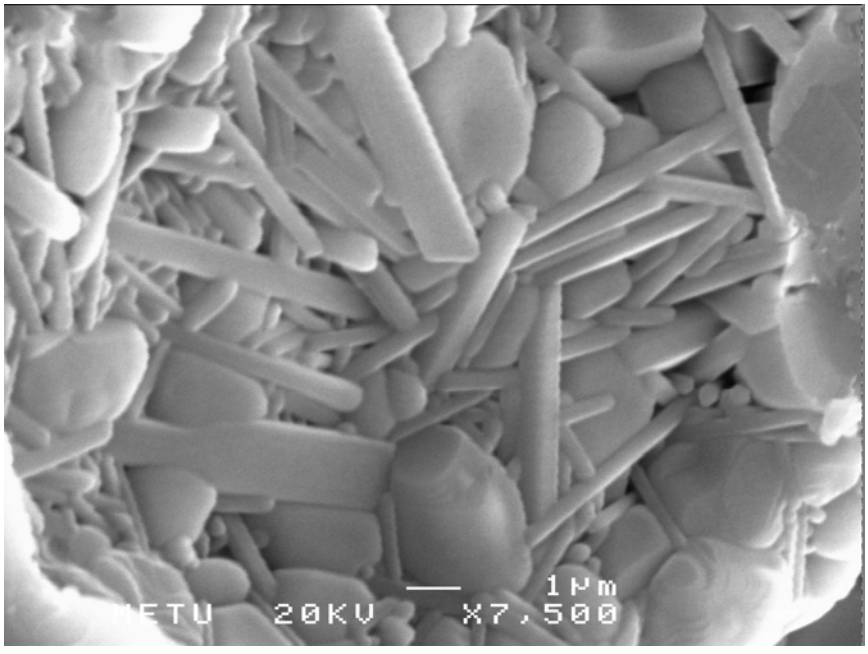

Figure 4.32 SEM micrograph of the sample containing 47.5 wt% Si-HAP_2 + 47.5 wt% W + 5 wt% NCAS frit.

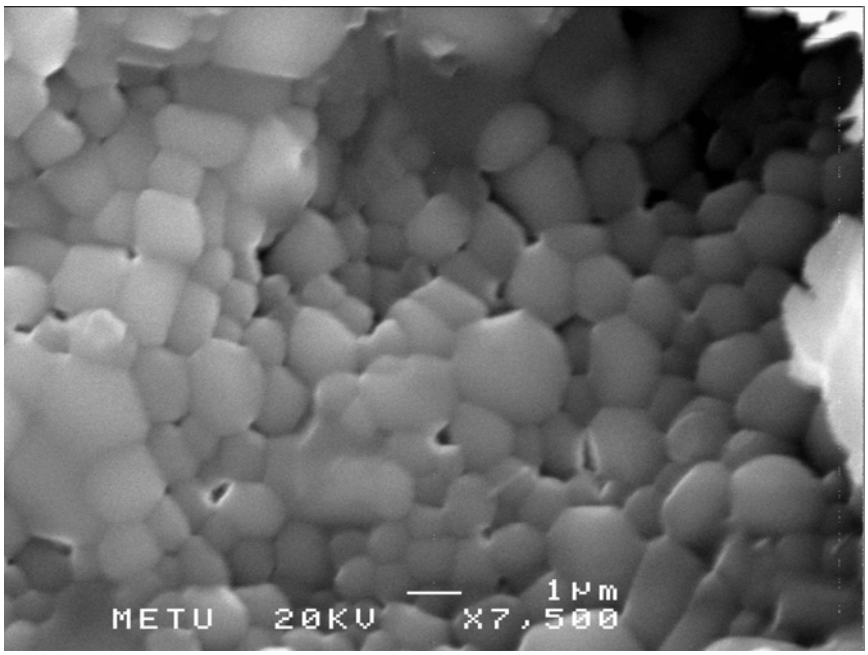

Figure 4.33 SEM micrograph of the sample containing 47.5 wt% Si-HAP_3 + 47.5 wt% W + 5 wt% NCAS frit.

The EDS scans over the wollastonite and "apatite" grains of the ceramic can be seen in **Figure 4.34** and **Figure 4.35**. The wollastonite was essentially in its pure chemical state of $CaO.SiO_2$. The chemical composition of the pure mineral silicocarnotite is 12.45% SiO_2, 29.46% P_2O_5 and 58.09% CaO. The EDS analysis of the silicocarnotite phase of the ceramic was very close to that of the pure mineral. These indicated that the wollastonite and silicocarnotite remained unaltered chemically although both of them had probably interacted with the flux component of the ceramic during the sintering process.

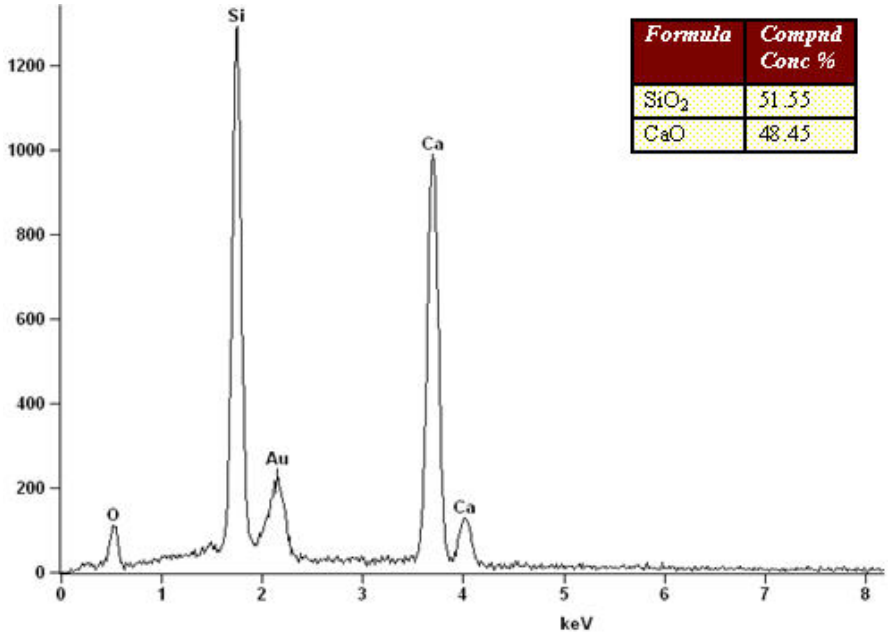

Figure 4.34 The EDS scan over the wollastonite component of the ceramic produced by sintering the mixture 47.5 wt% Si-HAP_3 + 47.5 wt %W + 5 wt% NCAS frit.

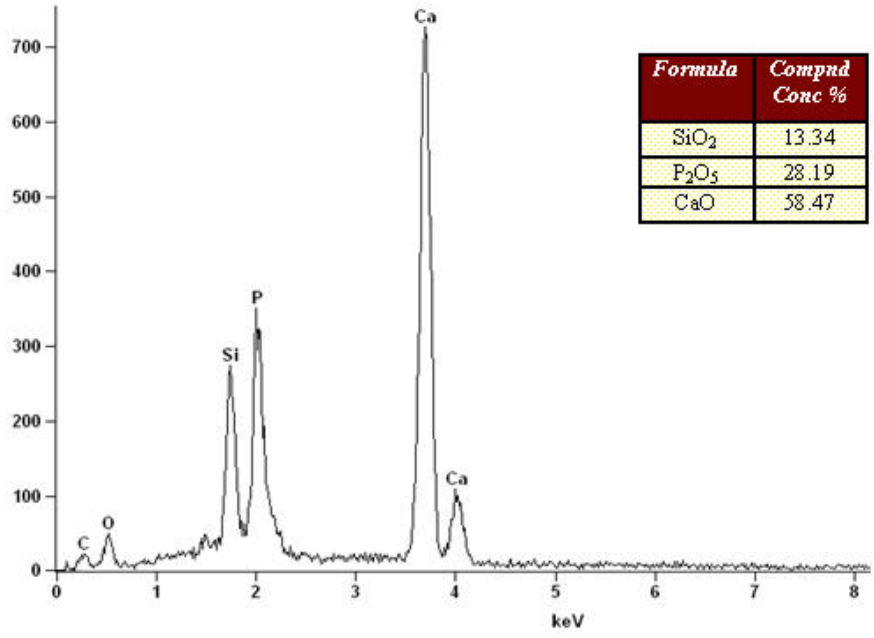

Figure 4.35 The EDS scan over the silico-phosphate component of the ceramic produced from the mixture 47.5 wt% Si-HAP_3 + 47.5 wt %W + 5 wt% NCAS frit.

4.3. MECHANICAL PROPERTIES

The determination of mechanical properties was confined to ceramics manufactured with the help of the NCAS frit. The properties evaluated involved bending strength, yield strength, elastic modulus, compressive strength, hardness, and fracture toughness. The data on these were obtained from tests including three point bending, cold crushing strength, and indentation, as described in Chapter 3.2.3.3.

The compositions of the ceramic samples used in mechanical tests are given in **Table 4.6**. In addition to the ceramics manufactured with NCAS frit, ceramics consisting of pure HAP, pure wollastonite, and a composite with 50 wt% HAP + 50 wt% wollastonite were included to serve as reference samples.

Table 4.6 Compositions of the ceramics used in mechanical testing.

Group Number	HAP (wt%)	Si-HAP_1 (wt%)	Si-HAP_2 (wt%)	α-W (wt%)	$NCAS_{frit}$ (wt%)
1	100	-	-	-	-
2	-	-	-	100	-
3	50	-	-	50	-
4	47.5	-	-	47.5	5
5	45	-	-	45	10
6	-	47.5	-	47.5	5
7	-	-	47.5	47.5	5

4.3.1. Results of Three-Point Bending Test

Three-point bending tests were performed using five samples from each group of ceramics specified in **Table 4.6**. Prior to the test, the sintered specimens were lapped on a polishing machine in order to produce flat and scratch-free surfaces. In order to calculate the flexural strength (σ_b, in MPa) and elastic modulus (E, in GPa) of each sample group, Equations 3.1-3.4 given in Chapter 3.2.3.3.1 were employed.

The data obtained on each group are tabulated in **Tables 4.7-4.13** along with a mean and standard deviation of the calculations. Given standard deviations were used for error detection only. They were not used for error comparison. Graphical representation of these data is shown in **Figure 4.36**.

Table 4.7 Results of the three-point bending test for sample group no:1, i.e. phase pure HAP.

Group 1	**Bending Strength (MPa)**	**Young's Modulus (GPa)**	**Strain to Failure (%)**
1a	50.01	18.39	0.272
1b	35.50	16.90	0.210
1c	34.33	16.67	0.206
1d	46.59	17.71	0.263
1e	66.21	21.57	0.307
Mean with Std	46.53 ± 12.94	18.25 ± 1.98	0.252 ± 0.04

Table 4.8 Results of the three-point bending test for sample group no:2, i.e. phase pure α-Wollastonite.

Group 2	Bending Strength (MPa)	Young's Modulus (GPa)	Strain to Failure (%)
2a	58.20	15.24	0.382
2b	56.64	16.14	0.351
2c	73.78	18.40	0.401
2d	69.50	17.82	0.390
2e	63.45	16.27	0.390
Mean with Std	64.31 ± 7.31	16.77 ± 1.30	0.383 ± 0.02

Table 4.9 Results of the three-point bending test for sample group no:3, i.e. 50 wt% HAP + 50 wt% wollastonite.

Group 3	Bending Strength (MPa)	Young's Modulus (GPa)	Strain to Failure (%)
3a	27.42	10.71	0.256
3b	25.60	10.80	0.237
3c	23.61	8.84	0.267
3d	28.13	10.82	0.239
3e	28.67	11.03	0.260
Mean with Std	26.69 ± 2.07	10.44 ± 0.90	0.252 ± 0.01

Table 4.10 Results of the three-point bending test for sample group no: 4, i.e. 47.5 wt% HAP + 47.5 wt% W + 5% NCAS frit.

Group 4	Bending Strength (MPa)	Young's Modulus (GPa)	Strain to Failure (%)
4a	36.83	11.80	0.312
4b	38.67	12.05	0.321
4c	34.56	11.96	0.289
4d	38.56	10.83	0.356
4e	34.39	9.27	0.371
Mean with Std	36.60 ± 2.08	11.18 ± 1.17	0.330 ± 0.03

Table 4.11 Results of the three-point bending test for sample group no: 5, i.e. 45 wt% HAP + 45 wt% W + 5 wt% NCAS frit.

Group 5	Bending Strength (MPa)	Young's Modulus (GPa)	Strain to Failure (%)
5a	65.33	21.14	0.309
5b	67.90	20.64	0.329
5c	71.88	19.59	0.367
5d	62.70	18.66	0.336
5e	67.04	20.04	0.334
Mean with Std	66.97 ± 3.39	20.01 ± 0.96	0.335 ± 0.02

Table 4.12 Results of the three-point bending test for sample group no: 6, i.e. 47.5 wt% Si-HAP_1 + 47.5 wt% W + 5 wt% NCAS frit.

Group 6	Bending Strength (MPa)	Young's Modulus (GPa)	Strain to Failure (%)
6a	70.94	22.81	0.311
6b	78.32	25.10	0.312
6c	67.03	21.03	0.319
6d	62.77	21.06	0.298
6e	75.92	21.03	0.361
Mean with Std	71.00 ± 6.35	22.21 ± 1.79	0.320 ± 0.02

Table 4.13 Results of the three-point bending test for sample group no: 7, i.e. 47.5 wt% Si-HAP_2 + 47.5 wt% W + 5 wt% NCAS frit.

Group 7	Bending Strength (MPa)	Young's Modulus (GPa)	Strain to Failure (%)
7a	83.61	28.34	0.295
7b	73.51	27.36	0.276
7c	93.77	31.89	0.294
7d	84.43	29.52	0.286
7e	82.65	28.50	0.290
Mean with Std	83.60 ± 7.19	29.12 ± 1.73	0.288 ± 0.01

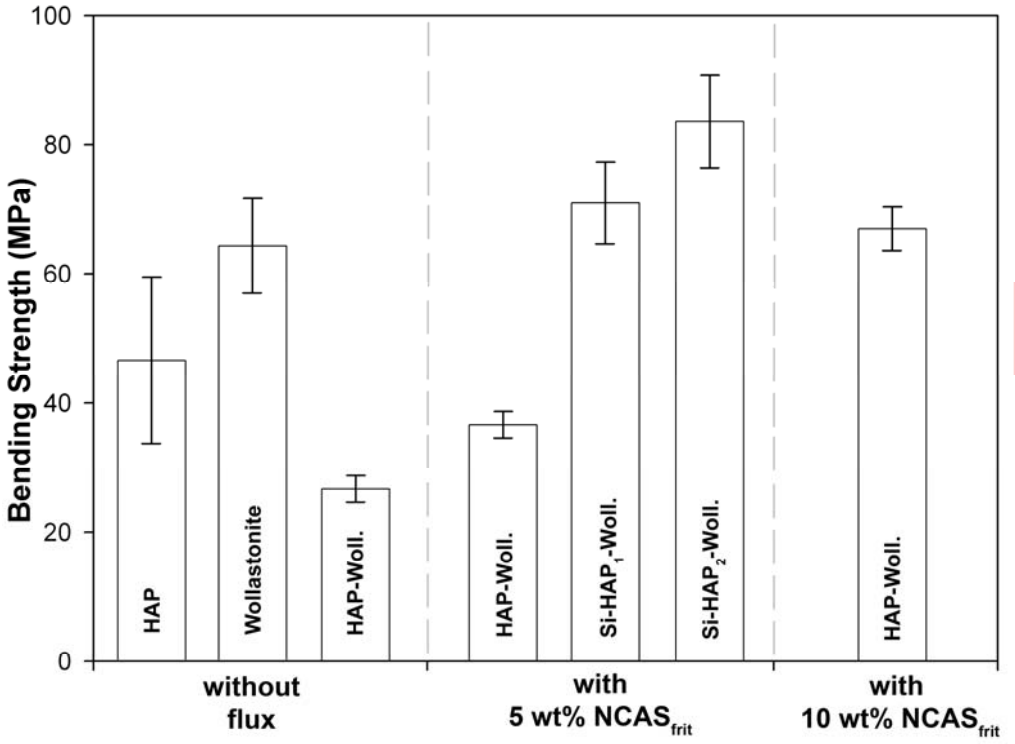

Figure 4.36 Bending strength of each group.

4.3.2. Results of Cold Crushing Strength Test

The ultimate compressive strengths of the sintered ceramics were determined as a procedure described in Chapter 3.2.3.3.2 from each of the selected compositions given in **Table 4.6**. The cylinders were compressed along their axes by placing them in between the platens of the machine. The cross-head speed was kept at 1 mm/min. In order to calculate the compressive strength (CCS, in MPa) for each sample group Equation 3.5 given in Chapter 3.2.3.3.2 was used. The data obtained on each group of samples are tabulated in **Tables 4.14-4.20** along with a mean and standard deviation of the calculations. Graphical representation of these data is shown in **Figure 4.37**.

Table 4.14 Results of the cold crushing strength tests for group no: 1, i.e. phase pure HAP.

Group 1	Compressive Strength (MPa)
1a	194.20
1b	175.70
1c	138.70
1d	171.86
1e	149.23
Mean with Std	165.94 ± 22.08

Table 4.15 Results of the cold crushing strength tests for group no: 2, i.e. phase pure α-wollastonite.

Group 2	Compressive Strength (MPa)
2a	246.22
2b	281.55
2c	280.81
2d	279.10
2e	262.13
Mean with Std	269.96 ± 15.50

Table 4.16 Results of the cold crushing strength tests for group no: 3, i.e. 50 wt% HAP + 50 wt% wollastonite.

Group 3	Compressive Strength (MPa)
3a	116.39
3b	135.59
3c	117.59
3d	148.79
3e	104.39
Mean with Std	124.55 ± 17.54

Table 4.17 Results of the cold crushing strength tests for group no: 4, i.e. 47.5 wt% HAP + 47.5 wt% W + 5 wt% NCAS frit.

Group 4	Compressive Strength (MPa)
4a	110.5
4b	143.3
4c	145.8
4d	145.0
4e	145.7
Mean with Std	138.06 ± 15.44

Table 4.18 Results of the cold crushing strength tests for group no: 5, i.e. 45 wt% HAP + 45 wt% W + 5 wt% NCAS frit.

Group 5	Compressive Strength (MPa)
5b	205.3
5c	271.0
5d	208.2
5e	209.2
5a	207.7
Mean with Std	220.28 ± 28.34

Table 4.19 Results of the cold crushing strength tests for group no: 6, i.e. 47.5 wt% Si-HAP_1 + 47.5 wt% W + 5 wt% NCAS frit.

Group 6	Compressive Strength (MPa)
6a	291.3
6b	303.8
6c	288.2
6d	213.4
6e	308.4
Mean with Std	281.02 ± 38.72

Table 4.20 Results of the cold crushing strength tests for group no: 7, i.e. 47.5 wt% Si-HAP_2 + 47.5 wt% W + 5 wt% NCAS frit

Group 7	Compressive Strength (MPa)
7a	229.9
7b	233.6
7c	242.5
7d	249.2
7e	261.4
Mean with Std	243.32 ± 12.61

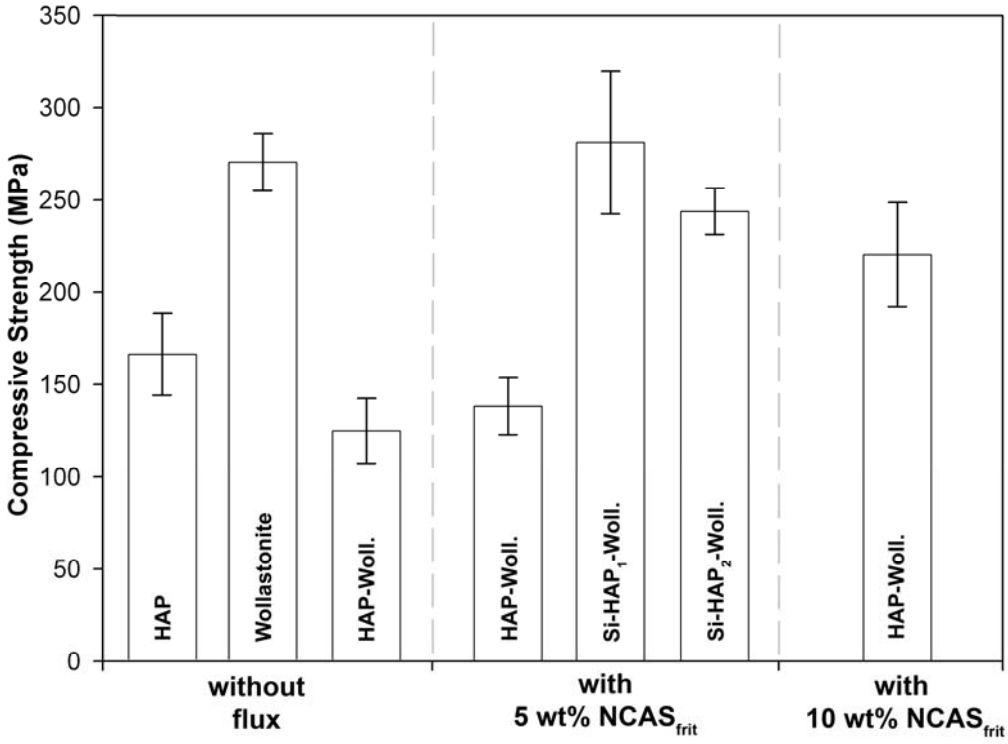

Figure 4.37 Compressive strength of each group.

4.3.3. Results of Indentation Test

The hardness and fracture toughness of the sintered samples were determined using the procedure described in Chapter 3.2.3.3.3. The data obtained on hardness of each sample group were tabulated in **Table 4.21.** They were the mean of at least 10 indentations taken from the each specimen group at room temperature. Indentations were made on polished surfaces of sintered ceramics and Equation 3.6 given in Chapter 3.2.3.3.3 was employed to calculate the values of Vickers hardness.

The measurement of indentation fracture toughness (IFT) of brittle solids has been given considerable attention in recent years. The inherent

simplicity of this technique, the requirement of small sized specimens, and the ease of specimen preparation have made it widely popular over the last two decades for evaluating fracture toughness of ceramics and glasses. As a result of this, great numbers of equations have been proposed to calculate the fracture toughness using Vickers indentation [81-82, 99-101].

These equations either consider that the crack emanating from the indentation is of mean half-penny shape or is a Palmqvist radial crack. However, equations in universal character have also been derived that adjust the formula to any kind of crack system [81, 101]. In any case, these equations are meant to reproduce the values obtained with conventional single edge notched beam (SENB) or double cantilever beam (DCB) specimens.

Evans [81] used dimensional analysis and curve fitting over a range of c/a from 1.5 to 7 for many ceramic materials and derived a universal formula for calculating fracture toughness data (B_4C, SiC, Si_3N_4, WC/Co, ZnS, ZnSe, PSZ, ZrO_2). This model should be applicable to both Palmqvist and median cracks, according to the following formula:

$$K_{1C} = (H)^{0.6} \times (E)^{0.4} \times \sqrt{a} \times (10)^{y} \qquad \textbf{(4.1)}$$

where,

$$y = -1.59 - (0.34x) - (2.02x^2) + (11.23x^3) - (24.97x^4) + (15.32x^5) \qquad \textbf{(4.2)}$$

and

$$x = \log(\frac{c}{a}) \qquad \textbf{(4.3)}$$

While Niihara et al. [82] derived two different formulas for each of Palmqvist and median type cracks. In the present study, the cracks formed belong to low l/a system (0.25<l/a<2.5, l=c-a) and therefore satisfy the relationship for a Palmqvist-type radial crack according to the information given by Niihara et al. [82]. Thus, the Niihara's [82] equation given below was additionally used to compare the results.

$$K_{1C} = 0.018 \times \left(\frac{c-a}{a}\right)^{-0.5} \times \left(\frac{E}{H}\right)^{0.4} \times H \times \sqrt{a} \qquad \textbf{(4.10)}$$

The Fracture toughness values calculated by using above equations are given in **Table 4.21**. Values for Group 2, 3 and 4 could not be determined. Because, it was not possible to initiate well defined radial cracks after indentation.

Table 4.21 Calculated hardness and fracture toughness, K_{1C}, values which were the mean of at least 10 indentations.

Group Number	(mean) a	(mean) c	l/a (l=c-a)	Vickers Hardness (GPa)	Fracture Toughness ($MPa.m^{1/2}$) -Evans'-	Fracture Toughness ($MPa.m^{1/2}$) -Niihara's-
1	58 µm	145 µm	1.50	2.70	0.68	0.65
2	172 µm	-	-	1.53	-	-
3	350 µm	-	-	0.36	-	-
4	117 µm	-	-	3.31	-	-
5	115 µm	360 µm	2.13	3.43	0.88	0.92
6	103 µm	310 µm	2.01	4.28	1.03	1.07
7	95 µm	300 µm	2.16	5.03	1.19	1.21

Here, it was worth to say that the short crack fracture toughness data as measured through Evans' and Niihara's equations, like any other semi-empirical equations for obtaining K_{1C} values from indentation crack length, were used in the present thesis study for making a relative toughness comparison for the newly developed ceramic material.

Figure 4.38 plots the K_{1C} values calculated according to the Evans' equation versus Niihara's equation. The line represents the 1:1 relationship between Evans and Niihara's K_{1C} values. As could be seen from the **Figure 4.38**, for every experimental measurement Niihara's approach correlated very well with Evans'.

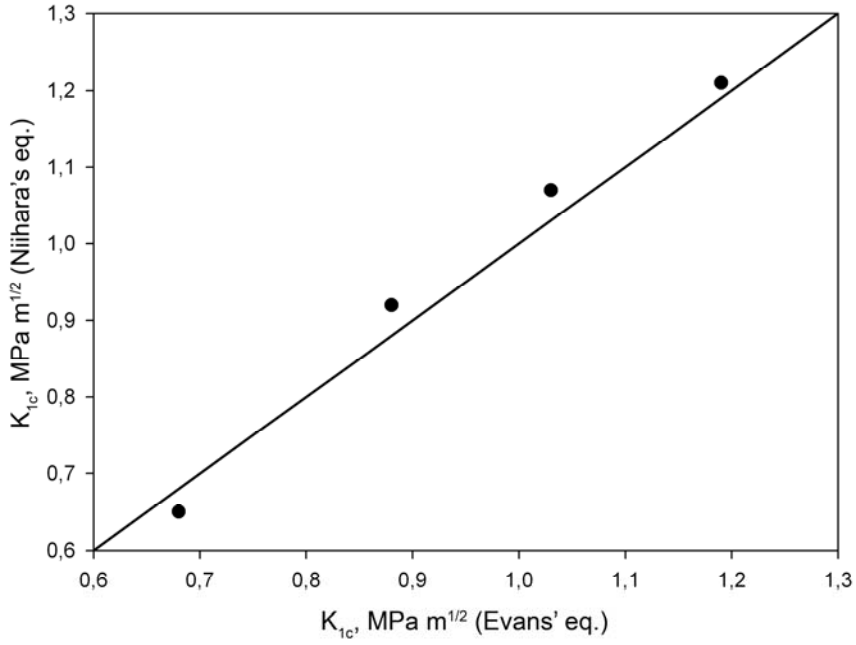

Figure 4.38 Fracture toughness (Evans' equation) versus fracture toughness (Niihara's equation).

CHAPTER V

DISCUSSION & CONCLUSION

Bone is the major component in the formation of the hard tissue in the human body. It has to be sufficiently strong so that it can provide structural support for the body and should act as a substrate to which the soft tissue can attach itself for muscular action development. In addition, it must be a host in which the body fluids may interact with the hard tissue for sustained biological activity.

Bone can be regarded as a composite of organic and inorganic materials. The organic part is mainly collagen and various proteins; on a dry basis, the proportion of these may reach 30 to 40 percent of the bone weight [111]. The inorganic part is a poorly crystallized calcium phosphate mineral very close in chemical composition to the natural calcium hydroxyapatite, HAP. Therefore, ceramics manufactured from synthetic HAP have found a prominent place in most clinical attempts involving the replacement or repair of natural bone. The first successful medical application of calcium phosphate bioceramics in humans was in 1920, and the first dental application in animals was reported to occur in 1975 [111].

Calcium phosphates can exist in different phases depending on temperature, impurities and the presence of water. Different phases of calcium phosphate ceramics are used by the modern health care industry, in accordance with resorbability or bioactivity requirements [111]. Two phases that are stable at body temperature and in contact with body fluids are dicalcium phosphate [$CaHPO_4.2H_2O$] at pH<4.2, and hydroxyapatite at pH>4.2. Human body stays in a very narrow pH range of about 7.3.

Therefore, HAP is the stable phase in that pH and also it is the ideal phase for applications inside the human body.

Despite chemical similarities of synthetic HAP to the mineral phase of the bone, it differs significantly in mechanical and biological properties of that of natural bone. As mentioned in Chapter II, biomedical applications of hydroxyapatites have been limited to low-load-bearing conditions due to their low mechanical reliability, especially low bending strength and low fracture toughness. Therefore, several studies in the past were devoted to find ways of improving the mechanical properties of HAP ceramics.

Introduction of other phases into HAP, which did not destroy the biological compatibility, was found to be quite effective. One such material with higher mechanical strength than HAP ceramics was the apatite-wollastonite glass ceramic produced by combining the conventional glass melting with ceramizing heat treatment. The wollastonite component of this material has been designated as the cause of higher strength [1, 58, 108].

Despite the vast amount of information on apatite-wollastonite glass ceramics, relatively little is known about the outcome of processes including liquid phase sintering of calcium hydroxyapatite and wollastonite powders. Clearly, the material obtained from the sintering process would be a composite ceramic consisting of apatite and wollastonite phases, with much lesser volume of the residual glass phase as compared to the conventional glass-ceramic product. The mechanical properties of the ceramic would be intermediate between pure HAP and the A-W glass ceramic, it would possess a higher bioactivity than pure HAP, and it would be amenable to manufacturing synthetic bones with customized pore architecture. Therefore the main objective of the present thesis project was to develop apatite-wollastonite composite ceramics manufactured by the sintering technique.

The preliminary efforts were directed towards searching for fluxes that could serve as effective liquid phase sintering additives. The fluxes were selected from silicate systems with compositions corresponding to low melting temperature eutectics. The one designated as MCAS did not produce liquid phase sintering effects, its failure was thought to be related to the probable high viscosity of the liquid and its non-wetting behavior. The second flux, which was sodium feldspar, failed also because of the large volume of liquid generated in the ceramic during sintering. Under the circumstances the liquid phase could not reach saturation. Therefore, attention was turned to a frit belonging to the system Na_2O-CaO-Al_2O_3-SiO_2.

The use of NCAS frit as the fluxing agent resulted in the expected microstructural formation typified by the residual porosity, a bimodal grain size distribution, and a glassy phase distributed at grain boundaries. The bimodal microstructure consisted of a mixture of rod-like apatite grains and equiaxed wollastonite grains which were bonded together with the help of the glassy phase. The distorted peaks of the apatite in the powder XRD pattern, shown in **Figure 4.25**, indicated that HAP was somehow modified during sintering. This was due to exchange of some of the (PO_4) of the HAP with (SiO_4) through the aid of the liquid phase.

During sintering studies, additional experiments were conducted in order to examine the effect of the starting HAP constitution on the sintered microstructural arrangements. Into these composite ceramics HAP was introduced in the siliconized version with different levels of (SiO_4) substitution. SEM investigations on sintered samples revealed that the elongated rod-like structure would come out as long as some (OH) was left in the HAP component of the ceramic. On the other hand, hexagonal grains would prevail when HAP would be replaced fully with the silicocarnotite version. This result indicated that, in addition to (SiO_4) substitution, a certain

degree of hydroxylation in the apatite was essential for the formation of rod-like morphology.

The sintering experiments conducted on HAP + Wollastonite mixtures in the presence of NCAS frit indicated that a reactive liquid phase sintering process was effective in obtaining the microstructural features aimed at the beginning of the thesis study. It is envisioned that during the sintering process, the apatite and wollastonite phases dissolved simultaneously in the liquid phase until the liquid became saturated with respect to calcium, phosphorus and silicon. In the next stage, rod-like elongated grains were re-precipitated from the saturated liquid, yielding the modified HAP constituent of the sintered ceramic. This modified version of HAP was siliconized calcium hydroxyapatite. Meanwhile, the remaining wollastonite grains tended to exhibit a faceted equiaxed morphology.

Following reaction could be postulated for the substitution of (SiO_4) for (PO_4) during the sintering process: Taking x=1, for example,

$$\mathbf{xCaO.SiO_2 + Ca_{10}(PO_4)_6(OH)_2 \rightarrow 6/5Ca_{10}(PO_4)_5(SiO_4)(OH) + 4/5(OH)} \quad \textbf{(c.1)}$$

The mechanism of substitution was probably the one depicted schematically by the diagram shown in **Figure 5.1**. It was observed that, in order to obtain well-developed rod-like apatite grains, the volume fraction of the liquid phase associated with NCAS frit during sintering should be maintained in between 5 to 10 percent. As the amount of liquid phase was increased beyond a threshold value reprecipitation was hindered due to inability of carrying the liquid to saturation.

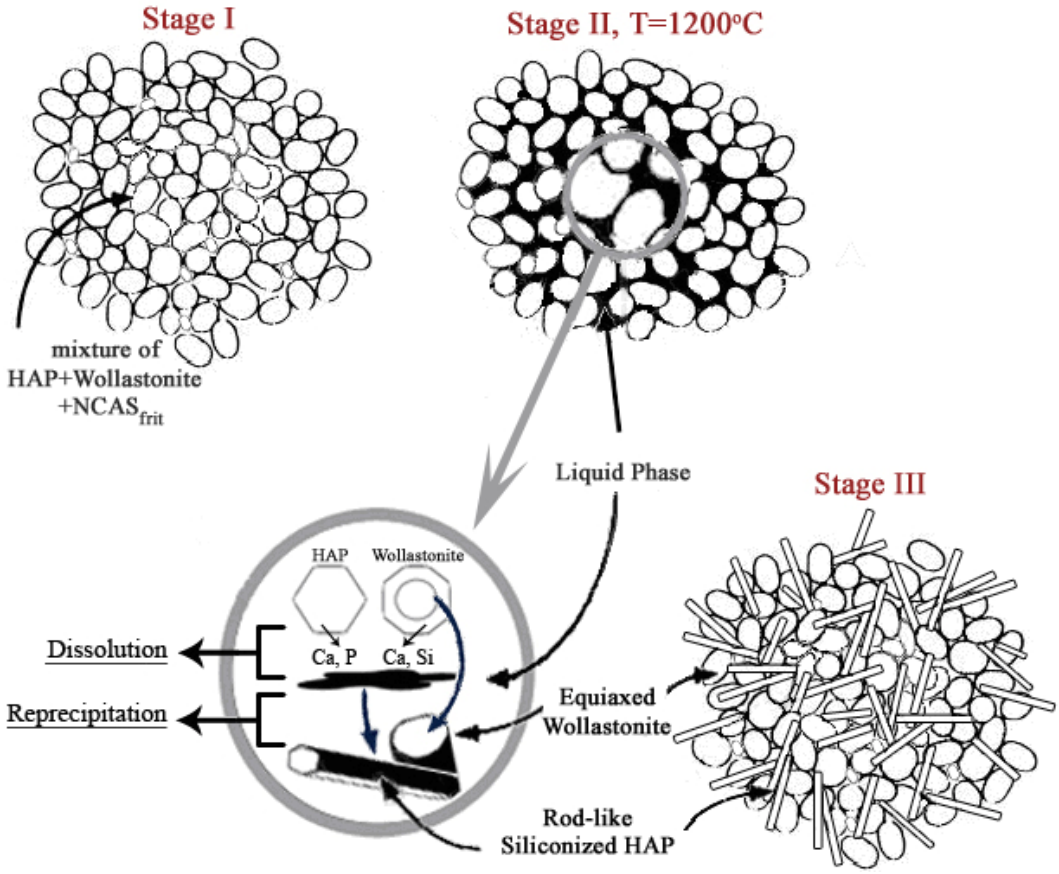

Figure 5.1 Mechanism of the reactive sintering process.

The mechanical properties of ceramics consisting of pure HAP, pure wollastonite, and HAP plus wollastonite composites with and without NCAS frit were determined in terms of the flexural strength, strength at failure under compression, and hardness. Fracture toughness determinations were confined to composite ceramics produced by the use of flux and siliconized HAP.

The data on mechanical properties, reported in Chapter IV, showed variations not only due to differences in the nature of phase assemblages but also due to differential densification. The values obtained for flexural strength, σ_f, and compressive strength, σ_c, hardness, H, and fracture toughness, K_{1c}, are summarized in **Table 5.1** in order to help in further

discussions. Following conclusions could be drawn with regard to the various ceramic groups in the table.

Table 5.1 – The summary of data on mechanical strength of the sintered ceramics.

#	HAP (wt%)	α-W (wt%)	Si-HAP$_1$ (wt%)	Si-HAP$_2$ (wt%)	NCAS (wt%)	%TD	σ_f MPa	σ_c MPa	H GPa	K_{1c} MPa.$m^{1/2}$
1	100	-	-	-	-	**90.3**	**46.3**	**165.9**	**2.70**	**0.65**
2	-	100	-	-	-	**77.1**	**64.3**	**269.0**	**1.53**	**-**
3	50	50	-	-	-	**68.6**	**26.7**	**124.6**	**0.36**	**-**
4	47.5	47.5	-	-	5	**75.0**	**36.6**	**138.1**	**3.31**	**-**
5	45	45	-	-	10	**90.5**	**67.0**	**220.3**	**3.43**	**0.88**
6	-	47.5	47.5	-	5	**95.2**	**71.0**	**281.0**	**4.28**	**1.03**
7	-	47.5	-	47.5	5	**93.6**	**83.6**	**243.3**	**5.03**	**1.19**

1) The average flexural strength of the sintered HAP ceramic was measured as 46.3 MPa. There was a considerable spread around this value (± 12.94 MPa) probably due to the variations in density and in the preparation of bending test samples. Despite the care spent in surface finish, scratches invisible to the naked eye could cause the spread noted. The average of the compressive strength was found as 165.9 MPa. For purposes of comparison, the data available in the literature on the flexural and compressive strength of HAP ceramics are summarized in **Table 5.2**. Values in the last raw in the table are taken from a review article, others were obtained from sources which contained direct experimentation.

Table 5.2 Summary of mechanical test data for hydroxyapatite ceramics.

σ_f : bending strength, σ_c : compressive strength, P: porosity, D: average powder particle size.

Reference	σ_f (MPa)	σ_c (MPa)	P (%)	D (μm)	Sintering Conditions, T (°C) / t (h)
Tancred et al [5]	31.4	-	2.2	1-1.5	1200°C for 3 h.
Akao et al.[74]	104	415	9.1	1.32	1200°C for 3 h.
Wang et al. [107]	70-80	-	1.9	0.5	1250°C for 2 h.
Kalita et al. [109]	-	158.4	12.7	-	1250°C for 3 h.
Present Study	47	166	9.7	~2	1200°C for 4 h.
Suchanek et al [3]	38-250	120-900	-	-	Review

The powder synthesis technique could play a dominant role in the strength values quoted. In the ceramics subject of the above table, the powder preparation techniques were almost same; the precipitation process was used some differences in the details. The highest experimental flexural strength was found by Akao et al [74]; their powder was prepared by partial calcination of the precursor at a low temperature (800 °C), which meant that the calcination product had a highly reactive surface, so that the ceramic could sinter with a finer grain size. The powder used by Wang et al [107] was a commercial one, it had a very fine particle size as well so that a low porosity ceramic of very fine grain size with high flexural strength could be produced. Although Tancred et al. [5] also used very fine powder, the reason why their HAP ceramics exhibited low levels of strength remain unclear.

The flexural and compressive strengths of the HAP ceramics produced in the present thesis were quite acceptable since they were manufactured from fully crystallized but low sinterability powders.

2) Despite the recognition of its high strength, until very recently, virtually no information has been available on the mechanical properties of wollastonite ceramics. The work reported by Lin et al. [108] showed that an α-wollastonite ceramic, sintered at 1200ºC for 3 hours, could have a bending strength of 53.48 MPa with 17.65% residual porosity. In the present study, the flexural strength of α-wollastonite with 22.9% porosity was found be 64.31 MPa. Thus a higher flexural strength was obtained at higher level of porosity. The differences in the strength values could be attributed to the powder synthesis method again. The method used by Lin et al [108] involved a chemical precipitation process in the presence of Na^+ ions. The presence of these, due to insufficient washing, could cause grain growth while sintering and therefore might lead to higher theoretical density but lower strength.

In addition to the bending strength, the compressive strength (269.96 MPa) and hardness (1.53 GPa) values for α-wollastonite ceramics were also measured. Since such data have not yet been reported in the previous literature no interpretation could be afforded on their magnitudes. However, it is quite clear that wollastonite ceramics sintered to high density would exhibit rather unusual strength values both under tension and in comparison. Because of this reason, it would be quite reasonable to expect wollastonite to enhance the mechanical properties of a composite ceramic considerably.

3) The bending strength and compressive strength of 50 wt% HAP + 50 wt% Wollastonite composite ceramics were found to be 26.69 MPa and 124.55 MPa, respectively. Both strength values were rather quite low, and just the opposite of the expectations from the presence of wollastonite. The low level of densification in the ceramic resulted in 31.4 % residual porosity; this was the main cause for the low strength for measured in this ceramic. The

results on sintered density and the microstructure showed that the components HAP and wollastonite had hampered their self sinterabilities mutually.

4) The addition of NCAS frit for upgrading the sintered density was useful not only in the densification process but also ceramics with increased flexural strength was produced. 10 wt% addition of frit raised the flexural strength of the composite by 150 %, hence a ceramic 2.5 times as strong as the bare HAP + Wollastonite mixture could be obtained. The density of the ceramic was also high, reaching 90 percent of the theoretical. Although the rod-like apatite morphology was also present, the increases observed in the strength values could be attributed more to the enhanced densification rather than the morphological change.

5) The increases observed in the densification and strength of the composite ceramics manufactured with the use of siliconized HAP were quite understandable. These were attained despite the reduction in the quantity of the frit used in ceramic preparation. It appears that using the siliconized version of HAP allowed the frit to function more like a sintering aid than acting as a reservoir of silicon for HAP. HAP did not need to deplete the SiO_2 of the liquid phase also the wollastonite component of the ceramic remained intact, thus the composite could attain higher strength levels both under tension and compression.

6) The average hardness and indentation fracture toughness (K_{1C}) values of sintered pure HAP ceramic was 2.70 GPa and 0.65 $MPa.m^{1/2}$, respectively. These results were in good agreement with those reported in literature [5, 38]. The hardness and indentation fracture toughness values of the composite A/W sintered ceramics made by the use of NCAS flux could reach 5.03 GPa, 1.21 $MPa.m^{1/2}$ respectively. These values represented double of what had been measured in the pure HAP ceramic. The higher fracture toughness of the

composite ceramics with NCAS flux was attributed to the bimodal grain size distribution. Most probably during crack propagation high-aspect ratio rod-like grains acted as crack-bridging zones and thereby increased the toughness of the ceramic.

When the results of this thesis work are compared with those of similar other studies published earlier, the composite apatite-wollastonite ceramics developed in the present study were noted to possess several advantages in terms of mechanical properties, structural features, and chemical stability.

For example, Santos et al. [53] used additives selected from the multicomponent oxide system $CaO-P_2O_5-Na_2O-Al_2O_3$ and Bioglass® ($CaO-P_2O_5-Na_2O-SiO_2$) as sintering additives for enhanced bioactivity and mechanical properties. They found that phosphate based additions would improve sintering but the Bioglass® additive failed to do so because of its SiO_2 content. No mentioned was made on strength enhancement, but the fracture toughness was increased to the 1.1-1.2 $MPa.m^{1/2}$ range by sintering HAP at 1300 °C in the presence of $CaO-P_2O_5-Na_2O-Al_2O_3$ Although densification was improved, the ceramic exhibited chemical unstability by transforming into β and then α forms of TCP.

Tancred et al. [62] sintered hydroxyapatite with $CaO-SiO_2$ based glass additions. They claimed that sintering was disrupted by the presence of $CaO-SiO_2$ glass, this verified the observations on poor sintering tendency of HAP + Wollastonite composites produced in the present study. Similar to the situation reported by Santos et al [53], they suffered the decomposition problem of HAP, turning into β-TCP and/or α-TCP. No improvement on flexural strength was recorded, the maximum value was around 35 MPa, which was almost half of what was measured in the composite ceramics of this study.

As mentioned earlier in this section, in a recent paper, Kalita et al [109] reported that a hydroxyapatite ceramic sintered with the addition of a $CaO-P_2O_5-Na_2O$ glass of specific composition, a maximum of 220 MPa could be achieved in the compressive strength. The ceramic was produced by sintering at 1300 °C for 3 hours. Although the necessity and desire of attaining higher strength levels were stressed as the major goals, no mention was made on the mechanical properties of their product.

Although calcium hydroxyapatite is described to exhibit excellent bioactivity its reactivity with the existing bone is reportedly quite low [112, 113]. The current approach which has become popular to speed up the rate of osseointegration is to incorporate biological entities, such as growth factors, proteins, and cells, onto the surface of the HAP implant. Another approach, which has potential for gaining popularity, is to adjust the chemical composition of the implant to more closely approximate that of the bone mineral. In this category, silicon substituted HAP is regarded as a good candidate for enhanced osseointegration.

Professor Hastings [114] claimed that preliminary studies conducted in his research group at the University of London have indicated that siliconized HAP enhanced in vitro biological response compared with stoichiometric HAP. The same observations have already been made by Professor Feza Korkusuz [115] of METU Medical Center who carried out in vitro studies by using a wollastonite-apatite ceramic that contained a certain grade of siliconized HAP. Therefore, initial results are quite encouraging to extend the research effort on bioceramics containing silicon substituted HAP in their constitution. It appears that the rod-like morphology in the modified HAP may add impetus to the osseointegration due the larger surface area provided for the in-vivo interactions.

Future studies on this subject may be directed towards attaining higher mechanical strength values by enhancing the level of densification. This can be achieved by variations in the method of ceramic powder synthesis, the modifications in the sintering schedules with respect to peak temperatures, soak times and/or ramp rates. Also, the alterations in the members of the composite, particularly the wollastonite component can be considered.

REFERENCES

[1] Hench L. L., Wilson J., editors. “An introduction to bioceramics”, advanced series in ceramics, vol. 1. Singapore: World Scientific, 1993

[2] Black J., ”Systemic Effects of Biomaterials”, Biomaterials 5, pp11, 1984.

[3] Suchanek W., Yoshimura M., “Processing and properties of hydroxyapatite-based biomaterials for use as hard tissue replacement implants”, Journal of Material Research, 13(1), pp97-17, 1998.

[4] Ruys A. J., Wei M., Sorrell C. C., Dickson, M.R., Brandwood A., Milthorpe B.K., ” Sintering effects on the strength of Hydroxyapatite”, Biomaterials 16, pp409-15, 1995.

[5] Tancred D. C., McCormack B. A. O., Carr A. J. "A Quantitative study of the sintering and mechanical properties of Hydroxyapatite/phosphate glass composites" Biomaterials, 19, pp1735-43, 1998

[6] Kokubo T, Ito S., Shigematsu, M., Sakka S., Yamamuro T., “Apatite and wollastonite containing glass ceramics for prosthetic application”, Journal of Materials Science, 20, pp2001-04, 1985.

[7] Juhasz J. A., Best S. M., Brooks R., Kawashita M., Miyata N., Kokubo T., Nakamura T., Bonfield W., ”Mechanical properties of glass-ceramic A–W-polyethylene composites: effect of filler content and particle size”, Biomaterials, 25, pp949–55, 2004.

[8] Black J., Hasting G., “Handbook of biomaterial properties", Chapman Hall, London, U.K., 1998.

[9] Thamaraiselvi T. V., Rajeswari S., “Trends in Biomaterials and Artificial Organs”, 18 (1), pp9-17, 2004.

[10] Marti A., “Inert bioceramics (Al_2O_3, ZrO_2) for medical application”, Injury International Journal, 31, pp33-36, 2000.

[11] Kanematsu N., Shibata K., Yamagami A., Kotera S., Yoshihara Y. “Cytotoxicity of anodized titanium and polycrystalline zirconia in cultured mammalian cells”, Japanese Journal of Oral Biology, 27, pp382–84, 1985.

[12] Hench L. L., “Bioceramics”, Journal of the American Ceramic Society, 81(7), pp1705-28, 1998.

[13] Kivrak N., "Synthesis of Hydroxyapatite (HA) / Tri-Calcium Phosphate (TCP) Composite Bioceramic Powders and Their Sintering Behavior", METU (Middle East Technical University, Ankara, Turkey), June 1996 (M.Sc. Thesis).

[14] Ryu H. S., Youn H. J., Hong K. S., Chang B. S., Lee C. K., Chung S. S., "An improvement in sintering property of beta-tricalcium phosphate by addition of calcium pyrophosphate", Biomaterials, 23(3), pp909-14, 2002.

[15] Taş A. C., Korkusuz F., Timuçin M. and Akkaş N., ”An Investigation of the Chemical Synthesis and High-Temperature Sintering Behavior of Calcium Hydroxyapatite (HA) and Tricalcium Phosphate (TCP) Bioceramics” Journal of Materials Science: Materials in Medicine, 8, pp91-96, 1997.

[16] Engin N. O., "Manufacture of Macroporous Calcium Hydroxyapatite (HA) and Tri-Calcium Phosphate (TCP) Bioceramics," METU (Middle East Technical University, Ankara, Turkey), January 1999 (M.Sc. Thesis).

[17] Raynaud S., Champion E., Lafon J. P., Bernache-Assollant D., "Calcium phosphate apatites with variable Ca/P atomic ratio III Mechanical properties and degradation in solution of hot pressed ceramics", Biomaterials, 23(4), pp1081-89, 2002.

[18] Engin N. O., Taş A. C., "Manufacture of macroporous calcium hydroxyapatite bioceramics", Journal of European Ceramic society, 19, pp2569-72, 1999.

[19] Lyckfeldt O., Ferreira J. M. F., “Processing of Porous Ceramics by Starch Consolidation”, Journal of European Ceramic society, 18, pp131-40, 1998.

[20] Fabbri M., Celotti G.C., Ravaflioli A. “Granulates Based on Calcium Phosphate with controlled Morphology and porosity for medical applications: Physico-Chemical Parameters and Production Technique”, Biomaterials, 15, pp474-77, 1994.

[21] Rodríguez-Lorenzo L. M., Vallet-Regí M., Ferreira J. M. F., Ginebra M. P., Aparicio C., Planell J. A., "Hydroxyapatite Ceramic Bodies with Tailored Mechanical Properties for Different Applications", Journal of Biomedical Material Research, 60 (1), pp159-66, 2002.

[22] Balçık C., "Biomechanics of porous ceramic implants used in long-bones segmental defect healing", METU (Middle East Technical University, Ankara, Turkey), 2002 (PhD. Thesis).

[23] De Aza P. N., Guitian F., De Aza S., "Bioeutectic: A new ceramic material for human bone replacement", Biomaterials, 18, pp1285-91, 1997.

[24] De Aza P. N., Luklinska Z. B., Anseau M. R., Guitian F., De Aza S., "Bioactivity of pseudowollastonite in human saliva", Journal of Dentistry, 27, 2, pp107-13, 1999.

[25] Seo J. H., Ryu H. S., Park K. S., Hong K. S., Kim H. , Lee J. H., Lee D. H., Chang B. S., Lee C. K., "Characterization of Bioactive Glass-Ceramics Prepared by Sintering Mixed Glass Powders of Cerabone® A-W Type Glass/CaO-SiO_2-B_2O_3 Glass", Bioceramics 16, pp147-50, 2004.

[26] Ramakrishna S., Mayer J., Wintermantelc E., Leongd K. W., "Biomedical applications of polymer-composite materials: a review", Composites Science and Technology, 61, 9, pp1189-24, 2001.

[27] Zhong J. P., Greenspan D. C., Feng J. W., "A microstructural examination of apatite induced by bioglass in vitro", Journal of Materials Science: Materials in Medicine, 13, pp321–26, 2002.

[28] DeWith G., Corbijn A. T. "Metal fiber reinforcement of hydroxyapatite Ceramics", Journal of Material Science, 24, pp3411-34, 1989.

[29] Yamashita K., Kanazawa T., "In Inorganic Phosphate Materials", Materials Science Monograph, 52, pp15, 1989.

[30] Ivanchenko L. A., Pinchuk N. D., "Making Calcium Phosphate Biomaterials" Powder Metallurgy and Metal Ceramics, 42, 7-8, pp357-71, 2003.

[31] Hench L. L., Ethridge B. C., "Biomaterials: An Interfacial Approach", Academic Press, New York, 1982.

[32] Takagi M., Mochida M., Uchida N., Saito K., Uematsu K., "Filter Cake Forming and Hot Isostatic Pressing for TZP-Dispersed Hydroxyapatite Composite", Journal of Materials Science: Materials in Medicine, 3, pp199–03, 1992.

[33] Rodríguez-Lorenzo L. M., Vallet-Regí M., Ferreira J. M. F., Ginebra M. P., Aparicio C., Planell J. A., "Hydroxyapatite Ceramic Bodies with Tailored Mechanical Properties for Different Applications", Journal of Biomedical Material Research, 60 (1), pp159-66, 2002.

[34] Zhijian S., Erik A., Mats N., Lian G., Hirokazu K., Koichi N., "Dense hydroxyapatite-zirconia ceramic composites with high strength for biological applications", Advanced Materials, 13(3), pp214-16, 2001.

[35] Ravaglioli A., Krajewski A., "Bioceramics – Materials, Properties, Applications", Chapman & Hall, London, 1992.

[36] Taş A. C., "Molten Salt Synthesis of Calcium Hydroxyapatite Whiskers", Journal of The American Ceramic Society, 84 (2), pp295-300, 2001.

[37] Taş A. C., "X-Ray Diffraction Data for Flux-Grown Calcium Hydroxyapatite Whiskers" Powder Diffraction, 16 (2), pp102-06 2001.

[38] Yoshimura M., Suda H., Okamoto K., Loku K., "Hydrothermal Synthesis of Biocompatible Whiskers," Journal of Material Science, 29, pp3399-402, 1994.

[39] Suchanek W., Suda H., Yashima M., Kakihaua M., Yoshimura M., "Biocompatible Whiskers with Controlled Morphology and Stoichiometry", Journal of Material Science, 10, pp521-29, 1995.

[40] Suchanek W., Yashima M., Kakihana M., Yoshimura M., "Hydroxyapatite/Hydroxyapatite-Whisker Composites without Sintering Additives: Mechanical Properties and Microstructural Evolution", Journal of American Ceramic Society, 80, pp2805-13, 1997.

[41] Suchanek W., Yoshimura M., "Preparation of Fibrous, Porous Hydroxyapatite Ceramics from Hydroxyapatite Whiskers", Journal of American Ceramic Society, 81, pp765-67, 1998.

[42] Zhang H., Wang Y., Yan Y., Li S., "Precipitation of biocompatible hydroxyapatite whiskers from moderately acid solution", Ceramics International, 29, 4, pp413-18, 2003.

[43] Zhang H., Wang Y., Yan Y., Li S., "Thermal Stability of hydroxyapatite whiskers prepared by homogenous precipitation", Advance Engineering Materials, 4, 12, pp916-19, 2002.

[44] Knowles J. C., Bonfield W., "Development of a glass-reinforced hydroxyapatite with enhanced mechanical properties: the effect of glass composition and its relationship to phase changes", Journal of Biomedical Material Research, 27, pp1591–98, 1993,

[45] Santos J. D., Knowles J. C., Reis R. L., Monteiro F. J., Hastings G. W., "Microstructural characterization of glass reinforced hydroxyapatite composites", Biomaterials, 15 ,pp5–10, 1994.

[46] Tancred D. C., Carr A. J., McCormack B. A. O. "The sintering and mechanical behavior of Hydroxyapatite with Bioglass additions", Journal of Materials Science: Materials in Medicine, 12, pp81–93, 2001.

[47] Santos J. D., Knowles J. C., Reis R. L., Monteiro F. J., Hastings G. W., "Liquid Phase Sintering of Hydroxyapatite by Phosphate and Silicate Glass Additions. Structure and Properties of the Composites", Journal of Materials Science: Materials in Medicine, 6, pp448-52, 1995.

[48] Salih V., Georgiou G., Knowles J. C., Olsen I. "Glass reinforced hydroxyapatite for hard tissue surgery-part II: in vitro evaluation of bone cell growth and function", Biomaterials, 22, 20, pp2817-24, 2001.

[49] Georgiou G., Knowles J. C., Barralet J. E., Kong Y. M., Kim H. E. "The effect of hot pressing on the physical properties of glass reinforced hydroxyapatite", Journal of Material Science: Materials in medicine, 15 (6), pp705-10, 2004.

[50] Hench L. L, Anderson O., "Bioactive glass". In: Hench LL, Wilson J, editors, "An introduction to bioceramics", USA: World Scientific, 1993, pp41–62.

[51] Merwin G.E., "Bioglass® middle ear prosthesis: preliminary report", Annals of Otology, Rhinology & Laryngology, 95, pp78–82, 1986.

[52] Wilson J., Merwin G. E., "Biomaterials for Facial Bone Augmentation: Comparative Studies", Journal of Applied Biomaterials, 22[A2], pp159-77, 1988.

[53] Li N., Jie Q., Zhu S., Wang R.,"A new route to prepare macroporous bioactive sol–gel glasses with high mechanical strength", Materials Letters, 58, 22-23, pp2747-50, 2004.

[54] Amaral M., Lopes M. A., Silva R. F., Santos J. D., "Densification route and mechanical properties of Si_3N_4–bioglass biocomposites", Biomaterials, 23, 3, pp857-62, 2002.

[55] Clupper D. C., "Bioactivity of Bioglass®-steel and Bioglass®-titanium laminate composites", Journal of Materials Science Letters, 20, 10, pp959-60, 2001.

[56] Brömer H., Pfeil E., Kas H. H., German Patent 2, 326, 100, 1973.

[57] Kokubo T., Ito S., Shigematsu M., Sakka S., Yamamuro T., "Fatigue and life-time of bioactive glass-ceramic A-W containing apatite and wollastonite", Journal of Material Science, 22, pp4067-70, 1987.

[58] Kokubo T., Ito S., Sakka S., Yamamuro T., "Formation of a high strength bioactive glass-ceramics in the system $MgO-CaO-SiO_2-P_2O_5$", Journal of Material Science, 21, pp536-40, 1986

[59] Carpanter P. R., Campbell M., Rawlings R. D., Rogers P. S., "Spherulitic growth of apatite in a glass-ceramic system", Journal of Materials Science Letters, 5, pp1309-12, 1986.

[60] Cho S. B., Miyaji F., Kokubo T., Nakamuro T. "Induction of bioactivity of a non-bioactive glass ceramic by a chemical treatment", Biomaterials, 18, pp1479-85, 1997.

[61] Ohgushi H, Yoshikawa T, Nakajima H, Tamai S, Dohi Y, Okunaga K.,"Al_2O_3 doped apatite-wollastonite containing glass ceramic provokes osteogenic differentiation of marrow stromal stem cells", Journal of Biomedical Material Research, 44 (4), pp381-88, 1998.

[62] Höland W., "Biocompatible and bioactive glass-ceramics - state of the art and new directions", Journal of Non-Crystalline Solids, 219, pp192-97, 1997.

[63] Beall G. H., Montierth M. R., Smith G. P., "Machinable Glass-Ceramics", Microtecnic, 26, pp173, 1972.

[64] Höland W., Rheinberger V., Frank M., "Mechanisms of nucleation and controlled crystallization of needle-like apatite in glass-ceramics of the SiO_2-Al_2O_3-K_2O-CaO-P_2O_5 system", Journal of Non-Crystalline Solids, 253, pp170-77, 1999.

[65] Hill R. G., Goat C., Wood D., "Thermal analysis of a SiO_2-Al_2O_3-CaO-CaF_2 glass", Journal of American Ceramic Society, 75, pp778–85, 1992.

[66] Hill R. G., Wood D., "Apatite-Mullite glass-ceramics", Journal of Materials Science: Materials in Medicine, 6, pp311-18, 1995.

[67] Calver A., Hill R. G., Stamboulis A., "Influence of fluorine content on the crystallization behavior of apatite-wollastonite glass-ceramics", Journal of Material Science, 39, pp2601-03, 2004.

[68] Kokubo T., Kim H. M., Kawashita M., "Novel Bioactive materials with different mechanical properties", Biomaterials 24, pp2161-75, 2003.

[69] Zhang Y., Santos J. D. "Microstructural characterization and in vitro apatite formation in CaO–P_2O_5–TiO_2–MgO–Na_2O glass-ceramics", Journal of the European Ceramic Society, 21, 2, pp169-75, 2001.

[70] Kasuga T., Abe Y., "Calcium phosphate invert glasses with soda and titania", Journal of Non-Crystalline Solids, 243, pp70–74, 1999.

[71] Pernot F., Rogier R., "Mechanical Properties of Phosphate Glass-Ceramic 316L Stainless-Steel Composites", Journal of Materials Science, 28, pp6676-82, 1993.

[72] Pernot F., Rogier R., “Phosphate glass-ceramic-cobalt-chromium composite materials”, Journal of Materials Science, 27, pp2914-21, 1992.

[73] Hayek E., Newesely H., “Pentacalciummonohydroxyorthophosphate”, Inorganic Synthesis, 7, pp63, 1963.

[74] Akao M., Aoki H., Kato K., "Mechanical properties of sintered hydroxyapatite for prosthetic applications", Journal of Materials Science, 16, pp809-12, 1981.

[75] Gibson I. R., Best S. M., Bonfield W., “Chemical Characterization of silicon-substituted hydroxyapatite”, Journal of Biomedical Materials Research, 44, pp422-29, 1999.

[76] Muan A., Osborn E. F., “Phase Equilibria among Oxides in Steelmaking”, Addison-Wesley Pub. Co., 1965.

[77] American Society for Testing and Materials (ASTM) C1161-90, “Standard Test Method for Flexural Strength of Advanced Ceramics at Ambient Temperature”, Annual Book of ASTM Standards, Volume 15.01, Philadelphia, PA, 1991.

[78] Downling, N. E. “Mechanical Behavior of Materials”, 2nd. Edition, Prentice-Hall Inc., New Jersey, 1999.

[79] American Society for Testing and Materials (ASTM) C773-88, “Standard Test Method for Compressive (Crushing) Strength of Fired Whiteware Materials”, Annual Book of ASTM Standards, Volume 15.02, Philadelphia, PA, 1999.

[80] American Society for Testing and Materials (ASTM) C1327-03, "Standard Test Method for Vickers Indentation Hardness of Advanced Ceramics", Annual Book of ASTM Standards, Volume 15.01, Philadelphia, PA, 2003.

[81] Evans A. G., "Fracture Toughness: The Role of Indentation Techniques", In S. W. Freiman, editor, Fracture Mechanics Applied to Brittle Materials, ASTM STP 678, pp112-135, American Society for Testing and Materials, 1979.

[82] Niihara K., Horena M. R., Hasselman D. Ph., "Evaluation of K_{IC} of brittle solids by the indentation method with low crack-to-indent ratio", Journal of Materials Science Letters, 1, pp13-18, 1982.

[83] PDF card no. 9-432, ICDD(JCPDS), Newton Square, Pennsylvania, USA.

[84] American Society for Testing and Materials (ASTM) F 1185-88(1993), "Standard Specification for Composition of Ceramic Hydroxylapatite for Surgical Implants," 1988.

[85] PDF card no. 31-300, ICDD(JCPDS), Newton Square, Pennsylvania, USA..

[86] Kim S. R., Lee J. H., Kim Y. T., Riu D. H., Jung S. J., Lee Y. J., Chung S. C., Kim Y. H., "Synthesis of Si, Mg substituted hydroxyapatites and their sintering behaviors", Biomaterials, 24, 8, pp1389-98, 2003.

[87] PDF card no. 40-393, ICDD(JCPDS), Newton Square, Pennsylvania, USA..

[88] Leventouri Th., Bunaciu C. E., Perdikatsis V., "Neutron powder diffraction studies of silicon-substituted hydroxyapatite", Biomaterials 24, pp 4205-11, 2003.

[89] Botelho C. M., Lopes M. A., Gibson I. R., Best S. M., Santos J. D., "Structural Analysis of Si-substituted Hydroxyapatite: Zeta Potential and X-ray Photoelectron Spectroscopy", Journal of Materials Science: Materials in Medicine, 13, 12, pp1123-27, 2002.

[90] Nyquist R. A., Putzig C. L., Leugers A. M.., "Infrared and Raman Spectral Atlas of Inorganic Compounds and Organic Salts", 3, 1995.

[91] Rehman I., Bonfield W. "Characterization of hydroxyapatite and carbonated apatite by photo acoustic FTIR spectroscopy", Journal of Materials Science: Materials in Medicine, 8, pp1–4, 1997.

[92] Iturriza I., Echeberria J., Gutiérrez I., Castro F., "Densification of silicon nitride ceramics under sinter-HIP conditions", Journal of Materials Science, 25, pp2548–69, 1990.

[93] Gomez E., Echeberria J., Iturriza I., Castro F., "Liquid phase sintering of SiC with additions of Y_2O_3, Al_2O_3 and SiO_2", Journal of the European Ceramic Society, 24, 9, pp2895-03, 2004.

[94] Yang J. F., Deng Z. Y., Ohji T., "Fabrication and characterization of porous silicon nitride ceramics using Yb_2O_3 as sintering additive", Journal of the European Ceramic Society, 23, 2, pp371-78, 2003.

[95] Perera D. S., Mitchell D. R. G., Leung S., "High aspect ratio β-Si_3N_4 grain growth", Journal of the European Ceramic Society, 20, 6, pp789-94, 2000.

[96] Yang J. F., Zhang G. J., Kondo N., Ohji T., **"**Synthesis and properties of porous Si_3N_4/SiC nanocomposites by carbothermal reaction between Si_3N_4 and carbon", Acta Materialia, 50, pp4831–40, 2000.

[97] Hayashi S., Sugai M., Nakagawa Z., Takei T., Kawasaki K., Katsuyama T., Yasumori A., Okada K., "Preparation of $CaSiO_3$ whiskers from alkali halide Fluxes", Journal of the European Ceramic Society, 20, pp1099-103, 2000.

[98] Park K., Ryu H. S., Seo J. H., Hong K. S., Kim H., Lee J. H., Lee D. H., Chang B. S., Lee C. K., "Effect of B_2O_3 on the Sintering Behavior and Phase Transition of Wollastonite Ceramics", Key Engineering Materials, 254-56, pp151-54, 2004.

[99] Anstis G. R., Chantikul P., Lawn B. R., Marshall D.B., "A critical evaluation of indentation techniques for measuring fracture toughness. I. Direct crack measurements" Journal of American Ceramic Society, 64 (9), pp533–38, 1981.

[100] Laugier M. T. "New formula for indentation toughness in ceramics", Journal of Materials Science Letters, 6, pp355-56, 1987

[101] Li Z., Ghosh A, Kobayashi A. S., Bradt R. C., "Indentation fracture toughness of sintered silicon carbide in the Palmqvist crack regime", Journal of the American Ceramic Society, 72, 6, pp904-11, 1989.

[102] Knowles J. C., Talal S., Santos J. D., "Sintering Effects in a Glass Reinforced Hydroxyapatite", Biomaterials, 17, 14, pp1437-42, 1996.

[103] Tadic D., Epple M., “A thorough physicochemical characterization of 14 calcium phosphate-based bone substitution materials in comparison to natural bone”, Biomaterials, 25, pp987-94, 2004.

[104] Rice W., ‘‘Microstructure Dependence of Mechanical Behavior of Ceramics’’, pp. 199–381 in Treatise on Materials Science and Technology, Vol. 11, Properties and Microstructure, Edited by R. K. MacCrone. Academic Press, New York, 1977.

[105] De Aza P. N., Luklinska Z. B., “Effect of glass-ceramics microstructure on its in vitro bioactivity”, Journal of Materials Science: Materials in Medicine, 14, pp891–98, 2003.

[106] Rao W. R., Boehm R. F., "A study of sintered apatites", Journal of Dental Resarch, 53, pp1351-54, 1974.

[107] Wang C. K., Ju C. P., Chern Lin J. H., “Effect of Doped bioactive glass on structure and properties of sintered Hydroxyapatite”, Materials Chemistry And Physics, 53, pp138-49, 1998.

[108] Lin K., Zhai W., Ni S., Chang J., Zeng Y., Qian W., "Study of the mechanical property and in vitro biocompatibility of $CaSiO_3$ ceramics", Ceramics International, 31, 2, pp323-26, 2005.

[109] Kalita S. J., Bose S., Hosick H. L., Bandyopadhyay A., "$CaO-P_2O_5-Na_2O$-based Sintering Additives for Hydroxyapatite (HAp) Ceramics", Biomaterials, 25, pp2331-39, 2004.

[110] Siriphannon P., Kameshima Y., Yasumori A., Okada K., Hayashi S., "Formation of hydroxyapatite on $CaSiO_3$ powders in simulated body fluid", Journal of the European Ceramic Society, 22, 4, pp511-20, 2002.

[111] Bilotte W. G., "Ceramic Biomaterials" In: The Biomedical Engineering Handbook, 2nd Edition, Boca Raton, Fl. CRC Press, London, 2000, Chapter 38, pp18, Editor: Bruzino J. D.

[112] Ikeda N., Kawanabe K., Nakamura T.,"Quantitative Comparison of Osteoconduction of Porous, Dense A-W Glass-Ceramic and Hydroxyapatite Granules", Biomaterials, 20, 12, pp1087-95, 1999.

[113] Gibson I. R., Serena M. B., Bonfield W., "Effect of Silicon Substitution on the sintering and Microstructure of Hydroxyapatite", Journal of the American Ceramic Society, 85, 11, pp2771-77, 2002.

[114] Gibson I. R, Huang J., Best S. M., Bonfield W., "Enhanced in vitro cell activity and surface apatite layer formation on novel silicon-substituted hydroxyapatites", In: Ohgushi H. , Hastings G. W. , Yoshikawa T. , editors. Proceedings of the 12th international symposium on ceramics in medicine, bioceramics 12, pp191-94, Singapore: World Scientific; 1999.

[115] Korkusuz P., Şenköylü A., Korkusuz F., "Hard Tissue-Implant Interactions-2: Bone-Ceramic and Bone-Polymer Interactions", Journal of Arthroplasty & Arthroscopic Surgery, 14, 2, pp109-25, 2003.